

EXCITED STATE METHODS FOR
STRONGLY-CORRELATED SYSTEMS

EXCITED STATE METHODS FOR STRONGLY-CORRELATED
SYSTEMS: FORMULATIONS BASED ON THE
EQUATION-OF-MOTION APPROACH.

By GABRIELA SANCHEZ-DIAZ, M.Sc.

A Thesis Submitted to the School of Graduate Studies in Partial
Fulfillment of the Requirements for
the Degree Doctor of Philosophy

McMaster University © Copyright by Gabriela Sanchez-Diaz,
September 2024

McMaster University

DOCTOR OF PHILOSOPHY (2024)

Hamilton, Ontario, Canada (Department of Chemistry and Chemical Biology)

TITLE: Excited state methods for strongly-correlated systems:
formulations based on the equation-of-motion approach.

AUTHOR: Gabriela Sanchez-Diaz
M.Sc., B.Sc., (University of Havana)

SUPERVISOR: Prof. Paul W. Ayers

NUMBER OF PAGES: xv, 206

Abstract

Most research on solving the N -electron Schrödinger equation has focussed on ground states; excited states are comparatively less studied, and represent a greater challenge for many *ab initio* methods. The challenge is exacerbated for systems with substantial multiconfigurational character (i.e., strongly-correlated systems) for which standard many-electron wavefunction methods relying on a single electronic configuration give qualitatively incorrect descriptions of electron correlation. This thesis explores approaches to molecular excited state properties that are computationally efficient, yet applicable to multiconfigurational systems. Specifically, we explore strategies that combine the Equation-of-Motion (EOM) approach with the types of correlated wavefunction ansätze that are suitable for strongly-correlated systems. While it is known that the EOM method provides a general strategy for computing electronic transition energies, the significant flexibility in how one formulates the EOM approach and how it can be applied as a post-processing tool for different wavefunctions is not always appreciated.

We begin by reviewing the EOM approach, focussing on methods that can be formulated using the 1- and 2-electron reduced density matrices. We assess the accuracy of different EOM approaches for neutral and ionic excited states. We focus on EOM-based alternatives to the traditional extended Koopmans' Theorem for ionization energies and electron affinities as well as an EOM formulation for double

ionization transitions that constitutes an extension of the hole-hole/particle-particle random phase approximation (RPA) to multideterminant wavefunction methods. Then we introduce FanEOM, an EOM extension of the Flexible Ansatz for N-electron Configuration Interaction (FANCI) [Comput. Theor. Chem. 1202, 113187 (2021)], and explore its application to spectroscopic properties. Using the EOM methods for electronic excitation and double ionization/double electron affinity transitions described in the initial part of this thesis (i.e., the extended random phase approximations, ERPA), we study adiabatic connection formulations (AC) for computing the residual dynamic correlation energy in correlated wavefunction methods. The key idea in these approaches is that the perturbation strength dependent 2-RDM that appears in the AC formula can be approximated through the solutions from the different variants of ERPA [Phys. Rev. Lett. 120, 013001 (2018)]. Finally, we present PyEOM, an open-source software package designed to help prototype and test EOM-based methods.

*To my dear Gilber and my loving parents Alicia and Gustavo
for believing in me*

Acknowledgements

Pursuing a Ph.D. has not been an easy journey, and I am certain it would not have been possible without the support of those who accompanied me through it.

I want to express my heartfelt gratitude to Dr. Paul W. Ayers, who has immensely impacted my professional career and personal growth. Paul, thank you for your dedication, patience and above all, for your vote of trust. I always felt reassured knowing that, in spite of your insanely busy schedule, I could count on your help.

I want to thank the staff of the department of Chemistry and Chemical Biology for always being amenable and helping me navigate the complexities of graduate school. Thank you to my committee, Dr. Randall Dumont and Dr. Spencer Smith, for their guidance over the past five years.

Visiting Poland had a tremendously positive impact on me both personally and professionally. I am very grateful to Dr. Katarzyna Pernal for hosting me and for her kindness and support. Kasia, your assistance was instrumental in helping me reach the finish line of my Ph.D. journey.

My graduate experience would not have been complete without the incredible members of the Ayers Lab. I would like to thank my fellow graduate students Valerii Chuiko, Menatalla Mohamed and Wesley Sanchez for the shared experiences, laughs and common worries; Michelle Richer, my research companion and coding mentor;

and Marco Martínez González, for his advice and huge assistance through this final stretch of my Ph.D. I am also grateful to the former lab members Xiaomin Huang, David Kim, Derrick Yang, Matt Chan, Fanwang Meng, Kumru Dikmenli, Cristina González Espinoza, Farnaz Heidar-Zadeh and Ramon Alain Miranda Quintana for making me feel so welcomed.

To my extended Cuban family, who have made Hamilton a true second home, thank you. I believed that, after certain age, one had already met all the closest friends. Annia, Eduardo and Mabel, you proved me wrong; thank you for always being there.

I am profoundly grateful to my parents, Alicia and Gustavo, for their endless support, understanding, and love. I know that having me far away has not been easy, and I am forever thankful for your sacrifices and encouragement. Last but not least, to my husband, Gilberto. I hope I didn't make it too difficult for you, but I am grateful that you stood by my side through it all. This achievement is as much yours as it is mine, and I couldn't have done it without you.

Table of Contents

Abstract	iii
Acknowledgements	vi
1 Introduction	1
1.1 Electronic structure problem	3
1.2 Variational method	6
1.3 Single Slater determinant model	8
1.4 Correlation energy	10
1.5 Multideterminant wavefunction models	12
1.6 Basic aspects of second quantization	18
1.7 Density matrices	23
1.8 Outline	25
2 Equation-of-motion approach	34
2.1 Introduction	34
2.2 General Equation-of-Motion (EOM) formalism	37
2.3 EOM approximations	45
2.4 Transition densities	63

2.5	Numerical illustrations	65
2.6	Summary	74
3	Calculation of spectroscopic properties via parameterized configuration interaction methods	89
3.1	Introduction	89
3.2	Excited states with FanCI: FanEOM	93
3.3	Linear response function	97
3.4	Computational considerations	101
3.5	Numerical illustrations	103
3.6	Summary	109
4	Dynamic correlation energy from extended random phase approximation approaches	115
4.1	Introduction	115
4.2	Correlation energy from the adiabatic connection	118
4.3	Exact two-electron reduced density matrix formulas	122
4.4	ERPA approximated 2-RDMs	125
4.5	AC-ERPA correlation energy	133
4.6	Examples	134
4.7	Computational details	142
4.8	Results and discussion	144
4.9	Conclusions	153
5	PyEOM: A software package for equations-of-motion methods.	165
5.1	What is PyEOM?	165

5.2	Why PyEOM?	166
5.3	Intended user	167
5.4	Structure of PyEOM	167
5.5	Using PyEOM	173
5.6	Extensions to PyEOM	183
5.7	Summary	184
6	Conclusion	193
6.1	Summary	193
6.2	Future work	196
A		202
	Appendix	202

List of Figures

1.1	Examples of electronic configuration generated from a reference Slater determinant with 4 orbitals, 2 electrons up and 2 down by different excitation operators. (a) Single, double and triple excited configurations. (b) Ionized configurations with single and double excitations.	21
2.1	Mean absolute errors (MAE) in the lowest ionization potentials of a small test set of atoms and molecules for KT, EKT, IPa and IPc methods relative to HCI results with the aug-cc-pVDZ basis set. . . .	70
4.1	General procedure for computing the correlation energy via AC-ERPA.	145
4.2	Dissociation curve of H ₂ in the cc-pVDZ basis set. (a) Total energies and (b) energy differences (relative to FCI).	148
4.3	Dissociation curve of FH in the 6-31G basis set. (a) Total energies and (b) energy differences calculated as the absolute value relative to HCI.	150
4.4	AC integrand for the DOCI reference for H ₆ with H–H distance of 1.0Å using 6-31G basis set. The correlation energy is given by the area under the $W(\lambda)$ curves. The hhDOCI underestimates the correlation energy relative to phDOCI.	152

4.5	Dissociation curve of N_2 in the cc-pVDZ basis set. (a) Total energies and (b) energy differences calculated as the absolute value relative to HCl.	154
5.1	PyEOM class inheritance diagram.	169
5.2	Dyson orbitals contour plots from Extended Koopmans' Theorem at the HCl/6-31G level of theory for CO molecule. (a) σ transition (b) π transition.	181

List of Tables

2.1	Approximations to the transition operator $(\hat{Q}_\lambda^{\pm\kappa})^\dagger$	46
2.2	Errors in the lowest ionization potentials (in eV) computed from 1- and 2-RDMs at the aug-cc-pVDZ HF (KT) and HCI levels (EKT, IPa, IPc). The errors are evaluated as the absolute value of the deviation from HCI, $\Delta_{method} = E(HCI) - E(method) $	68
2.3	Ionization potentials (in eV) computed from 1 and 2-RDMs at the aug-cc-pVDZ HF (KT) and HCI levels (EKT, IPa, IPc). The errors are given as $\Delta_{method} = E(HCI) - E(method) $	71
2.4	Errors in the lowest excitation energies (in eV) computed from 1 and 2-RDMs at the aug-cc-pVDZ HF (RPA) and HCI levels (ERPA, ETDA). RPA is short form for ph-RPA, ERPA for ph-ERPA and ETDA for ph-ETDA. The errors are given as $\Delta_{method} = E(HCI) - E(method) $. . .	73
2.5	Lowest double ionization potential (in eV) computed from 1 and 2-RDMs at the aug-cc-pVDZ HF (RPA) and HCI levels (ERPA, ETDA). RPA is short form for hh-RPA, ERPA for hh-ERPA and ETDA for hh-ETDA. The errors are given as $\Delta_{method} = E(HCI) - E(method) $. . .	74

3.1	Be ionization potentials (in Hartree) from FanEOM and EKT at the FCI/6-31G level of theory. The FanEOM projection space includes all unique one-electron removed configurations from the N-electron CISD model. Three procedures to solve the non-square matrix problem are compared, BDagger, LS and MPA. The transitions are labeled according to the main configuration from where the electron is removed	104
3.2	Convergence with size of projection space (PSpace) of Be ionization potentials (in Hartree) from FanEOM at the FCI/6-31G level of theory. The eigenstates from BDagger procedure are shown. The MAE is given relative to the projection on the full space of $(N - 1)$ -electron determinants. The transitions are labeled according to the main configuration from where the electron is removed	105
3.3	LiH ionization potentials (in Hartree) from FanEOM and EKT at the FCI/6-31G level of theory. The FanEOM projection space includes all unique one-electron removed configurations from CISD. Three procedures to solve the non-square matrix problem are compared, BDagger, LS and MPA. The transitions are labeled according to the symmetry of the orbital from where the electron is removed.	107
3.4	Be excitation energies (in Hartree) from FanEOM, ERPA and FCI with 6-31G levels of theory. The FanEOM projection space is CISDT. The transitions are labeled by the leading configuration in the FCI solution and the multiplicity of the state indicated by the spin (S=0, singlet or S=1, triplet).	108

3.5	LiH excitation energies (in Hartree) from FanEOM, ERPA and FCI with 6-31G levels of theory. The FanEOM projection space is CISDT. The transitions are labeled by the symmetry of the orbitals in the leading FCI configuration and the multiplicity of the state indicated by the spin (S=0, singlet or S=1, triplet).	108
3.6	Convergence of Be excitation energies (in Hartree) with size of projection space (PSPACE) computed with FanEOM at the FCI/6-31G level of theory. The eigenstates from BDagger method are shown. The transitions are labeled by the leading configuration in the FCI solution and the multiplicity of the state indicated by the spin (S=0, singlet or S=1, triplet).	109
5.1	Supported EOM Methods.	168
5.2	Excited states in PyEOM.	170
A.1	Lowest ionization potentials (in eV) computed from 1- and 2-RDMs at the aug-cc-pVDZ HF (KT) and HCI levels (EKT, IPa, IPc, IPam, IPcm)	206
A.2	Lowest ionization potentials (in eV) computed from 1- and 2-RDMs at the aug-cc-pVDZ HCI level (EKT, EKT1/2, IPc, IPc1/2)	206

Chapter 1

Introduction

Electronic excited states of molecules and materials are central to photochemical and photophysical processes with far-reaching implications for diverse areas of science, environment, and technology. For example, the key step in photochemical processes such as CO₂ reduction [1, 2], water splitting [3, 4], and atmospheric pollutant degradation [5] is frequently the excitation of a molecule to a higher-energy state. In materials science, photovoltaic devices use electronic excitations to harness the energy of sunlight [6]. Finally, observing how molecules and materials are excited to higher-energy states is central to spectroscopic methods for the quantitative and qualitative characterization of substances and their physicochemical processes.

The physical and chemical properties of excited states are governed by their electronic structure. For example, because a molecule's electronic structure typically changes *qualitatively* when it is excited, molecular excited states typically have very different reactivity, with different nucleophilic/electrophilic propensities. Typically, molecules tend to react more rapidly in excited states, and activation barriers tend to be lower on excited-state potential energy surfaces [7–9]. This is why photochemistry

has emerged as a distinct field of inquiry, with rules and principles that are often different (and sometimes even reversed) from those of ground-state chemistry.

The other area of chemistry where excited states are ubiquitous is spectroscopy, which is defined by its focus on excited states, and the transitions to, from, and between them. Ultraviolet-visible (UV/visible) spectroscopy measures the energy and amount of radiation absorbed by a substance through a spectrophotometer, and can provide valuable information about the identity of a molecule, its structure, its molecular environment, and how the molecule and its environment change over time. Thermodynamic and kinetic information about a chemical reaction can be inferred from these measurements [10, 11].

Predicting photochemical processes and interpreting a molecule’s spectrum can be challenging, especially for new substances. This motivates the development of theoretical approaches and computational methods to model excited states. Specifically, quantum chemistry methods can provide an atomistic understanding of excited state processes and aid interpret experimental observations [12]. In the quantum world, the central variable encoding all information about a system is the wavefunction. By solving the Schrödinger equation, one can determine the wavefunction and energy of ground and excited states. However, this equation cannot be solved exactly except for the simplest systems. Therefore, developing approximate methods that are both accurate and computationally feasible is essential.

Balancing computational cost with accuracy is the central challenge of quantum chemistry, and it is especially acute for excited states, which are often more challenging to describe than ground states because they are less likely to be well-described by a single electron configuration. That is, many excited states cannot be well described by

specifying a set of occupied molecular orbitals and antisymmetrizing their product in a Slater determinant wavefunction. Such multi-configurational character indicates that there is a significant correlation between the electrons, which is not well captured by black-box methods based on single-reference wavefunctions like configuration interaction singles (CIS) [13], time-dependent density functional theory (TD-DFT) [14], or coupled-cluster (CC) methods [15, 16]. To treat multiconfigurational character, or strong electron correlation, one must use more elaborate wavefunction approximations [17–19]. However, these advanced methods often scale poorly with system size, highlighting the need for ongoing research into efficient wavefunction methods for excited states.

This thesis focuses on developing cost-effective *ab initio* methods for treating electron correlation in ground and excited states and, thus, is a contribution to the development of theoretical approaches and computational methods for strong electron configuration. This chapter introduces the theoretical framework and notation essential for understanding the thesis, outlining the electronic structure problem, presenting the electronic Schrödinger equation, and reviewing standard many-electron wavefunction methods. It also introduces second-quantized notation, a formalism that describes many-electron systems in a compact and elegant way, and (reduced) many-electron density matrices.

1.1 Electronic structure problem

The nature and evolution of a quantum system are governed by the Schrödinger equation, which is the fundamental equation of quantum mechanics [20]. In its most

general form, the time-dependent Schrödinger equation,

$$i\hbar\frac{\partial\Psi(\mathbf{r},t)}{\partial t} = \hat{H}\Psi(\mathbf{r},t) \quad (1.1.1)$$

describes the how one or more nonrelativistic particles, at spatial (and possibly spin) coordinates, \mathbf{r} , evolve in time, t . The evolution of these particles is governed by the Hamiltonian, \hat{H} , which is the energy operator associated with the quantum particles and their environment. The solution to the Schrödinger equation, $\Psi(\mathbf{r},t)$, is the wavefunction, which encodes all the observable physical information about the quantum system.

Quantum chemists in general, and electronic structure theorists in particular, are often interested in the time-independent systems, where \hat{H} does not depend on time. This allows one to separate the spatial- and time-dependent parts of the wavefunction; the spatial wavefunction is then obtained by solving the time-independent Schrödinger equation:

$$\hat{H}\Psi_\lambda(\mathbf{r}) = E_\lambda\Psi_\lambda(\mathbf{r}) \quad (1.1.2)$$

which has the form of an eigenvalue problem. According to the postulates of quantum mechanics, the (infinite) set of solutions $\{\Psi_\lambda\}$ provides a complete basis set in the Hilbert space of wavefunctions. The lowest energy state, indexed with $\lambda = 0$, corresponds to the ground state; higher energies correspond with excited states. Our main focus is the ground state and, for notational concision, we neglect the subscript in Ψ_λ when referring to the ground state wavefunction if there is no ambiguity.

For a molecule with M atomic nuclei and N electrons, their pairwise interactions can be described by the non-relativistic Hamiltonian operator which, in atomic units,

is given by:

$$\begin{aligned}\hat{H} &= -\frac{1}{2} \sum_{A=1}^M \frac{\nabla_A^2}{m_A} - \frac{1}{2} \sum_{i=1}^N \nabla_i^2 - \sum_{i=1}^N \sum_{A=1}^M \frac{Z_A}{r_{iA}} + \sum_{i<j}^N \frac{1}{r_{ij}} + \sum_{A<B}^M \frac{Z_A Z_B}{R_{AB}} \\ &= \hat{T}_n + \hat{T}_e + \hat{V}_{ne} + \hat{V}_{ee} + \hat{V}_{nn}\end{aligned}\tag{1.1.3}$$

where ∇^2 is the Laplace operator, m_A and Z_A are the mass and charge of nucleus A, and r_{iA} , r_{ij} and R_{AB} are the distances between an electron and a nucleus, two electrons, and two nuclei, respectively. The first two sums are the kinetic energy operators for the nuclei and electrons, \hat{T}_n and \hat{T}_e , respectively. The next sums correspond to the potential energy operators, including the nuclei-electron Coulomb attraction, \hat{V}_{ne} (this term is also known as external potential), the interelectron Coulomb repulsion, \hat{V}_{ee} , and internuclear Coulomb repulsion, \hat{V}_{nn} .

The Schrödinger equation for atoms and molecules can be further simplified because the atomic nuclei are thousands of times heavier than electrons and, thus, move much more slowly. Consequently, the nuclei can often be considered to have fixed positions relative to the movement of electrons and the electronic and nuclear wavefunctions can be separated. From the viewpoint of the electrons, then, coupling to the nuclei's motion (encapsulated in \hat{T}_n) can be neglected, and because the nuclear positions are fixed, \hat{V}_{nn} becomes a constant. While there are several different ways to justify this *adiabatic approximation*, the most pervasive in quantum chemistry is the Born-Oppenheimer (BO) approach [21, 22]. Within the BO approximation, after factorizing the molecular wavefunction into its nuclear and electronic components, one obtains,

at each molecular geometry, the electronic Schrödinger equation:

$$(\hat{T}_e + \hat{V}_{ne} + \hat{V}_{ee})\Psi(\mathbf{x}_1, \mathbf{x}_2, \dots, \mathbf{x}_N) = E\Psi(\mathbf{x}_1, \mathbf{x}_2, \dots, \mathbf{x}_N) \quad (1.1.4)$$

The solution to the electronic Schrödinger equation provides the electronic energy, E , at a given nuclear geometry and the associated N -electron wavefunction, $\Psi(\mathbf{x}_1, \mathbf{x}_2, \dots, \mathbf{x}_N)$. Here \mathbf{x} denotes the combined spatial (\mathbf{r}) and spin (σ) coordinates of the electrons. Equation (1.1.4) depends parametrically on the nuclear coordinates through \hat{V}_{ne} and the potential energy surface (PES) for the nuclei is obtained by adding \hat{V}_{nn} to E . The PES is the key quantity in modelling molecular thermodynamics, kinetics, and spectroscopy.

Even after introducing the separation of time and nuclear motion variables, the Schrödinger equation cannot be solved exactly for multielectron systems because the electron-electron repulsion term, \hat{V}_{ee} , couples the electrons' coordinates, leading to electron correlation. Therefore, one needs to introduce further approximations; this is the goal of electronic structure methods in quantum chemistry. In this chapter and this thesis, we focus on approximations based on the wavefunction as opposed to density functional or perturbation theory approaches.

1.2 Variational method

One approach to solving the Schrodinger equation, Eq.(1.1.4), is to guess a suitable trial wavefunction, $\tilde{\Psi}$. (An N -electron wavefunction is suitable if it is single-valued, antisymmetric with respect to exchange of electronic coordinates, square-integrable, has finite kinetic energy, and satisfies appropriate boundary conditions.) Then, the

best wavefunction of the trial form can be determined by the variational principle, i.e., minimizing the energy of the trial wavefunction [21].

The energy of a given trial wavefunction can be obtained left multiplying Eq. (1.1.4) by the complex conjugate of the wavefunction and integrating:

$$\begin{aligned} E[\tilde{\Psi}] &= \frac{\int \tilde{\Psi}^*(\mathbf{x}_1, \mathbf{x}_2, \dots, \mathbf{x}_N) \hat{H} \tilde{\Psi}(\mathbf{x}_1, \mathbf{x}_2, \dots, \mathbf{x}_N) d\mathbf{x}_1 \dots d\mathbf{x}_N}{\int \tilde{\Psi}^*(\mathbf{x}_1, \mathbf{x}_2, \dots, \mathbf{x}_N) \tilde{\Psi}(\mathbf{x}_1, \mathbf{x}_2, \dots, \mathbf{x}_N) d\mathbf{x}_1 \dots d\mathbf{x}_N} \\ &= \frac{\langle \tilde{\Psi} | \hat{H} | \tilde{\Psi} \rangle}{\langle \tilde{\Psi} | \tilde{\Psi} \rangle} \end{aligned} \quad (1.2.1)$$

This expression represents the expectation value of the Hamiltonian operator, where, in the second line, we have introduced Dirac's bra-ket notation, $\langle | \rangle$:

$$|\tilde{\Psi}\rangle = \tilde{\Psi}(\mathbf{x}_1, \mathbf{x}_2, \dots, \mathbf{x}_N) \quad (1.2.2)$$

$$\langle \tilde{\Phi} | = \tilde{\Phi}^*(\mathbf{x}_1, \mathbf{x}_2, \dots, \mathbf{x}_N) \quad (1.2.3)$$

$$\langle \tilde{\Psi} | \tilde{\Psi} \rangle = \int \tilde{\Psi}^*(\mathbf{x}_1, \mathbf{x}_2, \dots, \mathbf{x}_N) \tilde{\Psi}(\mathbf{x}_1, \mathbf{x}_2, \dots, \mathbf{x}_N) d\mathbf{x}_1 \dots d\mathbf{x}_N \quad (1.2.4)$$

$$\langle \tilde{\Phi} | \hat{H} | \tilde{\Psi} \rangle = \int \tilde{\Phi}^*(\mathbf{x}_1, \mathbf{x}_2, \dots, \mathbf{x}_N) \hat{H} \tilde{\Psi}(\mathbf{x}_1, \mathbf{x}_2, \dots, \mathbf{x}_N) d\mathbf{x}_1 \dots d\mathbf{x}_N \quad (1.2.5)$$

Then the variational principle states that the expectation value of the energy of $\tilde{\Psi}$ is never below the exact ground state energy, E_0 :

$$E[\tilde{\Psi}] = \frac{\langle \tilde{\Psi} | \hat{H} | \tilde{\Psi} \rangle}{\langle \tilde{\Psi} | \tilde{\Psi} \rangle} \geq \frac{\langle \Psi_0 | \hat{H} | \Psi_0 \rangle}{\langle \Psi_0 | \Psi_0 \rangle} = E_0 \quad (1.2.6)$$

The variational principle provides a systematic approach to construct upper bounds to the ground-state energy. The *variational method* consists of choosing a trial wavefunction, $\tilde{\Psi}$, that depends on a set of parameters, and then minimizing the

energy functional, $E[\tilde{\Psi}]$, with respect to these parameters.

1.3 Single Slater determinant model

Because electrons are fermions, the simplest approximation to $|\Psi\rangle$ that preserves their permutational antisymmetry is a single Slater determinant.[21] This determinant, expressed in terms of a basis of orthonormal one-electron functions $\chi_i(\mathbf{x})$ called spin-orbitals, is denoted as follows:

$$\Phi(\mathbf{x}_1, \mathbf{x}_2, \dots, \mathbf{x}_N) = \frac{1}{\sqrt{N!}} \begin{vmatrix} \chi_1(\mathbf{x}_1) & \chi_2(\mathbf{x}_1) & \dots & \chi_N(\mathbf{x}_1) \\ \chi_1(\mathbf{x}_2) & \chi_2(\mathbf{x}_2) & \dots & \chi_N(\mathbf{x}_2) \\ \vdots & \vdots & & \vdots \\ \chi_1(\mathbf{x}_N) & \chi_2(\mathbf{x}_N) & \dots & \chi_N(\mathbf{x}_N) \end{vmatrix} \quad (1.3.1)$$

In the Slater determinant, where the columns correspond to orbitals and the rows to electronic coordinates, the pre-factor ensures normalization, accounting for the number of electrons N . The Slater determinant wavefunction explicitly satisfies Pauli's exclusion principle, ensuring that if two columns in Eq. (1.3.1) were identical, Φ would be zero. Additionally, permutation of two rows or columns changes the sign of the determinant, ensuring the permutational antisymmetry.

Spin-orbitals are commonly defined as the product of a spatial function $\phi(\mathbf{r})$ and a spin function $\sigma(\omega)$, which can take the values α or β :

$$\chi_i(\mathbf{x}) = \phi_i(\mathbf{r})\sigma(\omega) \quad (1.3.2)$$

They can be classified as restricted, unrestricted, or generalized. Restricted spin-orbitals have the same spatial component for the alpha and beta spin functions; unrestricted spin-orbitals have no such constraints on the spatial part. Generalized spin-orbitals can be constructed as linear combinations of alpha- and beta-spin basis functions. We always choose our spin-orbitals to be orthogonal and normalized,

$$\langle \chi_i(\mathbf{x}) | \chi_j(\mathbf{x}) \rangle = \delta_{ij} \quad (1.3.3)$$

The Hartree-Fock method, which is arguably the simplest electronic structure approach, results when the trial wavefunction is chosen to be a Slater determinant and the variational method is applied. To determine the optimal set of occupied orbitals, one derives an expression for the expectation value of the energy for a Slater determinant and minimizes it, using Lagrange multipliers to enforce the orthonormality of the spin-orbitals. After some algebraic manipulations, one obtains the Hartree-Fock (HF) equations [21]:

$$\hat{f}(\mathbf{x}_1)\chi_i(\mathbf{x}_1) = \epsilon_i\chi_i(\mathbf{x}_1) \quad i = 1, 2, \dots, N \quad (1.3.4)$$

where, \hat{f} , the Fock operator, is an effective one-electron operator, defined as:

$$\hat{f}(\mathbf{x}_1) = -\frac{1}{2}\nabla_1^2 - \sum_{A=1}^M \frac{Z_A}{r_{1A}} + \sum_{j=1}^N (\hat{J}_j(\mathbf{x}_1) - \hat{K}_j(\mathbf{x}_1)) \quad (1.3.5)$$

The operators \hat{J}_j and \hat{K}_j are the Coulomb and exchange operators, defined by their

action on a spin-orbital as follows:

$$\hat{J}_j(\mathbf{x}_1) |\chi_i\rangle = \int d\mathbf{x}_2 |\chi_j(\mathbf{x}_2)|^2 \frac{1}{r_{12}} \chi_i(\mathbf{x}_1) \quad (1.3.6)$$

and

$$\hat{K}_j(\mathbf{x}_1) |\chi_i\rangle = \int d\mathbf{x}_2 \chi_j^*(\mathbf{x}_2) \frac{1}{r_{12}} \chi_j(\mathbf{x}_1) \chi_i(\mathbf{x}_2) \quad (1.3.7)$$

respectively.

The i -th eigenvalue ϵ_i is interpreted as the energy of spin-orbital χ_i . The HF method represents an effective mean-field approach given that it accounts for the electron-electron interactions \hat{V}_{ee} in an average manner. It gives rise to the concept of molecular orbitals, which are building blocks for more advanced approximate electronic structure methods.

1.4 Correlation energy

The probability of observing an electron at \mathbf{x} depends on the positions/spins of the other electrons. That is, electrons are correlated. Mean-field approximations like HF (where one electron interacts with the field generated by the others in an average way) fail to describe electron correlation. Nonetheless, Hartree-Fock usually provides a good approximation to molecule's total electronic energy. (Typically the Hartree-Fock energy is within 1% of the exact energy for a given basis set; in absolute numbers, the error is typically 1 eV per valence electron pair.) However, this seemingly small error in absolute energies becomes highly significant for quantitative accuracy in energy differences, especially when predicting bond dissociation or any other process that involves breaking/forming/rearranging electron pairs. The correlation energy is also

important for predicting spectroscopic energy differences (e.g., excitation energies, ionization potentials, electron affinities), as these energy differences are typically a small percentage of the total energy, comparable to the error in the Hartree-Fock approximation.

The difference between the HF energy in the limit of a complete basis set E_{HF} and the exact one E_{exact} is *defined* as the correlation energy E_{corr} ,

$$E_{corr} = E_{exact} - E_{HF} \quad (1.4.1)$$

Since the HF result is an upper bound to E_{exact} (as can be proved through the variational principle) the correlation energy is negative.

The electron correlation can be further divided into contributions depending on the physical effects that originate it. Dynamic and static correlation are the most common classifications used among the quantum chemistry community. The former, as its name indicates, is related to the movement of the electrons in a system trying to avoid each other at all times: every multi-electron systems has dynamic correlation. Static, or strong, correlation is associated with the failure of the single electron configuration (Slater determinant) to describe the qualitative electronic structure of a system; it arises from near degeneracy in the molecular orbitals. Recalling that electron correlation arises from V_{ee} , one may infer that static correlation is more pronounced when the electron-electron integrals between molecular orbitals (e.g., the J_{ij} and K_{ij} integrals that appear in the matrix representation of the Fock operator in the Hartree-Fock method [21]) are comparable to, or even larger than, the magnitude of the associated orbital energy differences, $\varepsilon_i - \varepsilon_j$.

Correlated wavefunction approximations, which recover E_{corr} , are often known as

post-Hartree-Fock methods since they usually build upon the Hartree-Fock reference. Some of the most popular approximations are the configuration interaction (CI) [21] and Coupled Cluster (CC) models [15, 16, 23]. However, when static correlation is important, it is necessary to include additional Slater determinants in the “starting” approximation, leading to alternative methods called multideterminant, or multiconfiguration, approaches. MRCI [24, 25] and MRCC [26] are the multireference analogues of configuration interaction and coupled cluster methods, respectively.

1.5 Multideterminant wavefunction models

This section provides a brief overview of standard correlated wavefunction models within the CI and CC hierarchy of methods. Each method offers a unique approach to approximating the many-electron wavefunction by expanding it in a space of Slater determinants. Both CI and CC approaches, while powerful, have their own sets of advantages and limitations, making them complementary tools in the study of electronic structure.

1.5.1 Configuration Interaction

The set of all possible Slater determinants $\{\Phi_p\}$ that can be formed from m spin-orbitals and N electrons comprises a complete basis, in which the N -electron wavefunction can be expanded. Configuration interaction (CI) use this idea, writing the N -electron wavefunction as a linear combination of Slater determinants:

$$|\Psi\rangle = \sum_{p=1} c_p |\Phi_p\rangle \quad (1.5.1)$$

where the coefficient c_p determines the weight of each configuration Φ_p in the expansion.

Commonly, the HF determinant $|\Phi_0\rangle$ is chosen as the leading term in the expansion, and further terms include excited configurations relative to the HF reference:

$$|\Psi\rangle = c_0 |\Phi_0\rangle + \sum_{i,a} c_{ia} |\Phi_i^a\rangle + \sum_{i<j,a<b} c_{ij,ab} |\Phi_{ij}^{ab}\rangle + \sum_{i<j<k,a<b<c} c_{ijk,abc} |\Phi_{ijk}^{abc}\rangle + \dots \quad (1.5.2)$$

This equation denotes single excitations from an occupied HF orbital χ_i to an unoccupied/virtual HF orbital χ_a , $|\Phi_i^a\rangle$; double $|\Phi_{ij}^{ab}\rangle$, triple $|\Phi_{ijk}^{abc}\rangle$, and higher-order excitations are denoted similarly.

In CI methods, it follows from the variational principle that the stationary states of the Schrödinger equation can be found by solving the matrix eigenvalue problem:

$$\mathbf{H}\mathbf{c} = E\mathbf{c} \quad (1.5.3)$$

where \mathbf{c} is the vector of coefficients, E is the corresponding energy eigenvalue, and the matrix \mathbf{H} is the Hamiltonian operator projected onto the CI basis set, defined by its elements $H_{mn} = \langle \Phi_m | \hat{H} | \Phi_n \rangle$. The Hamiltonian matrix is sparse and, using iterative diagonalization methods, one can find eigenvectors and eigenvalues at a computational cost proportional to the number of nonzero matrix elements in \mathbf{H} .

If the complete set of determinants is considered, one gets the Full CI (FCI) wavefunction model, which gives the exact ground and excited-state energies and corresponding wavefunctions, subject only to the approximation inherent in truncating the orbital basis set. However, the computational scaling of FCI is $m!$ (there are $\binom{m}{N}$ possible configurations), which is prohibitively expensive for all but the smallest systems. For example, in a 10-electron system such as water, doubling the size of

the basis set from 10 to 20 spatial orbital gives a 3000-fold increase in the number of determinants in FCI.

In chemical applications, or any system where the Hamiltonian operator (ergo its eigenfunctions) have favorable differentiability properties, most configurations in Eq. (1.5.2) have very small magnitude. Therefore, one can truncate the FCI expansion and design a guess wavefunction that minimizes the computational cost while retaining a target accuracy by choosing the most important terms in Eq. (1.5.2). This is the idea behind the selected/truncated CI methods (SCI) [27]. For example, because more highly-excited determinants tend to have smaller coefficients, one can truncate the expansion at a certain excitation level, leading to the excitation hierarchy of configuration interaction singles CIS, singles and doubles (CISD), etc.. Alternatively, the seniority—the number of unpaired electrons—of the electronic configurations can be the selection criteria [28, 29]. This results in the seniority hierarchy of CI methods; the seniority-zero wavefunction model (including all electron configurations with all electrons paired) is quite old, and is often called doubly-occupied CI (DOCI) in deference to the traditional CI literature [30]. However, there are more efficient techniques that attempt to estimate the magnitude of each configuration, then include all configurations whose predicted weight is larger than a threshold. One of the most expensive and accurate of these approaches is configuration interaction by perturbatively selecting iteratively (CIPSI) [31], which uses perturbation theory to determine the most important missing CI coefficients, then systematically expands the CI space. One of the simplest of these approaches is the family of Griebel-Knappek configuration interaction (GKCI) methods [32], which approximate the CI coefficients based on mathematical properties of the Hamiltonian. A favorable compromise

between expensive but accurate estimates of the CI coefficients (like CIPSI) and cheap but less-accurate Hamiltonian-independent methods (like GKCI) is the Heat-bath Configuration Interaction (HCI) approach, devised by Holmes et al. [33]. HCI involves two main steps: (1) the selection of determinants to be included in the variational wavefunction space, Equation (1.5.2), followed by the optimization of this trial wavefunction; (2) the computation of a second-order PT correction to approximate the importance of neglected determinants. HCI relies on two parameters, denoted by epsilon variables, ϵ_1 and ϵ_2 . The first parameter governs the selection of the determinants to add in step (1), while the second controls the choice of those used in step (2). These parameters are crucial in balancing the trade-off between computational speed and accuracy. The deterministic heat-bath sampling algorithm guides the selection process in both steps. It ensures that only determinants connected by a Hamiltonian matrix element H_{mn} with a magnitude higher than an ϵ to a given reference determinant are considered. In practice, HCI and closely-related algorithms provide an excellent compromise between cost and accuracy, and are nearly "ideal" for many chemical applications.

Truncated CI methods avoid the ($m!$) scaling of FCI, typically reducing it to a polynomial (e.g., m^6 for CISD). However, except for orbital-optimized seniority-zero (DOCI), the aforementioned truncated CI methods are not size-extensive or size-consistent [21, 34]. Both properties have to do with the additivity of the energy and are critical for the correct qualitative description of the thermodynamic limit (size-extensivity) and molecular dissociation (size-consistency). Nonetheless, these errors are often manageable in practice (e.g., for HCI methods with sufficiently small values of ϵ_1 and ϵ_2).

1.5.2 Coupled Cluster

Size-extensivity and size-consistency is restored in the coupled cluster (CC) model, which employs an exponential wavefunction parametrization rather than a linear one:

$$|\Psi\rangle = e^{\hat{T}} |\Phi_0\rangle \quad (1.5.4)$$

Here, $|\Phi_0\rangle$ is a single Slater determinant (typically the HF solution) and the cluster operator, $e^{\hat{T}}$, is defined by the Taylor series:

$$e^{\hat{T}} = 1 + \hat{T} + \frac{\hat{T}^2}{2!} + \frac{\hat{T}^3}{3!} + \dots = \sum_{k=1}^{\infty} \frac{\hat{T}^k}{k!} \quad (1.5.5)$$

$$\hat{T} = \hat{T}_1 + \hat{T}_2 + \hat{T}_3 + \dots + \hat{T}_N = \sum_{k=1}^N \hat{T}_k \quad (1.5.6)$$

where in the second line the cluster operator \hat{T} is defined as the sum of excitation operators up to the N th-order. Each \hat{T}_k operator directly creates k th-order excited Slater determinants from the reference $|\Phi_0\rangle$. For example, when applied to $|\Phi_0\rangle$, the operators \hat{T}_1 and \hat{T}_2 generate linear combinations of singly and doubly excited determinants $|\Phi_i^a\rangle$ and $|\Phi_{ij}^{ab}\rangle$, respectively:

$$\hat{T}_1 |\Phi_0\rangle = \sum_{ia} t_{ia} |\Phi_i^a\rangle \quad (1.5.7)$$

$$\hat{T}_2 |\Phi_0\rangle = \sum_{ijab} t_{ij,ab} |\Phi_{ij}^{ab}\rangle \quad (1.5.8)$$

The coefficients t_{ia} , $t_{ij,ab}$, known as cluster amplitudes, are the variables one seeks to determine in CC approaches. Instead of solving the variational form of the Schrödinger Equation, Eq. (1.2.1), in CC methods a set of non-linear equations is

solved by projecting onto a set of Slater determinants $\{\Phi_m\}$:

$$\langle \Phi_m | \hat{H} | \Psi \rangle = E_\lambda \langle \Phi_m | \Psi \rangle \quad \forall \Phi_m \quad (1.5.9)$$

When the complete expansion of the cluster operator is used, the CC ansatz spans the same space of N-electron determinants as Full Configuration Interaction (FCI). However, full CC is as computationally demanding as FCI, so truncated CC variants, analogues to truncated CI, are frequently used. For example, coupled cluster singles and doubles, CCSD, is the CC analogue of CISD, where only the \hat{T}_1 and \hat{T}_2 cluster operators are included. Triple excitations are also important, but because they are expensive, one often uses perturbation theory to estimate their contribution, leading to the CCSD(T) approximation [35]. Although CCSD(T) is relatively expensive computationally, $\mathcal{O}(m^7)$, it usually has excellent performance for dynamic correlation and is often referred to as the "gold standard" for computational chemistry applications. Conventional excitation-based CC methods are unreliable for systems with strong multireference character (where static correlation effects are predominant) because they rely on a single Slater determinant. Multireference CC methods are an active area of research [36], but are complicated because many of the mathematical features one exploits to make single-reference CC methods computationally efficient are lost when the Hartree-Fock determinant is replaced by a multiconfigurational wavefunction.

1.6 Basic aspects of second quantization

Post-HF methods, including CI-based and CC-based methods, are most conveniently expressed using the notation of second quantization. In second quantization, one introduces operators that create and remove electrons in spin-orbitals; this allows one to directly model processes where the number of electrons changes (e.g., ionization and electron attachment) and to model excitation processes (as ionization followed by electron attachment, or vice versa). We now briefly look at how to express the wavefunction and the Hamiltonian using second quantization [21, 37].

1.6.1 The wavefunction

In the notation of second quantization an N -electron Slater determinant Φ can be represented by an occupation number vector (ON) $|\mathbf{k}\rangle$ with dimensions of the number of spin-orbitals m :

$$\Phi(\mathbf{x}_1, \mathbf{x}_2, \dots, \mathbf{x}_N) = |\mathbf{k}\rangle = |k_1, k_2, \dots, k_m\rangle \quad (1.6.1)$$

where k_i , the occupation number is one if ϕ_i is occupied and zero otherwise. The state with all occupations set to zero is the vacuum state ($|\rangle$). The set of $\binom{m}{N}$ vectors $|\mathbf{k}\rangle$ forms a basis for the N -electron Hilbert space. The set of 2^m occupation vectors is the m -dimensional Fock space. As an illustration, given a basis set with 4 spin-orbitals, an ON for a two electron system where the first two orbitals ϕ_1 and ϕ_2 are occupied is written as:

$$|\mathbf{k}\rangle = |1, 1, 0, 0\rangle \quad (1.6.2)$$

The elementary operators a_p^\dagger and a_p , called the creation and annihilation operators, respectively, are central to this formalism. They add and remove, respectively, an electron from the p th spin-orbital in an ON. For instance, building on our previous example, we can define a new ON with an electron added to ϕ_3 through:

$$a_3^\dagger |\mathbf{k}\rangle = |1, 1, 1, 0\rangle \quad (1.6.3)$$

or destroy the electron in ϕ_2 with:

$$a_2 |\mathbf{k}\rangle = |1, 0, 0, 0\rangle \quad (1.6.4)$$

However, creating an electron on an already occupied spin-orbital or removing it from an empty one, is not permitted, in accordance with Pauli's exclusion principle. These examples are generalized and formally expressed through the following relations:

$$a_p^\dagger |k_1, \dots, 0_p, \dots, k_m\rangle = \prod_{i=1}^{p-1} (-1)^{k_i} |k_1, \dots, 1_p, \dots, k_m\rangle \quad (1.6.5)$$

$$a_p |k_1, \dots, 1_p, \dots, k_m\rangle = \prod_{i=1}^{p-1} (-1)^{k_i} |k_1, \dots, 0_p, \dots, k_m\rangle \quad (1.6.6)$$

$$a_p^\dagger |k_1, \dots, 1_p, \dots, k_m\rangle = 0 \quad (1.6.7)$$

$$a_p |k_1, \dots, 0_p, \dots, k_m\rangle = 0 \quad (1.6.8)$$

In the first Slater determinant on the left-hand-side, Equation (1.6.5), ϕ_p is virtual (i.e. it has zero occupation) while in the second equation it is occupied. The operators act on the immediate orbital on the left of $|\mathbf{k}\rangle$, therefore $(p - 1)$ permutations are necessary to bring k_p to that position. Every permutation changes the sign of the

wavefunction by -1 , reflecting fermionic antisymmetry.

All the key characteristics of the second-quantized operators are encapsulated by the anticommutation relations,

$$\{a_p^\dagger, a_q^\dagger\} = a_p^\dagger a_q^\dagger + a_q^\dagger a_p^\dagger = 0 \quad (1.6.9)$$

$$\{a_p, a_q\} = a_p a_q + a_q a_p = 0 \quad (1.6.10)$$

$$\{a_p^\dagger, a_q\} = a_p^\dagger a_q + a_q a_p^\dagger = \delta_{pq} \quad (1.6.11)$$

The first two of these relations arise from the antisymmetric requirement of the N -electron wavefunction; the third relation uses the orthonormality of the spin-orbitals. The creation and annihilation operators are Hermitian conjugates of each other: a annihilator (creator) acting on the ket (bra) is the creator (annihilator) acting on the bra (ket).

Every quantum-mechanical operator and state can be expressed as a linear combination of concatenated second-quantized operators. For example, Figure 1.1 illustrates the Slater determinants generated by number of particle conserving (excitation) or changing (ionization) operators acting on a reference determinant $|\Phi_0\rangle$ with 4 spatial orbitals, and 2 up-spin and 2 down-spin electrons:

Thus, we can rewrite our multideterminant expression for the FCI model, Eq. (1.5.2), in terms of single, double and up to N th order excitation operator strings as:

$$\begin{aligned} |\Psi\rangle = & c_0 |\Phi_0\rangle + \sum_{i,a} c_{ia} a_a^\dagger a_i |\Phi_0\rangle \\ & + \sum_{i<j,a<b} c_{ij,ab} a_a^\dagger a_b^\dagger a_j a_i |\Phi_0\rangle + \sum_{i<j<k,a<b<c} c_{ijk,abc} a_a^\dagger a_b^\dagger a_c^\dagger a_k a_j a_i |\Phi_0\rangle + \dots \end{aligned} \quad (1.6.12)$$

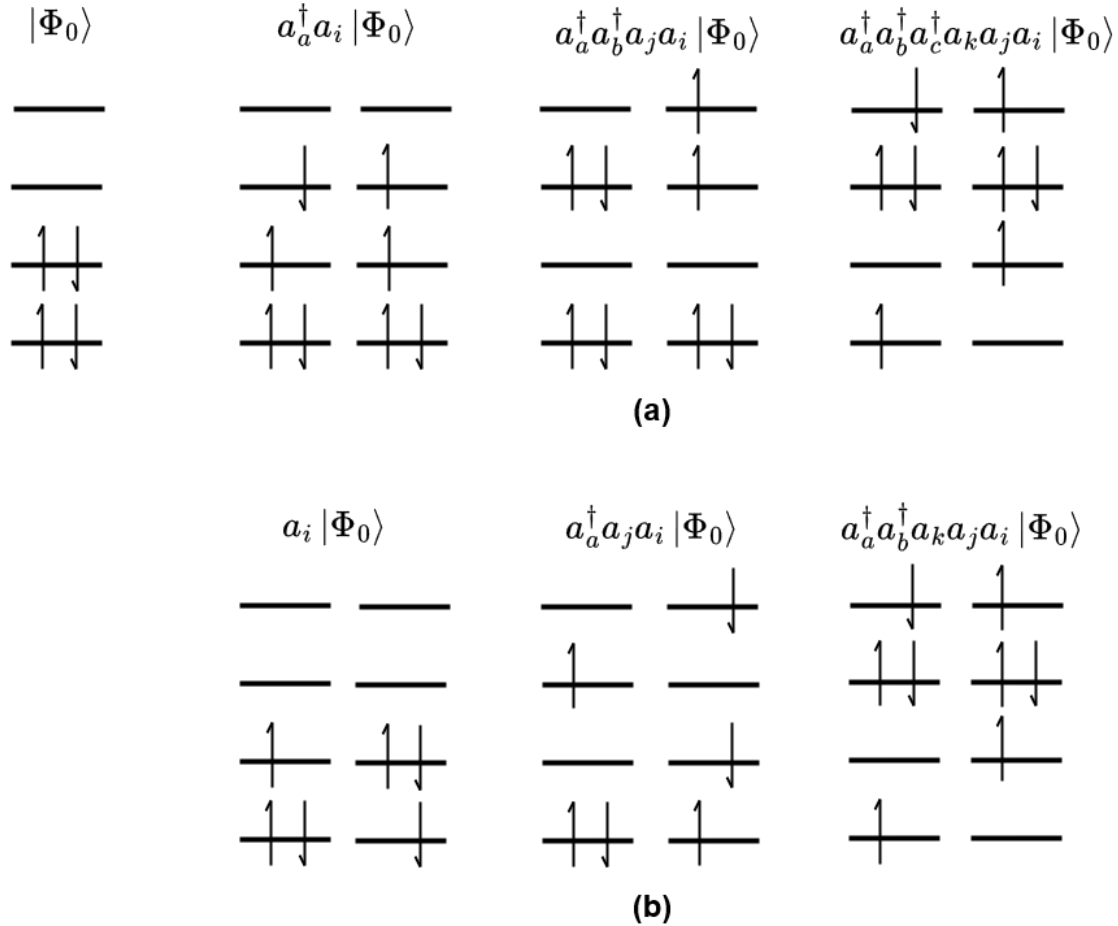


Figure 1.1: Examples of electronic configuration generated from a reference Slater determinant with 4 orbitals, 2 electrons up and 2 down by different excitation operators. (a) Single, double and triple excited configurations. (b) Ionized configurations with single and double excitations.

1.6.2 The Hamiltonian operator

In second quantization, the Hamiltonian operator becomes independent of the number of particles in the system and depends only on the chosen spin-orbital basis set. The sum over the number of electrons in the Hamiltonian (Eq. 1.1.3) is replaced by one over the spin-orbitals, permitting its generalization to cases where the number

of electrons changes. The nonrelativistic time-independent electronic Hamiltonian is then written as:

$$\hat{H} = \sum_{pq}^m h_{pq} a_p^\dagger a_q + \frac{1}{2} \sum_{pqrs}^m g_{pqrs} a_p^\dagger a_q^\dagger a_s a_r \quad (1.6.13)$$

where the matrix elements h_{pq} are the Hamiltonian one-electron interaction terms, integrated over the spatial and spin coordinates \mathbf{x} for each pair of function in the basis set:

$$h_{pq} = \int \phi_p^*(\mathbf{x}) \left(-\frac{\nabla^2}{2} - \sum_A \frac{Z_A}{r_{1A}} \right) \phi_q(\mathbf{x}) d\mathbf{x} \quad (1.6.14)$$

and equivalently for the elements g_{pqrs} , corresponding to the electron-electron repulsion contributions:

$$\begin{aligned} g_{pqrs} &= \int \int \phi_p^*(\mathbf{x}_1) \phi_q^*(\mathbf{x}_2) \frac{1}{r_{12}} \phi_r(\mathbf{x}_1) \phi_s(\mathbf{x}_2) d\mathbf{x}_1 d\mathbf{x}_2 \\ &= \langle pq|rs \rangle \end{aligned} \quad (1.6.15)$$

The notation $g_{pqrs} = \langle pq|rs \rangle$ is called physicists' notation.

Finally, the expectation value of the Hamiltonian operator for a normalized wavefunction can be written as:

$$\begin{aligned} E &= \langle \Psi | \hat{H} | \Psi \rangle \\ &= \sum_{pq}^m h_{pq} \langle \Psi | a_p^\dagger a_q | \Psi \rangle + \frac{1}{2} \sum_{pqrs}^m g_{pqrs} \langle \Psi | a_p^\dagger a_q^\dagger a_s a_r | \Psi \rangle \\ &= \sum_{pq}^m h_{pq} \gamma_{pq} + \frac{1}{2} \sum_{pqrs}^m g_{pqrs} \Gamma_{pqrs} \end{aligned} \quad (1.6.16)$$

In this expression, the matrix elements $\langle \Psi | a_p^\dagger a_q | \Psi \rangle = \gamma_{pq}$ and $\langle \Psi | a_p^\dagger a_q^\dagger a_s a_r | \Psi \rangle = \Gamma_{pqrs}$, correspond to the one- and two-electron reduced density matrices, which are introduced in the next section.

1.7 Density matrices

Because the electronic Hamiltonian depends only on one- and two-electron operators, one doesn't need the full wavefunction to evaluate the energy, just the one- and two-electron reduced density matrices (RDMs). Superficially, this means that one can envision using the RDMs, instead of the wavefunction, as the fundamental descriptor of an electronic system [38]. In density-functional theory (DFT), one uses an even simpler quantity, the ground-state electron density, $\rho(\mathbf{r})$, as the fundamental descriptor. The electron density is the probability of finding an electron in the element of volume $d\mathbf{r}$,

$$\rho(\mathbf{r}) = N \int \Psi^*(\mathbf{x}_1, \mathbf{x}_2, \dots, \mathbf{x}_N) \Psi(\mathbf{x}_1, \mathbf{x}_2, \dots, \mathbf{x}_N) d\sigma_1 d\mathbf{x}_2 \dots d\mathbf{x}_N \quad (1.7.1)$$

DFT is philosophically appealing because the electron density can be measured experimentally and computationally appealing because it only depends on the three spatial coordinate variables, which is much simpler than the wavefunction's dependence on $3N$ spatial and N dichotomic spin variables.

Reduced density matrices generalize the electron density to include additional variables. For example, the one-electron reduced density matrix (1-RDM) in coordinate representation is defined in terms of the N -electron wavefunction by integration over

all but one electron coordinate,

$$\rho(\mathbf{x}_1; \mathbf{x}'_1) = N \int d\mathbf{x}_2 \dots d\mathbf{x}_N \Psi(\mathbf{x}_1, \mathbf{x}_2, \dots, \mathbf{x}_N) \Psi(\mathbf{x}'_1, \mathbf{x}_2, \dots, \mathbf{x}_N)$$

Similarly, the two-electron reduced density matrix (2-RDM) is defined as:

$$\rho(\mathbf{x}_1 \mathbf{x}_2; \mathbf{x}'_1 \mathbf{x}'_2) = N(N-1) \int d\mathbf{x}_3 \dots d\mathbf{x}_N \Psi(\mathbf{x}_1, \mathbf{x}_2, \dots, \mathbf{x}_N) \Psi(\mathbf{x}'_1, \mathbf{x}'_2, \dots, \mathbf{x}_N)$$

Evaluation of the density matrices requires integration over a grid of points or expansion in a basis. If one expands the RDMs in a basis of m one-electron functions $\{\phi_p\}$,

$$\rho(\mathbf{x}; \mathbf{x}') = \sum_{pq}^m \gamma_{pq} \phi_p^*(\mathbf{x}) \phi_q(\mathbf{x}') \quad (1.7.2)$$

$$\rho(\mathbf{x}_1 \mathbf{x}_2; \mathbf{x}'_1 \mathbf{x}'_2) = \sum_{pqrs}^m \Gamma_{pqrs} \phi_p^*(\mathbf{x}_1) \phi_q^*(\mathbf{x}_2) \phi_r(\mathbf{x}'_1) \phi_s(\mathbf{x}'_2) \quad (1.7.3)$$

a compact representation that maps the three-dimensional spatial dependence of the electron density functions into a matrix space is obtained, where γ_{pq} and Γ_{pqrs} denote matrix elements of the 1- and 2-RDMs, respectively (compare Eq. (1.6.16)).

Not every choice of γ_{pq} and Γ_{pqrs} corresponds to an N -electron system; those which do are said to be N -representable. For example, N -representable 1- and 2-RDMs are positive semidefinite [39]. The diagonal elements of the 1-RDM, $w_p = \gamma_{pp}$, are the probabilities, or occupation numbers, for occupying the spin-orbital p and according to the Pauli principle $0 \leq w_p \leq 1$. Therefore, the trace of the 1-RDM is the number

of electrons in the system:

$$N = \text{Tr}(\boldsymbol{\gamma})$$

On the other hand, the diagonals of the 2-RDM, $w_{pq} = \Gamma_{ppqq}$, represent the probability of occupying the pair of orbitals p and q , with values in the interval $0 \leq w_{pq} \leq 1$. Correspondingly, its trace gives the number of unique electron pairs $N(N - 1)$.

If the 2-RDM is known the 1-RDM can be determined by the partial trace,

$$\gamma_{pq} = \frac{1}{(N - 1)} \sum_i \Gamma_{pi,qi}$$

In some instances, working in the eigenbasis for the 1-RDM, known as the natural-spin-orbital (NSO) basis, is convenient. For example, many functions that depend on the 1-RDM, such as the energy, Eq. 1.6.16, have simpler mathematical expressions, CI expansions tend to converge more rapidly, and operators tend to be more sparse. The NSOs are found through a unitary transformation of the 1-RDM:

$$\boldsymbol{\gamma} = \mathbf{U}\mathbf{n}\mathbf{U}^\dagger \tag{1.7.4}$$

where \mathbf{n} is a diagonal matrix containing the eigenvalues of the 1-RDM, called the natural occupation numbers ($0 < n_k < 1$).

1.8 Outline

All of the many-electron wavefunction methods described in the preceding sections can be used to predict excited states properties but their accuracy and computational

cost vary significantly. The more expensive methods generally scale poorly with system size and computationally-tractable variants of single-reference approaches (e.g., excitation-truncated CI and CC methods) fail for strongly-correlated systems. Additionally, numerical convergence of projected methods like coupled cluster for excited states is often poor.

This thesis focuses on alternative wavefunction methodologies for predicting and characterizing excited states in strongly-correlated many-electron systems, with a focus on the development and application of the Equation-of-Motion (EOM) framework. Chapter 2 describes the EOM approach for direct computation of electronic transitions' energies and properties. This versatile method can be combine with any ground-state or excited-state wavefunction method because it relies on the reduced density matrices of a reference state.

Building upon the EOM framework, Chapter 3 introduces the FanEOM method, an extension of our Flexible Ansatz for N-electron Configuration Interaction (FanCI) method for multideterminant wavefunctions to spectroscopic properties. FanCI provides a common framework for wavefunction approaches, including CI and CC, and can be used to derive new wavefunction approximations. Within FanCI the parameters of the wavefunction are optimized through a projected Schrodinger equation which, as already mentioned, can be challenging to converge to excited states. FanEOM can be thought of as a projected EOM equation whereby electronic transitions are obtained using the FanCI ground-state solution as the reference state.

The EOM framework can also be used to improve the accuracy of *ground states* using the extended random phase approximation. Chapter 4 uses the adiabatic connection to add dynamic correlation to multireference wavefunctions, providing an

alternative to traditional MRCI and MRCC approaches. The key idea is to express the correlation energy equation in terms of the perturbation-strength-dependent 2-RDMs, which can be estimated by using excitation-based (particle-hole) or ionization-based (particle-particle/hole-hole) EOM.

The final chapter introduces PyEOM, a Python-based software library developed to facilitate exploration of EOM-based methods for modelling electronic transitions starting from reduced density matrices. We provide an overview of the library’s architecture, functionalities, and user interface. Through a series of examples, we demonstrate PyEOM’s capabilities as a post-processing tool for efficient excited-state prediction and quick prototyping of new EOM-based methods.

References

- [1] Shenzhen Xu and Emily A. Carter. Theoretical insights into heterogeneous (photo)electrochemical co₂ reduction. *Chemical Reviews*, 119(11):6631–6669, 2019. PMID: 30561988.
- [2] Siyuan Fang, Motiar Rahaman, Jaya Bharti, Erwin Reisner, Marc Robert, Geoffrey A. Ozin, and Yun Hang Hu. Photocatalytic co₂ reduction. *Nature Reviews Methods Primers*, 3(1):61, 2023. ISSN 2662-8449.
- [3] Nicholas Cox, Dimitrios A. Pantazis, Frank Neese, and Wolfgang Lubitz. Artificial photosynthesis: understanding water splitting in nature. *Interface Focus*, 5(3):20150009, 2015.
- [4] Ji Wu, Zhonghuan Liu, Xinyu Lin, Enhui Jiang, Shuai Zhang, Pengwei Huo, Yan Yan, Peng Zhou, and Yongsheng Yan. Breaking through water-splitting bottlenecks over carbon nitride with fluorination. *Nature Communications*, 13(1):6999, 2022. ISSN 2041-1723.
- [5] Chi Him A. Tsang, Kai Li, Yuxuan Zeng, Wei Zhao, Tao Zhang, Yujie Zhan, Ruijie Xie, Dennis Y.C. Leung, and Haibao Huang. Titanium oxide based photocatalytic materials development and their role of in the air pollutants

- degradation: Overview and forecast. *Environment International*, 125:200–228, 2019. ISSN 0160-4120.
- [6] Jeroen Hustings, Robin Bonn , Rob Cornelissen, Filippo Morini, Roland Valcke, Koen Vandewal, and Jean V. Manca. Charge-transfer states in photosynthesis and organic solar cells. *Frontiers in Photonics*, 3, 2022. ISSN 2673-6853.
- [7] Juan C. Scaiano. A beginners guide to understanding the mechanisms of photochemical reactions: things you should know if light is one of your reagents. *Chem. Soc. Rev.*, 52:6330–6343, 2023. doi: 10.1039/D3CS00453H. URL <http://dx.doi.org/10.1039/D3CS00453H>.
- [8] Farzaneh Mohamadpour and Ali Mohammad Amani. Photocatalytic systems: reactions, mechanism, and applications. *RSC Adv.*, 14:20609–20645, 2024. doi: 10.1039/D4RA03259D.
- [9] S. Yu. Grebenshchikov, Z.-W. Qu, H. Zhu, and R. Schinke. New theoretical investigations of the photodissociation of ozone in the hartley, huggins, chappuis, and wulf bands. *Phys. Chem. Chem. Phys.*, 9:2044–2064, 2007. doi: 10.1039/B701020F. URL <http://dx.doi.org/10.1039/B701020F>.
- [10] James Doble, Grace Wilson, and Jacob W. Wainman. Kinetic and thermodynamic analysis of the adsorption of methylene blue onto biochar. *Journal of Chemical Education*, 100(10):4040–4046, 2023.
- [11] Laura M. Hancock, David J. McGarvey, and Daniela Plana. An investigation of the temperature dependence of a monomer–dimer equilibrium using uv–vis and 1h nmr spectroscopies. *Journal of Chemical Education*, 100(3):1283–1288, 2023.

- [12] Luis Serrano-Andrés and Juan José Serrano-Pérez. *Calculation of Excited States: Molecular Photophysics and Photochemistry on Display*, pages 1–88. Springer Netherlands, Dordrecht, 2016. ISBN 978-94-007-6169-8. doi: 10.1007/978-94-007-6169-8_14-2. URL https://doi.org/10.1007/978-94-007-6169-8_14-2.
- [13] James B. Foresman, Martin Head-Gordon, John A. Pople, and Michael J. Frisch. Toward a systematic molecular orbital theory for excited states. *The Journal of Physical Chemistry*, 96:135–149, 1 1992. ISSN 0022-3654.
- [14] Andreas Dreuw and Martin Head-Gordon. Single-reference ab initio methods for the calculation of excited states of large molecules. *Chemical Reviews*, 105:4009–4037, 11 2005. ISSN 0009-2665.
- [15] T Daniel Crawford and Henry F Schaefer III. *An Introduction to Coupled Cluster Theory for Computational Chemists*, pages 33–136. John Wiley & Sons, Ltd, 2007. ISBN 9780470125915.
- [16] Dmitry I. Lyakh, Monika Musiał, Victor F. Lotrich, and Rodney J. Bartlett. Multireference nature of chemistry: The coupled-cluster view. *Chemical Reviews*, 112(1):182–243, 2012. PMID: 22220988.
- [17] Daniel Roca-Sanjuán, Francesco Aquilante, and Roland Lindh. Multiconfiguration second-order perturbation theory approach to strong electron correlation in chemistry and photochemistry. *WIREs Computational Molecular Science*, 2(4):585–603, 2012.
- [18] Hans Lischka, Dana Nachtigallová, Adélia J. A. Aquino, Péter G. Szalay, Felix

- Plasser, Francisco B C Machado, and Mario Barbatti. Multireference approaches for excited states of molecules. *Chemical Reviews*, 118:7293–7361, 8 2018. ISSN 0009-2665.
- [19] Pierre-François Loos, Anthony Scemama, and Denis Jacquemin. The quest for highly accurate excitation energies: A computational perspective. *The Journal of Physical Chemistry Letters*, 11:2374–2383, 3 2020. ISSN 1948-7185.
- [20] I.N. Levine. *Quantum Chemistry*. Pearson advanced chemistry series. Pearson, 2014. ISBN 9780321890603. URL <https://books.google.ca/books?id=ht6jMQEACAAJ>.
- [21] Attila Szabo and Neil S Ostlund. *Modern Quantum Chemistry: Introduction to Advanced Electronic Structure Theory*. Courier Corporation, 2012.
- [22] F. Jensen. *Introduction to Computational Chemistry*. Wiley, 2007. ISBN 9780470058046. URL <https://books.google.ca/books?id=RDIG48UcZfYC>.
- [23] I. Shavitt and R.J. Bartlett. *Many-Body Methods in Chemistry and Physics: MBPT and Coupled-Cluster Theory*. Cambridge Molecular Science. Cambridge University Press, 2009. ISBN 9780521818322. URL <https://books.google.ca/books?id=SWw6ac1NHZYC>.
- [24] Hans-Joachim Werner and Peter J. Knowles. An efficient internally contracted multiconfiguration reference configuration interaction method. *The Journal of Chemical Physics*, 89(9):5803–5814, 11 1988. ISSN 0021-9606.
- [25] Felix Plasser and Hans Lischka. *Multi-Reference Configuration Interaction*, chapter 9, pages 277–297. John Wiley & Sons, Ltd, 2020. ISBN 9781119417774.

- [26] Bogumil Jeziorski and Hendrik J. Monkhorst. Coupled-cluster method for multideterminantal reference states. *Phys. Rev. A*, 24:1668–1681, Oct 1981.
- [27] Robert J. Buenker and Sigrid D. Peyerimhoff. Individualized configuration selection in ci calculations with subsequent energy extrapolation. *Theoretica chimica acta*, 35(1):33–58, 1974. ISSN 1432-2234.
- [28] Laimutis Bytautas, Thomas M. Henderson, Carlos A. Jimenez-Hoyos, Jason K. Ellis, and Gustavo E. Scuseria. Seniority and orbital symmetry as tools for establishing a full configuration interaction hierarchy. *The Journal of Chemical Physics*, 135(4):044119, 07 2011. ISSN 0021-9606.
- [29] Diego R. Alcoba, Alicia Torre, Luis Lain, Gustavo E. Massaccesi, and Ofelia B. OÃ±a. Configuration interaction wave functions: A seniority number approach. *The Journal of Chemical Physics*, 140(23):234103, 06 2014. ISSN 0021-9606.
- [30] Peter A Limacher, Taewon D Kim, Paul W Ayers, Paul A Johnson, Stijn De Baerdemacker, Dimitri Van Neck, and Patrick Bultinck. The influence of orbital rotation on the energy of closed-shell wavefunctions, 2013.
- [31] B. Huron, J. P. Malrieu, and P. Rancurel. Iterative perturbation calculations of ground and excited state energies from multiconfigurational zeroth-order wavefunctions. *The Journal of Chemical Physics*, 58(12):5745–5759, 06 1973. ISSN 0021-9606.
- [32] James SM Anderson, Farnaz Heidar-Zadeh, and Paul W Ayers. Breaking the curse of dimension for the electronic schrödinger equation with functional analysis. *Computational and Theoretical Chemistry*, 1142:66–77, 2018.

- [33] Adam A. Holmes, Norm M. Tubman, and C. J. Umrigar. Heat-bath configuration interaction: An efficient selected configuration interaction algorithm inspired by heat-bath sampling. *Journal of Chemical Theory and Computation*, 12:3674–3680, 8 2016. ISSN 1549-9618.
- [34] John A. Pople, J. Stephen Binkley, and Rolf Seeger. Theoretical models incorporating electron correlation. *International Journal of Quantum Chemistry*, 10(S10):1–19, 1976.
- [35] Krishnan Raghavachari, Gary W. Trucks, John A. Pople, and Martin Head-Gordon. A fifth-order perturbation comparison of electron correlation theories. *Chemical Physics Letters*, 157(6):479–483, 1989. ISSN 0009-2614.
- [36] Dmitry I. Lyakh, Victor F. Lotrich, and Rodney J. Bartlett. The ‘tailored’ ccsd(t) description of the automerization of cyclobutadiene. *Chemical Physics Letters*, 501:166–171, 1 2011. ISSN 00092614.
- [37] Trygve Helgaker, Poul Jørgensen, and Jeppe Olsen. *Molecular Electronic-Structure Theory*. John Wiley & Sons, 2013.
- [38] David A Mazziotti. Two-electron reduced density matrix as the basic variable in many-electron quantum chemistry and physics. *Chemical Reviews*, 112:244–262, 2012. PMID: 21863900.
- [39] Caitlin Lanssens, Paul W. Ayers, Dimitri Van Neck, Stijn De Baerdemacker, Klaas Gunst, and Patrick Bultinck. Method for making 2-electron response reduced density matrices approximately n-representable. *Journal of Chemical Physics*, 148, 7 2017.

Chapter 2

Equation-of-motion approach

2.1 Introduction

Modern electronic structure methods are able to describe the behavior of molecular ground states with impressive accuracy [1–4]. For example, coupled cluster singles doubles and perturbative triplets (CCSD(T)) [5] is regarded as the gold-standard for achieving chemical accuracy, with results typically within 1 kcal/mol (0.04 eV) from the experimental data. On the other hand, the study of excited states remains a challenge, in part due to the diverse nature of these states (valence, Rydberg, charge transfer, radical, etc.).

In principle, any wavefunction-based electronic structure method has the potential to evaluate excitation energies by solving the Schrödinger equation for two stationary states of interest. For example, to obtain the energy associated to an electronic excitation, it is necessary to compute the corresponding wavefunctions (Ψ_0^N , Ψ_λ^N) and energies (E_0^N , E_λ^N) of the involved states. The energy of the transition then corresponds to the energy difference between the states $\Delta E_\lambda = E_\lambda^N - E_0^N$. In practice,

it can be difficult to converge variational methods to the targeted excited state, especially if it has the same symmetry as the ground state [6–8]. On the other hand, with projected approaches, like coupled cluster methods (CC), it can be challenging to find higher-energy roots of the CC equations or to assign these roots to a given state [9, 10]. In addition, many methods (such as selected CI approaches) often provide an unbalanced treatment of electron correlation in the ground- and excited-states, leading to systematic errors in excitation energies.

One alternative is to directly compute transition energies using the equation-of-motion approximation to excited states (EOM), an approach formulated by Rowe in the 1960s [11]. EOM methods compute ΔE directly by defining a transition operator that transforms a reference N -electron stationary (ground) state Ψ_0^N into the neutral or charged excited state $\Psi_\lambda^{N\pm k}$, where $k \geq 0$. Like the Full Configuration Interaction (FCI) or Coupled Cluster (CC) wavefunction models, EOM is exact when the transition operator is complete and the reference state is exact.

Several approximations to EOM for molecular spectroscopic applications have been derived [12–16]. The simplest approaches rely on the Hartree-Fock solution as the ground state reference and a few-electron description of the transition operator. For instance, choosing the electronic excitation operator to be described by a one-electron excitations (i.e., the particle-hole operator) results in the particle-hole random phase approximation, which is identical to time-dependent Hartree-Fock if the reference wavefunction is the Hartree-Fock ground state. Approaches that go beyond the single Slater determinant description have been devised both for electronic excitations, electron attachment, and electron removal [12, 13, 17]. However, these latter formulations rely on a self-consistent iterative process for the optimization of the excited state

wavefunction, which can be challenging to converge and computationally expensive. Other popular approaches use a CC wavefunction model as the reference ground state and find the transition energies diagonalizing a similarity transformed Hamiltonian in a basis of excited configurations [16, 18–21]. The EOM-CC hierarchy of methods, and related linear response CC methods [22], have been very successful in the description of electronically excited and open-shell species within a single reference formalism. However, it is known that conventional CC approaches struggle with multireference systems whereas more sophisticated CC formulations [23, 24], suitable for strong correlation, are generally not black-box approaches and result computationally demanding.

Alternatively, a framework based on reduced density matrices (RDMs) can be employed. By expanding the transition operator in a suitable basis set of few-electron transition operators, the EOM working equations can be written in terms of the reference state RDMs. The transition energies and associated wavefunction parameters can then be determined by matrix diagonalization, similar to configuration interaction methods. This EOM approach presents two distinct advantages: it reduces the computational costs to that of the matrix diagonalization and, by combining it with multideterminant wavefunction approaches, it is applicable to strongly-correlated system.

Employing EOM within the context of reduced density matrices is not new. In fact, it has been previously used to derive the particle-hole extended Random Phase Approximation (ERPA) [25] and the extended Koopman’s Theorem (EKT) [26, 27]. Here we focus on efficient formulations that require at most the ground state two-electron reduced density matrix (2-RDM) to evaluate the transition energies. We extend previous studies by exploring the most common, and simplest, approximations

to the transition operator, and analyzing the performance of different (in principle equivalent) formulations for the working equations. In addition to well established approximations, such as the two aforementioned ones, alternative equations to compute ionization potentials (IPs), electron affinities (EAs), and double ionization potentials (DIPs) are explored.

In the subsequent Section 2.2, the theoretical framework of EOM is presented. From this background, in Section 2.3, an overview of the traditional working equations for the processes of ionization, electron excitation, and double ionization (DIPs) is provided and alternative expressions are proposed. The transition energies computed from the described methods are then compared in Section 2.5.

It is important to note that this chapter does not attempt to offer a comprehensive review of the EOM approaches. Instead, it focuses on the development and application of EOM techniques for excitation energies that can be formulated using the 1- and 2-electron reduced density matrices. Moreover, the relationship between the EOM formulations and the closely related linear response or Green’s function approaches is not discussed. Readers interested in the broader connections to these theoretical approaches are encouraged to consult the relevant literature [28–32].

2.2 General Equation-of-Motion (EOM) formalism

The equation-of-motion (EOM) approach is a general approach for directly computing energy differences in quantum mechanics. The basic idea is to introduce a transition operator, $(\hat{Q}_\lambda^{\pm\kappa})^\dagger$, which generates the λ -th excited state of the system with $N \pm \kappa$ ($\kappa \geq 0$) electrons, $\Psi_\lambda^{N\pm\kappa}$, starting from a reference N -electron stationary state (usually

the ground state):

$$|\Psi_\lambda^{N\pm\kappa}\rangle = (\hat{Q}_\lambda^{\pm\kappa})^\dagger |\Psi_0^N\rangle \quad (2.2.1)$$

The Schrödinger equation for the final (post-transition) wavefunction is

$$\hat{H} |\Psi_\lambda^{N\pm\kappa}\rangle = \hat{H} (\hat{Q}_\lambda^{\pm\kappa})^\dagger |\Psi_0^N\rangle = E_\lambda (\hat{Q}_\lambda^{\pm\kappa})^\dagger |\Psi_0^N\rangle \quad (2.2.2)$$

where \hat{H} is the time-independent non-relativistic electronic Hamiltonian operator, which can be written in second quantization as

$$\hat{H} = \sum_{pq} h_{pq} a_p^\dagger a_q + \frac{1}{2} \sum_{pqrs} \langle pq|rs\rangle a_p^\dagger a_q^\dagger a_s a_r \quad (2.2.3)$$

Here h_{pq} and $\langle pq|rs\rangle$ are the one- and two-electron integrals, a_p^\dagger (a_p) are the creation (annihilation) operators that add (remove) an electron from the p th spin orbital, and the labels p, q, r, s denote arbitrary spin-orbitals.

Traditional excited state methods solve Eq. 2.2.2 separately from the corresponding equation for the ground state:

$$\hat{H} |\Psi_0^N\rangle = E_0 |\Psi_0^N\rangle \quad (2.2.4)$$

and then explicitly compute the energy difference between the states ($\Delta E_\lambda = E_\lambda - E_0$). The EOM approach directly computes the transition energy ΔE_λ by multiplying Eq. 2.2.4 by $(\hat{Q}_\lambda^{\pm\kappa})^\dagger$ on the left, and subtracting it from Eq. 2.2.2:

$$\begin{aligned} \hat{H} (\hat{Q}_\lambda^{\pm\kappa})^\dagger |\Psi_0^N\rangle - (\hat{Q}_\lambda^{\pm\kappa})^\dagger \hat{H} |\Psi_0^N\rangle &= (E_\lambda - E_0) (\hat{Q}_\lambda^{\pm\kappa})^\dagger |\Psi_0^N\rangle \\ \left[\hat{H}, (\hat{Q}_\lambda^{\pm\kappa})^\dagger \right] |\Psi_0^N\rangle &= \Delta E_\lambda (\hat{Q}_\lambda^{\pm\kappa})^\dagger |\Psi_0^N\rangle \end{aligned} \quad (2.2.5)$$

Since Ψ_0^N is an eigenstate of the Hamiltonian and E_0 its expectation value, this shifts the spectrum of the Hamiltonian.

Equation 2.2.5 has the advantage that $[\hat{H}, (\hat{Q}_\lambda^{\pm\kappa})^\dagger]$ is a simpler operator (i.e., it has fewer creation/annihilation operators) than $\hat{H}(\hat{Q}_\lambda^{\pm\kappa})^\dagger$, hence reducing the computational cost. For example, $[a_p^\dagger a_q^\dagger a_s a_r, a_t^\dagger a_u]$, the commutator between the two-electron operator, $a_p^\dagger a_q^\dagger a_s a_r$, and a one-orbital excitation, $a_t^\dagger a_u$, is a two-electron, rather than a three-electron operator. Moreover, by directly evaluating energy differences, one may benefit from systematic cancellation of errors due, for example, to the incompleteness of the spin-orbital basis set.

2.2.1 The transition operator

Eq. (2.2.1) implies that $(\hat{Q}_\lambda^{\pm\kappa})^\dagger$ can be exactly written as:

$$(\hat{Q}_\lambda^{\pm\kappa})^\dagger = |\Psi_\lambda^{N\pm\kappa}\rangle \langle \Psi_0^N| \quad (2.2.6)$$

The complex conjugate of this operator satisfies the *killer condition*:

$$\hat{Q}_\lambda^{\pm\kappa} |\Psi_0^N\rangle = |\Psi_0^N\rangle \langle \Psi_\lambda^{N\pm\kappa} | \Psi_0^N\rangle = 0 \quad (2.2.7)$$

Many problems with EOM formulations arise because the killer condition is sometimes invoked even when it is not always satisfied [25, 33]. When the killer condition is satisfied, it guarantees that the excited states generated by the transition operator will be orthogonal to the reference state.

Although expression Eq. (2.2.6) for the transition operator is an elegant mathematical derivation, it is impractical for electronic structure calculations because it requires

foreknowledge of the exact excited states $\Psi_\lambda^{N\pm\kappa}$. In practice, $(\hat{Q}_\lambda^{\pm\kappa})^\dagger$ is expanded in a suitable basis constructed from strings of second-quantized operators, which is then truncated in practical computations. For example, one can exactly model any electronic excitation with:

$$(\hat{Q}_\lambda^0)^\dagger = \sum_{pq} c_{pq} a_p^\dagger a_q + \sum_{pqrs} c_{pqrs} a_p^\dagger a_q^\dagger a_s a_r + \sum_{pqrst} c_{pqrst} a_p^\dagger a_q^\dagger a_r^\dagger a_u a_t a_s + \dots \quad (2.2.8)$$

were single ($a_p^\dagger a_q$), double ($a_p^\dagger a_q^\dagger a_s a_r$), triple ($a_p^\dagger a_q^\dagger a_r^\dagger a_u a_t a_s$), ... and N th order electron excitation operators are included. The indexes p, q, r, s, u, t in the summations run over all spin-orbitals. This expansion is almost always truncated, so it is convenient to write $(\hat{Q}_\lambda^{\pm\kappa})^\dagger$ in a general notation,

$$(\hat{Q}_\lambda^{\pm\kappa})^\dagger = \sum_n c_{n;\lambda} \hat{q}_n^\dagger \quad (2.2.9)$$

where \hat{q}_n^\dagger denotes a general element in the basis set expansion and $c_{n;\lambda}$ denotes its coefficient.

2.2.2 Derivation of the EOM equations

Inserting Eq. (2.2.9) for $(\hat{Q}_\lambda^{\pm\kappa})^\dagger$ into Eq. (2.2.5), we get an eigenvalue problem with the form:

$$\left[\hat{H}, \sum_n c_{n;\lambda} \hat{q}_n^\dagger \right] |\Psi_0^N\rangle = \Delta E_\lambda \sum_n c_{n;\lambda} \hat{q}_n^\dagger |\Psi_0^N\rangle \quad (2.2.10)$$

To find the transition energies and excited states that satisfy this equation, we express it as a matrix eigenvalue problem by left-multiplying by a set of arbitrary states

$\langle \Psi_0^N | \hat{R}$:

$$\sum_n \langle \Psi_0^N | \hat{R} [\hat{H}, \hat{q}_n^\dagger] | \Psi_0^N \rangle c_{n;\lambda} = \Delta E_\lambda \sum_n \langle \Psi_0^N | \hat{R} \hat{q}_n^\dagger | \Psi_0^N \rangle c_{n;\lambda} \quad (2.2.11)$$

Usually, it is convenient to use the states $\langle \Psi_0^N | \hat{q}_m$ generated by the basis elements which expand the transition operator $(\hat{Q}_\lambda^{\pm\kappa})^\dagger$ for this step in the derivation. This choice is especially convenient because the resulting equations require only the reduced density matrices (RDMs) of the reference state. This leads to the basic form of the equation-of-motion:

$$\sum_n \langle \Psi_0^N | \hat{q}_m [\hat{H}, \hat{q}_n^\dagger] | \Psi_0^N \rangle c_{n;\lambda} = \Delta E_\lambda \sum_n \langle \Psi_0^N | \hat{q}_m \hat{q}_n^\dagger | \Psi_0^N \rangle c_{n;\lambda} \quad \forall m \quad (2.2.12)$$

corresponding to a generalized eigenvalue problem (GEVP). Moreover, if the reference state Ψ_0^N is an eigenfunction of the Hamiltonian, this formulation is equivalent to the variational procedure. In this case, the computed transition energy will be an upper bound to the exact one.

Further progress can be made using the killer condition Eq. (2.2.7), which implies that the following terms are zero:

$$\langle \Psi_0^N | \sum_n c_{n;\lambda} \hat{q}_n^\dagger = \langle \Psi_0^N | \hat{H} \sum_n c_{n;\lambda} \hat{q}_n^\dagger = 0 \quad (2.2.13)$$

These conditions are valid if the $(\hat{Q}_\lambda^{\pm\kappa})^\dagger$ is expanded in a complete basis set, but we cannot guarantee that they are satisfied when the expansion is truncated. Nonetheless, they are often invoked because they can lead to simpler EOM expressions. For example, the killer conditions allow one to add or subtract a term that is nominally

zero from the left-hand-side of equation Eq. (5.4.3):

$$\begin{aligned} & \left\langle \Psi_0^N \left| \hat{q}_m \left[\hat{H}, \sum_n c_{n;\lambda} \hat{q}_n^\dagger \right] \pm \left[\hat{H}, \sum_n c_{n;\lambda} \hat{q}_n^\dagger \right] \hat{q}_m \right| \Psi_0^N \right\rangle \\ &= \sum_n \left\langle \Psi_0^N \left| \left[\hat{q}_m, \left[\hat{H}, \hat{q}_n^\dagger \right] \right]_{\pm} \right| \Psi_0^N \right\rangle c_{n;\lambda} = \Delta E_\lambda \sum_n \langle \Psi_0^N | \hat{q}_m \hat{q}_n^\dagger | \Psi_0^N \rangle c_{n;\lambda} \end{aligned} \quad (2.2.14)$$

or from both the left-hand and right-hand sides, giving:

$$\sum_n \left\langle \Psi_0^N \left| \left[\hat{q}_m, \left[\hat{H}, \hat{q}_n^\dagger \right] \right]_{\pm} \right| \Psi_0^N \right\rangle c_{n;\lambda} = \Delta E_\lambda \sum_n \left\langle \Psi_0^N \left| \left[\hat{q}_m, \hat{q}_n^\dagger \right]_{\pm} \right| \Psi_0^N \right\rangle c_{n;\lambda} \quad (2.2.15)$$

Although both of these expressions are valid when the killer condition holds, usually one applies the killer condition to both sides of the basic EOM equation.

By inserting the killer condition in different ways, one has four (equivalent) formulations of EOM. If one subtracts using the killer condition on the left, or on both sides, one obtains commutators:

$$\sum_n \left\langle \Psi_0^N \left| \left[\hat{q}_m, \left[\hat{H}, \hat{q}_n^\dagger \right] \right] \right| \Psi_0^N \right\rangle c_{n;\lambda} = \Delta E_\lambda \sum_n \langle \Psi_0^N | \hat{q}_m \hat{q}_n^\dagger | \Psi_0^N \rangle c_{n;\lambda} \quad (2.2.16)$$

and

$$\sum_n \left\langle \Psi_0^N \left| \left[\hat{q}_m, \left[\hat{H}, \hat{q}_n^\dagger \right] \right] \right| \Psi_0^N \right\rangle c_{n;\lambda} = \Delta E_\lambda \sum_n \langle \Psi_0^N | \left[\hat{q}_m, \hat{q}_n^\dagger \right] | \Psi_0^N \rangle c_{n;\lambda} \quad (2.2.17)$$

respectively. Alternatively, if one adds the killer condition on the left or on both sides, one obtains anticommutators:

$$\sum_n \left\langle \Psi_0^N \left| \left[\hat{q}_m, \left[\hat{H}, \hat{q}_n^\dagger \right] \right]_{+} \right| \Psi_0^N \right\rangle c_{n;\lambda} = \Delta E_\lambda \sum_n \langle \Psi_0^N | \hat{q}_m \hat{q}_n^\dagger | \Psi_0^N \rangle c_{n;\lambda} \quad (2.2.18)$$

and

$$\sum_n \left\langle \Psi_0^N \left| \left[\hat{q}_m, \left[\hat{H}, \hat{q}_n^\dagger \right] \right]_+ \right| \Psi_0^N \right\rangle c_{n;\lambda} = \Delta E_\lambda \sum_n \left\langle \Psi_0^N \left| \left[\hat{q}_m, \hat{q}_n^\dagger \right]_+ \right| \Psi_0^N \right\rangle c_{n;\lambda} \quad (2.2.19)$$

respectively. Introducing higher-order (anti)commutators is beneficial because it reduces order of the fermionic operators, hence the order of the RDMs that are needed to evaluate the terms in the equations above, and therefore the computational cost. Which formulation is used, anticommutator or double commutator, depends on the transition operator $(\hat{Q}_\lambda^{\pm\kappa})^\dagger$. Generally the expression that gives the operators with lower particle rank is chosen, so anticommutators are preferred when the number of creation and annihilation operators in the transition operator is odd (i.e., when describing removal/attachment of an odd number of electrons). The double commutator expression is preferred when the transition operator has an even number of creation and annihilation operators, like the one-body excitation operator considered earlier, $a_p^\dagger a_q$.

There is yet another, rarely used, form of EOM, where the outermost commutator, rather than the innermost, involves the transition operator [14, 34]:

$$\begin{aligned} & \left\langle \Psi_0^N \left| \left[q_m, \hat{H} \right] \sum_n c_{n;\lambda} \hat{q}_n^\dagger \right| \Psi_0^N \right\rangle - \left\langle \Psi_0^N \left| \sum_n c_{n;\lambda} \hat{q}_n^\dagger \left[q_m, \hat{H} \right] \right| \Psi_0^N \right\rangle = \\ & \left\langle \Psi_0^N \left| \left[\left[q_m, \hat{H} \right], \sum_n c_{n;\lambda} \hat{q}_n^\dagger \right] \right| \Psi_0^N \right\rangle = \Delta E_\lambda \sum_n \left\langle \Psi_0^N \left| \hat{q}_m \hat{q}_n^\dagger \right| \Psi_0^N \right\rangle c_{n;\lambda} \end{aligned} \quad (2.2.20)$$

This means that we can also write the equations:

$$\sum_n \left\langle \Psi_0^N \left| \left[[q_m, \hat{H}], \hat{q}_n^\dagger \right] \right| \Psi_0^N \right\rangle c_{n;\lambda} = \Delta E_\lambda \sum_n \left\langle \Psi_0^N \left| q_m q_n^\dagger \right| \Psi_0^N \right\rangle c_{n;\lambda} \quad (2.2.21)$$

$$\sum_n \left\langle \Psi_0^N \left| \left[[q_m, \hat{H}], \hat{q}_n^\dagger \right] \right| \Psi_0^N \right\rangle c_{n;\lambda} = \Delta E_\lambda \sum_n \left\langle \Psi_0^N \left| [q_m, q_n^\dagger] \right| \Psi_0^N \right\rangle c_{n;\lambda} \quad (2.2.22)$$

Adding these equations to the previous commutator-based eigenvalue equations, Eqs. (5.4.5) and (2.2.17), gives a more symmetric eigenproblem, namely:

$$\sum_n \left\langle \Psi_0^N \left| \frac{1}{2} [q_m, [\hat{H}, \hat{q}_n^\dagger]] + \frac{1}{2} [[q_m, \hat{H}], q_n^\dagger] \right| \Psi_0^N \right\rangle c_{n;\lambda} = \Delta E_\lambda \sum_n \left\langle \Psi_0^N \left| q_m q_n^\dagger \right| \Psi_0^N \right\rangle c_{n;\lambda} \quad (2.2.23)$$

and:

$$\sum_n \left\langle \Psi_0^N \left| \frac{1}{2} [q_m, [\hat{H}, \hat{q}_n^\dagger]] + \frac{1}{2} [[q_m, \hat{H}], q_n^\dagger] \right| \Psi_0^N \right\rangle c_{n;\lambda} = \Delta E_\lambda \sum_n \left\langle \Psi_0^N \left| [q_m, q_n^\dagger] \right| \Psi_0^N \right\rangle c_{n;\lambda} \quad (2.2.24)$$

Notice that all of the EOM formulations considered, Eqs. (5.4.3) and (5.4.5) - (2.2.24), are subsumed by the following generalized matrix eigenproblem,

$$\mathbf{AC}_\lambda = \Delta E_\lambda \mathbf{MC}_\lambda \quad (2.2.25)$$

Taking Eq. 2.2.17 as an example, the elements of the left-hand-side (LHS) and right-hand-side (RHS) matrices, \mathbf{A} and \mathbf{M} , are defined as:

$$A_{mn} = \langle \Psi_0^N | [\hat{q}_m, [\hat{H}, \hat{q}_n^\dagger]] | \Psi_0^N \rangle \quad (2.2.26)$$

$$M_{mn} = \langle \Psi_0^N | [\hat{q}_m, \hat{q}_n^\dagger] | \Psi_0^N \rangle \quad (2.2.27)$$

2.3 EOM approximations

All the EOM expressions presented, Eqs. (5.4.3) and (5.4.5) to (2.2.24), are equivalent and produce exact solutions for the excited states, $\Psi_\lambda^{N\pm\kappa}$ and excitation energies, when one uses a complete basis for the transition operator and the reference wavefunction is exact. However, turning these equations into practical methods for computation of spectroscopic properties of molecular systems requires introducing approximations. There are two main approximations used in applications of EOM methods, namely:

- (a) Truncation of the transition operator expansion, Eq. (2.2.9).
- (b) The selection of the wavefunction approximation to describe the reference state Ψ_0^N (for instance choosing a single Slater determinant like Hartree-Fock (HF) or a multideterminant method).

Our emphasis is on truncating the transition-operator expansion so that the EOM equations can be solved in terms of the one- and two-electron reduced density matrices (RDMs) of the reference state Ψ_0^N ,

$$\gamma_{pq} = \langle \Psi_0^N | a_p^\dagger a_q | \Psi_0^N \rangle \quad (2.3.1)$$

$$\Gamma_{pqrs} = \langle \Psi_0^N | a_p^\dagger a_q^\dagger a_s a_r | \Psi_0^N \rangle \quad (2.3.2)$$

The resulting methods are applicable to any electronic structure method for which the 1-RDM and 2-RDM are available.

Table 2.1: Approximations to the transition operator $(\hat{Q}_\lambda^{\pm\kappa})^\dagger$

Operator	Process
$\hat{Q}_\lambda^{-1} = \sum_p c_p a_p$	Ionization
$\hat{Q}_\lambda^{+1} = \sum_p c_p a_p^\dagger$	Electron addition
$\hat{Q}_\lambda^0 = \sum_{pq} c_{pq} a_p^\dagger a_q$	Electron excitation
$\hat{Q}_\lambda^{-2} = \sum_p c_{pq} a_p a_q$	Double ionization
$\hat{Q}_\lambda^{+2} = \sum_p c_{pq} a_p^\dagger a_q^\dagger$	Double electron addition

For this condition to be met, the most common approximate $(\hat{Q}_\lambda^{\pm\kappa})^\dagger$ choices correspond to truncating the linear expansion in Eq. (2.2.9) so that no more than two creation or annihilation operators are present in the transition operator, as indicated in table 2.1. From top to bottom these operators model the processes of single-electron removal, \hat{Q}_λ^{-1} , single-electron attachment, \hat{Q}_λ^{+1} , electron excitation, \hat{Q}_λ^0 , double-electron removal, \hat{Q}_λ^{-2} , and double-electron attachment \hat{Q}_λ^{+2} . The following sections present the working EOM equations for these electronic transitions.

2.3.1 Ionization potentials and electron affinities

Describing electron removal and attachment requires, at the simplest level, only a single electron annihilation or creation operator. The associated ionization and attachment processes are relevant to photoelectron spectroscopy, understanding charge-transfer and redox processes, and acid/base chemistry [35–37].

The wavefunction for an $N - 1$ electron system, $|\Psi_\lambda^{N-1}\rangle$, can be generated from the ground state $|\Psi_0^N\rangle$ considering the simplest form of the operator $(\hat{Q}_\lambda^{\pm\kappa})^\dagger$, Eq. (2.2.9),

expanded in a basis of one-electron annihilation operators, $\hat{q}_n^\dagger = a_n$:

$$\hat{Q}_\lambda^{-1} = \sum_p c_{p;\lambda} a_p \quad (2.3.3)$$

where $\kappa = -1$. The associated vertical ionization potential is the transition energy, $\Delta E_n^{N-1} = E_n^{N-1} - E_0^N$, and \hat{Q}_λ^{-1} determines the spin-orbital from which the electron should be removed in the ground state, $|\Psi_0^N\rangle$, to produce the $N - 1$ electron system's wavefunction.

With this form of the ionization operator all EOM equations, Eqs. (5.4.3) and (5.4.5) to (2.2.24), can be evaluated using the 1-RDM and 2-RDM. Here three representative cases of these equations are analyzed.

Extended Koopman's Theorem (EKT)

The EKT is the generalization of the Koopman's theorem (relating ionization potentials to Hartree-Fock occupied molecular orbital energies) to correlated wavefunction methods allowing computation of ionization energies from any level of theory [38–41]. Its applications encompass highly accurate and cost effective predictions of ionization energies of atomic and molecular systems [42–45] as well as computation of chemical reactivity descriptors (such as chemical potential and chemical hardness) [46, 47].

EKT can be derived from EOM substituting Eq. (2.3.3) into the basic equation of motion Eq. (5.4.3) to give the system of linear equations:

$$\sum_n \langle \Psi_0^N | a_m^\dagger [\hat{H}, a_n] | \Psi_0^N \rangle c_{n;\lambda} = \Delta E_\lambda^{N-1} \sum_n \langle \Psi_0^N | a_m^\dagger a_n | \Psi_0^N \rangle c_{n;\lambda}; \forall m \quad (2.3.4)$$

where the set of ionized configurations $\langle \Psi_0^N | a_m^\dagger$ are projected on the left-hand-side.

Solving Eq. (2.3.4) produces the approximated wavefunctions of the $N - 1$ electron system and the corresponding ionization energies ΔE_λ^{N-1} .

The matrix elements on the right-hand-side of above equation, here on denoted M_{mn} , correspond to the 1-RDMs:

$$M_{mn} = \langle \Psi_0^N | a_m^\dagger a_n | \Psi_0^N \rangle = \gamma_{mn} \quad (2.3.5)$$

whereas those on the left-hand-side, labeled as A_{mn} , are associated to the generalized Fock matrix (or the orbital Lagrangian) and are given by:

$$\begin{aligned} A_{mn} &= \langle \Psi_0^N | a_m^\dagger [\hat{H}, a_n] | \Psi_0^N \rangle \\ &= - \sum_q h_{nq} \gamma_{mq} - \frac{1}{2} \sum_{qrs} \langle nq || rs \rangle \Gamma_{mqr s} \end{aligned} \quad (2.3.6)$$

where the notation $\langle pq || rs \rangle$ denotes the antisymmetrized two-electron integrals. This formula for the elements A_{mn} as a function of the RDMs can be derived inserting the definition of the Hamiltonian operator, Eq. (2.2.3), and applying the fundamental anticommutation properties:

$$\begin{aligned} a_p^\dagger a_q + a_q a_p^\dagger &= \delta_{pq} \\ a_p^\dagger a_q^\dagger + a_q^\dagger a_p^\dagger &= 0 \\ a_p a_q + a_q a_p &= 0 \end{aligned} \quad (2.3.7)$$

to arrange all creation operators a_p^\dagger to the left of the annihilators a_p (i.e., place the operators in normal order).

An analogous EKT equation for the process of electron attachment:

$$\Delta E_n^{N+1} = E_n^{N+1} - E_0^N \quad (2.3.8)$$

can be derived considering the $N + 1$ electron wavefunction, Ψ_λ^{N+1} , produced from Ψ_0^N by a one-electron addition operator defined as a linear combination of creation operators a_p^\dagger :

$$\hat{Q}_\lambda^{+1} = \sum_p c_{p;\lambda} a_p^\dagger \quad (2.3.9)$$

This corresponding matrix elements that result from Eq. (5.4.3) are:

$$A_{mn} = \langle \Psi_0^N | a_m [\hat{H}, a_n^\dagger] | \Psi_0^N \rangle \quad (2.3.10)$$

$$M_{mn} = \langle \Psi_0^N | a_m a_n^\dagger | \Psi_0^N \rangle \quad (2.3.11)$$

The explicit expressions for these matrices are given in the Appendix [39, 48].

The matrices \mathbf{A} and \mathbf{M} in EKT can be built in principle from any post-Hartree-Fock method that provides the 1- and 2-RDMs. However, the orbital Lagrangian \mathbf{A} is only Hermitian (guaranteeing physical solutions) for those wavefunction approximations which are eigenfunctions of the Hamiltonian operator. This potentially limits the application of EKT to variational methods like configuration interaction or multiconfiguration approaches although the extensions to other (non-variational) correlated approaches have been developed [39, 40].

Ionization potential from anticommutator (IPa)

For certain correlated wavefunction approaches, such as the coupled cluster method, obtaining the 2-RDMs needed in EKT left-hand-side matrix Eq. (2.3.6) is challenging. This difficulty arises because these methods generally produce 2-RDMs that do not correspond to physical N -electron wavefunctions, meaning they are not N -representable [49]. In cases like these, taking the ionization operator \hat{Q}_λ^{-1} , as defined in Eq. 2.3.3, together with the anticommutator form of EOM, Eq. (2.2.19), may be preferable:

$$\sum_n \left\langle \Psi_0^N \left| \left[a_m^\dagger, \left[\hat{H}, a_n \right] \right]_+ \right| \Psi_0^N \right\rangle c_{n;\lambda} = \Delta E_\lambda^{N-1} \sum_n \left\langle \Psi_0^N \left| \left[a_m^\dagger, a_n \right]_+ \right| \Psi_0^N \right\rangle c_{n;\lambda}; \forall m \quad (2.3.12)$$

given that the alternative orbital Lagrangian matrix terms:

$$\begin{aligned} A_{mn} &= \left\langle \Psi_0^N \left| \left[a_m^\dagger, \left[\hat{H}, a_n \right] \right]_+ \right| \Psi_0^N \right\rangle \\ &= \left\langle \Psi_0^N \left| a_m^\dagger \left[\hat{H}, a_n \right] \right| \Psi_0^N \right\rangle + \left\langle \Psi_0^N \left| \left[\hat{H}, a_n \right] a_m^\dagger \right| \Psi_0^N \right\rangle \end{aligned} \quad (2.3.13)$$

and metric matrix M_{mn} :

$$M_{mn} = \left\langle \Psi_0^N \left| \left[a_m^\dagger, a_n \right]_+ \right| \Psi_0^N \right\rangle \quad (2.3.14)$$

only depend on the 1-RDM of the reference state Ψ_0^N .

This reduction in the order of the RDMs can be understood considering that due to the anticommutation properties (Eq. 2.3.7) the operators defining the matrices \mathbf{A} and \mathbf{M} above have one less creation and annihilation operator than the corresponding operators $a_m^\dagger \left[\hat{H}, a_n \right]$ and $a_p^\dagger a_q$ in the EKT matrices (Eqs. (2.3.6) and (2.3.5), respectively).

This EOM method will be referred to as IPa.

The explicit expressions for the LHS and RHS matrix elements in the anticommutator EOM, Eq. (2.3.12), read:

$$A_{mn} = -(h_{nm} + \sum_{qr} \langle nq || mr \rangle \gamma_{qr}) \quad (2.3.15)$$

$$M_{mn} = \delta_{mn} \quad (2.3.16)$$

where the metric matrix is simply the identity matrix, and A_{mn} is an effective one body operator. Solving the eigenvalue equation (2.3.12) produces two sets of solutions from a single computation. Positive eigenvalues, $\Delta E_\lambda > 0$, correspond to the ionization energies (ΔE_λ^{N-1}), whereas negative eigenvalues $\Delta E_\lambda < 0$ are the electron affinities (ΔE_λ^{N+1}). The respective $(N-1)$ and $(N+1)$ -electron wavefunctions and the spectroscopic intensities of the associated electron-removal and electron-attachment processes can be deduced from the eigenvectors.

The origin of the two sets of solutions in the IPa eigenvalue equation can be understood considering that the anticommutator matrix \mathbf{A} for the process of ionization differs by a minus sign from the complementary matrix for the process of adding one electron to the ground state, $\langle \Psi_0^N | [a_n, [\hat{H}, a_m^\dagger]]_+ | \Psi_0^N \rangle$. This relationship is expressed in the following anticommutator identity:

$$\langle \Psi_0^N | [a_m^\dagger, [\hat{H}, a_n]]_+ | \Psi_0^N \rangle = - \langle \Psi_0^N | [a_n, [\hat{H}, a_m^\dagger]]_+ | \Psi_0^N \rangle + \langle \Psi_0^N | [\hat{H}, [a_m^\dagger, a_n]]_+ | \Psi_0^N \rangle \quad (2.3.17)$$

The second term on the right-hand side of this equation corresponds to the commutator between the Hamiltonian operator and a one-body operator. This term vanishes if

the ground state wavefunction is invariant under orbital rotations.

Ionization potential with double commutator (IPc)

Another variant of EOM that simultaneously yields ionization energies and electron affinities arises from the commutator form of EOM, Eq. (2.2.17):

$$\sum_n \langle \Psi_0^N | [a_m^\dagger, [\hat{H}, a_n]] | \Psi_0^N \rangle c_{n;\lambda} = \Delta E_\lambda^{N-1} \sum_n \langle \Psi_0^N | [a_m^\dagger, a_n] | \Psi_0^N \rangle c_{n;\lambda}; \forall m \quad (2.3.18)$$

This approach will be labeled as IPc method, denoting the form of the EOM equation used.

In this case the formula for the elements on the LHS of the eigenvalue equation, A_{mn} , is

$$\begin{aligned} A_{mn} &= \langle \Psi_0^{(N)} | [a_m^\dagger, [\hat{H}, a_n]] | \Psi_0^{(N)} \rangle \\ &= -2 \sum_q h_{nq} \gamma_{mq} - \sum_{qrs} \langle nq || rs \rangle \Gamma_{mqr s} + h_{nm} + \sum_{qs} \langle nq || ms \rangle \gamma_{qs} \end{aligned} \quad (2.3.19)$$

and the metric matrix on the RHS, M_{mn} , is

$$M_{mn} = \langle \Psi_0^{(N)} | [a_m^\dagger, a_n] | \Psi_0^{(N)} \rangle = 2\gamma_{mn} - \delta_{nm} \quad (2.3.20)$$

Both expressions essentially represent a linear combination between the corresponding matrix terms in the EKT and IPa formulas (compare, for example, the matrix \mathbf{M} above with the ones from EKT and IPa, Eqs. (2.3.5) and (2.3.16), respectively).

Solving the eigenvalue problem, Eq. (2.3.18), determined by the matrices \mathbf{A} and \mathbf{M} as defined above, produces two set of solutions; positive eigenvalues corresponding

to the ionization energies, ΔE_λ^{N-1} , and transitions with negative sign corresponding to the electron affinities, ΔE_λ^{N+1} , with corresponding $(N-1)$ and $(N+1)$ -electron wavefunction approximations in each case.

In summary, this subsection described three EOM-based approaches, namely EKT, IPa and IPc methods, to compute ionization energies from the low-order density matrices of an N -electron ground state, Ψ_0^N . These approximations for ionized wavefunctions have a low computational scaling corresponding to the cost of the matrix diagonalization step in the solutions of the eigenvalue equations in their matrix form, Eq. (2.2.25). The cost is at most M^3 , determined by the number of spin-orbitals (M). To our knowledge, the alternative approximations, Eqs. (2.3.12) and (2.3.18), have not been studied numerically.

Notice that when the reference wavefunction, Ψ_0^N , is the Hartree-Fock ground state, the anticommutator (IPa; Eq. 2.3.12) and commutator EOM (IPc; Eq. 2.3.18) equations produce the same ionization spectrum as EKT, which reduces to the conventional Koopmans' theorem (KT).

We conclude this section by discussing the orthogonality of the approximate $(N-1)$ electron wavefunctions obtained by solving these equations. Orthogonality of the ionized states leads to the condition

$$\langle \Psi_\lambda^{(N-1)} | \Psi_\nu^{(N-1)} \rangle = \delta_{\lambda\nu} \quad (2.3.21)$$

which can be enforced after completing the calculations by requiring that the states are orthogonal with the specified metric, i.e., $\mathbf{C}_\lambda^T \mathbf{M} \mathbf{C}_\nu = \delta_{\lambda\nu}$.

2.3.2 Excitation energies

The EOM formulation can also be used to estimate vertical excitations and their associated energies, $\Delta E_\lambda^N = E_\lambda^N - E_0^N$, based on low-order density matrices of a correlated wavefunction method. The simplest approximation to an N -electron excited state wavefunction based on the EOM ansatz:

$$|\Psi_\lambda^N\rangle = \hat{Q}_\lambda^0 |\Psi_0^N\rangle \quad (2.3.22)$$

corresponds to an excitation operator, $(\hat{Q}_\lambda^{\pm\kappa})^\dagger = \hat{Q}_\lambda^0$, expressed as a linear combination of one-electron excitation operators (or particle-hole operators, $\hat{q}_n^\dagger = a_p^\dagger a_q$):

$$\hat{Q}_\lambda^0 = \sum_{pq} c_{pq,\lambda} a_p^\dagger a_q \quad (2.3.23)$$

where the indices p and q label arbitrary spin-orbitals and n is a multi-index. This approximation is most suitable for excited states dominated by single electron excitations.

Extended random phase approximation (particle-hole ERPA)

Taking the truncated excitation operator Eq. 2.3.23 with the commutator form of the EOM, Eq. (2.2.17), leads to the particle-hole extended random phase approximation method (ph-ERPA) of Chatterjee and Pernal [25]:

$$\sum_{ij} \langle \Psi_0^N | [a_k^\dagger a_l, [\hat{H}, a_i^\dagger a_j]] | \Psi_0^N \rangle c_{ij;\lambda} = \Delta E_\lambda^N \sum_{ij} \langle \Psi_0^N | [a_k^\dagger a_l, a_i^\dagger a_j] | \Psi_0^N \rangle c_{ij;\lambda} \quad \forall k, l \quad (2.3.24)$$

The solutions to this equation provide the excitation energies, ΔE_λ^N , and the optimized coefficients, $c_{pq;\lambda}$, that parameterize the excited state wavefunction, Ψ_λ^N .

The term on the RHS of Eq. (2.3.24) are elements of a metric matrix,

$$M_{kl,ji} = \left\langle \Psi_0^N \left| \left[a_k^\dagger a_l, a_i^\dagger a_j \right] \right| \Psi_0^N \right\rangle = \gamma_{kj} \delta_{li} - \delta_{kj} \gamma_{li} \quad (2.3.25)$$

and the double commutator terms on the LHS gives the transition-energy operator $A_{kl,ji}$ (also known as the orbital Hessian), with elements:

$$\begin{aligned} A_{kl,ji} &= \left\langle \Psi_0^N \left| \left[a_k^\dagger a_l, \left[\hat{H}, a_i^\dagger a_j \right] \right] \right| \Psi_0^N \right\rangle \\ &= h_{li} \gamma_{kj} + h_{jk} \gamma_{il} - \delta_{li} \sum_q h_{jq} \gamma_{kq} + \delta_{jk} \sum_q h_{qi} \gamma_{ql} \\ &+ \sum_{qs} \langle lq || is \rangle \Gamma_{kqjs} + \sum_{qs} \langle jq || ks \rangle \Gamma_{iqsl} \\ &+ \frac{1}{2} \sum_{rs} \langle jl || rs \rangle \Gamma_{kirs} + \frac{1}{2} \sum_{pq} \langle pq || ik \rangle \Gamma_{pqlj} \\ &+ \frac{1}{2} \delta_{li} \sum_{rsq} \langle qj || rs \rangle \Gamma_{kqrs} + \frac{1}{2} \delta_{jk} \sum_{pqs} \langle pq || si \rangle \Gamma_{pqsl} \end{aligned} \quad (2.3.26)$$

where the terms $\langle pq || rs \rangle$ are the anti-symmetrized two-electron integrals in physicist's notation. With the matrices \mathbf{A} and \mathbf{M} written in this form, they can be evaluated using any correlated electronic structure method for which the 1- and 2-RDMs are available.

The non-zero matrix elements in \mathbf{A} correspond to Hamiltonian terms between two singly-excited states like $\left\langle \Psi_0^N \left| a_k^\dagger a_l \hat{H} a_i^\dagger a_j \right| \Psi_0^N \right\rangle$, and off-diagonal elements corresponding to the coupling between the ground state and a doubly-excited configuration described as two one-electron excitations, $\left\langle \Psi_0^N \left| \hat{H} a_k^\dagger a_l a_i^\dagger a_j \right| \Psi_0^N \right\rangle$ expressed in terms of two single

excitations. (While we find it beneficial to discuss single- and double-excitations, we caution the reader that when the reference state is strongly multi-reference, this terminology can be misleading.)

A characteristic of the ph-ERPA method, (2.3.24), is that it produces (mirror) opposite sign solutions; excitation energies and excited states correspond to the positive eigenvalues ($\Delta E_\lambda > 0$, C_λ); the corresponding negative eigenvalues and their eigenvectors are traditionally interpreted as de-excitations ($\Delta E_\lambda < 0$, $C_{-\lambda}$). This feature of ERPA arises because the commutators impose the following symmetries on the left- and right-hand-side matrices:

$$A_{kl,ji} = A_{lk,ij} \quad (2.3.27)$$

$$M_{kl,ji} = -M_{lk,ij} \quad (2.3.28)$$

It can also be loosely understood considering the basis set of the transition operator, Eq. (2.3.23), as composed of single excitation elements $a_p^\dagger a_q$ that take an electron from q th occupied spin-orbital to the p th virtual one, and corresponding de-excitation terms $a_q^\dagger a_p$.

Particle-hole ERPA eigenvectors fulfill a normalization condition through the metric matrix: $\mathbf{C}_\lambda^T \mathbf{M} \mathbf{C}_\nu = \pm \delta_{\lambda\nu}$, which is positive if the states correspond to excitations and negative for the inverse process.

Particle-hole ERPA has been applied to describe excited state properties of atomic and molecular systems, including those with a strong multiconfigurational character, employing various methods for approximating the ground-state RDMs [25, 50, 51]. Even the simpler method, particle-hole RPA, to which ERPA reduces when the 1- and 2-RDMs originate from Hartree-Fock, was already successfully applied in the 60s

for the prediction of atomic and molecular electronic absorption energies [52–54].

Extended Tamm-Dancoff approximation (particle-hole ETDA)

Although the EOM equation with the killer condition applied to both sides is the traditional form used to obtain approximated excited states, taking equation (5.4.5) (without commutator on the right-hand-side term) also leads to a formulation that only requires the reference state’s 1- and 2-RDMs. The significant change relative to ph-ERPA, Eq. 2.3.24, is the definition of the metric matrix which now depends also on the 2-RDM:

$$M_{kl,ji} = \left\langle \Psi_0^N \left| a_k^\dagger a_l a_i^\dagger a_j \right| \Psi_0^N \right\rangle = \gamma_{kj} \delta_{li} - \Gamma_{kijl} \quad (2.3.29)$$

As a result, only positive energies (excitations), $\Delta E_\lambda > 0$, appear in the solutions of the corresponding eigenvalue problem. Based on this resemblance of this approach to the Tamm-Dancoff approximation to excited states [55, 56] which decouples the excitation and de-excitation processes in RPA, we will refer to this approach as extended Tamm-Dancoff approximation (particle-hole ETDA).

It is worth pointing out that because the matrix \mathbf{A} present in the ph-ERPA and ETDA methods corresponds to the orbital Hessian (this is, the second derivative of the ground state energy relative to the orbital rotations), both approaches are sensitive to instabilities in the reference ground state wavefunction, Ψ_0^N . This can be diagnosed by the presence of negative eigenvalues in the spectrum of the matrix \mathbf{A} , indicating that there is another solution with lower energy than the current state. In practice, this means that one should use spin-(un)restricted excitation operators in ph-ERPA or ETDA if the underlying wavefunction used spin-(un)restricted orbitals.

In terms of computational scaling, both ph-ERPA and ETDA methods scale as the

sixth power of the spin-orbital basis set size. Moreover, for closed-shell systems (which have an even number of electrons, each pair sharing the same spatial component of a spin-orbital) one can use spin-adapted implementations to reduce the cost to the sixth power of the spatial-orbital basis set size, attaining a nominal 2^6 -fold speedup.

2.3.3 Double ionization potentials and double electron affinities

The wavefunction for a doubly-ionized system, Ψ_λ^{N-2} , can be generated from the N -electron ground state Ψ_0^N applying a transition operator, \hat{Q}_λ^{-2} , defined in terms of a basis set of operators that remove two-electrons from the reference wavefunction, $q_\lambda = a_p a_q$ (or hole-hole operator):

$$\hat{Q}_\lambda^{-2} = \sum_{pq} c_{pq,\lambda} a_p a_q \quad (2.3.30)$$

Here the sum runs over all spin-orbitals p, q and the coefficient c_{pq} determines the weight of a given $(N - 2)$ -electron configuration generated from Ψ_0^N . One can think of this approximation as finding the best electron pair, or geminal, to remove from an N -electron wavefunction.

The double ionized wavefunction parameters $c_{pq;\lambda}$ and the corresponding double ionization potentials (DIPs) $\Delta E_\lambda^{N-2} = E_\lambda^{N-2} - E_0^N$ can be determined solving the eigenvalue equation:

$$\sum_{ij} \langle \Psi_0^N | a_k^\dagger a_l^\dagger [\hat{H}, a_i a_j] | \Psi_0^N \rangle c_{ij;\lambda} = \Delta E_\lambda^{N-2} \sum_{ij} \langle \Psi_0^N | a_k^\dagger a_l^\dagger a_i a_j | \Psi_0^N \rangle c_{ij;\lambda}; \quad \forall k, l \quad (2.3.31)$$

that results from inserting the operator \hat{Q}_λ^{-2} , Eq. (2.3.30), into the fundamental EOM

equation, Eq. (5.4.3). Here the projection space is given by the $(N - 2)$ -electron configurations $\langle \Psi_0^N | a_p^\dagger a_q^\dagger$. This set of equations corresponds to the extension of EKT to double ionization energies. Therefore, for a variational approximations to the ground state wavefunction Ψ_0^N , the lowest double ionization energy obtained from the solutions to this equation would correspond to an upper bound to the exact result.

However, evaluating the matrix elements $\langle \Psi_0^N | a_k^\dagger a_l^\dagger [\hat{H}, a_i a_j] | \Psi_0^N \rangle$ would require the 3-electron reduced density matrices. Therefore, to reduce the order of the density matrices needed in the EOM formulation, the double commutator expression of the EOM, Eq. (2.2.17), is taken instead, giving the system of equations:

$$\sum_{ij} \langle \Psi_0^N | [a_k^\dagger a_l^\dagger, [\hat{H}, a_i a_j]] | \Psi_0^N \rangle c_{ij;\lambda} = \Delta E_\lambda \sum_{ij} \langle \Psi_0^N | [a_k^\dagger a_l^\dagger, a_i a_j] | \Psi_0^N \rangle c_{ij;\lambda}; \forall k, l \quad (2.3.32)$$

By using the fundamental anticommutation properties of the creation and annihilation operators, it can be shown that the LHS term in above's equation, labeled as $A_{kl,ji}$,

can be expressed as follows:

$$\begin{aligned}
A_{kl,ji} &= \left\langle \Psi_0^N \left| \left[a_k^\dagger a_l^\dagger, \left[\hat{H}, a_i a_j \right] \right] \right| \Psi_0^N \right\rangle \\
&= 2h_{ik}\gamma_{lj} - 2h_{il}\gamma_{kj} - 2h_{jl}\delta_{ik} + 2h_{jk}\delta_{il} + 2\delta_{ik} \sum_q h_{jq}\gamma_{lq} - 2\delta_{il} \sum_q h_{jq}\gamma_{kq} \\
&+ \langle ji||kl \rangle + \sum_r \langle ji||lr \rangle \gamma_{kr} - \sum_r \langle ji||kr \rangle \gamma_{lr} + 2 \sum_q \langle qj||kl \rangle \gamma_{qi} \\
&+ 2\delta_{lj} \sum_{qr} \langle iq||rk \rangle \gamma_{qr} + 2\delta_{kj} \sum_{qr} \langle iq||lr \rangle \gamma_{qr} \\
&+ 2 \sum_{qr} \langle jq||rk \rangle \Gamma_{qlri} + 2 \sum_{qr} \langle jq||lr \rangle \Gamma_{qkri} \\
&+ \delta_{ki} \sum_{qrs} \langle qj||rs \rangle \Gamma_{qlrs} - \delta_{li} \sum_{qrs} \langle qj||rs \rangle \Gamma_{qkrs}
\end{aligned} \tag{2.3.33}$$

and those of the RHS, $M_{kl,ji}$, are given by:

$$\begin{aligned}
M_{kl,ji} &= \left\langle \Psi_0^N \left| \left[a_k^\dagger a_l^\dagger, a_i a_j \right] \right| \Psi_0^N \right\rangle \\
&= \delta_{ik}\delta_{jl} - \delta_{il}\delta_{jk} - \delta_{ik}\gamma_{lj} + \delta_{il}\gamma_{kj} - \delta_{jl}\gamma_{ki} + \delta_{jk}\gamma_{li}
\end{aligned} \tag{2.3.34}$$

are determined from the 1- and 2-RDMs of the ground state.

Solving the eigenvalue equation, Eq. (4.4.10), produces two sets of eigenvalue/eigenvector pairs. The DIPs and approximated $(N - 2)$ -electron states from the positive side of the spectrum ($\Delta E_\lambda > 0, C_\lambda$), and the double electron affinities (DEAs) and $(N + 2)$ -electron states from the negative side of the spectrum ($\Delta E_\lambda < 0, C_{-\lambda}$). This is a result of the introduction of an extra commutator in the derivation of the EOM. The

nested commutator matrix \mathbf{A} and the metric matrix \mathbf{M} satisfy the relations:

$$\begin{aligned} \langle \Psi_0^N | [a_k^\dagger a_l^\dagger, [\hat{H}, a_i a_j]] | \Psi_0^N \rangle &= \langle \Psi_0^N | [a_i a_j, [\hat{H}, a_k^\dagger a_l^\dagger]] | \Psi_0^N \rangle + \langle \Psi_0^N | [\hat{H}, [a_k^\dagger a_l^\dagger, a_i a_j]] | \Psi_0^N \rangle \\ \langle \Psi_0^N | [a_k^\dagger a_l^\dagger, a_i a_j] | \Psi_0^N \rangle &= - \langle \Psi_0^N | [a_i a_j, a_k^\dagger a_l^\dagger] | \Psi_0^N \rangle \end{aligned} \quad (2.3.35)$$

where the first term on the right-hand-side of the double commutator identity can be identified as the LHS matrix for the process of adding two electrons to Ψ_0^N and there is a minus sign associated with its corresponding metric matrix $\langle \Psi_0^N | [a_i a_j, a_k^\dagger a_l^\dagger] | \Psi_0^N \rangle$. The additional term $\langle \Psi_0^N | [\hat{H}, [a_k^\dagger a_l^\dagger, a_i a_j]] | \Psi_0^N \rangle$ in the first line of the equation above, will take the form of a commutator between the Hamiltonian and a one-electron operator, and therefore it will vanish for ground states given by wavefunction models that are invariant to orbital rotations. These commutator identities lead to the two sets of eigenvalues in the solution of Eq. 4.4.10.

Furthermore, analyzing the non-zero elements in the matrix \mathbf{A} would show that they correspond to Hamiltonian elements between two $(N-2)$ -electron configurations like $\langle \Psi_0^N | a_k^\dagger a_l^\dagger \hat{H} a_i a_j | \Psi_0^N \rangle$, or two $(N+2)$ -electron configurations, $\langle \Psi_0^N | a_i a_j \hat{H} a_k^\dagger a_l^\dagger | \Psi_0^N \rangle$, and off-diagonal couplings terms between the ground state and a double excited configurations like $\langle \Psi_0^N | \hat{H} a_i a_j a_k^\dagger a_l^\dagger | \Psi_0^N \rangle$. Correspondingly, the metric matrix \mathbf{M} has overlaps between double ionized configurations $\langle \Psi_0^N | a_k^\dagger a_l^\dagger a_i a_j | \Psi_0^N \rangle$ and with opposite sign those for two-electron added configurations $-\langle \Psi_0^N | a_i a_j a_k^\dagger a_l^\dagger | \Psi_0^N \rangle$.

When the ground state is approximated by the Hartree-Fock ground state, equation is the particle-particle RPA method [57]. Therefore, following the naming convention in the work by Chatterjee and Pernal, we label the EOM method that produces double ionization energies from correlated 2-RDMs as the hole-hole extended random phase approximation (hh-ERPA).

Another EOM approach for the double ionization process that would only require the 2-RDMs from the ground state corresponds to taking Eq. (5.4.5), which does not have a commutator on the right-hand side:

$$\sum_{ij} \left\langle \Psi_0^N \left| \left[a_k^\dagger a_l^\dagger, \left[\hat{H}, a_i a_j \right] \right] \right| \Psi_0^N \right\rangle c_{ij;\lambda} = \Delta E_\lambda \sum_{ij} \left\langle \Psi_0^N \left| a_k^\dagger a_l^\dagger a_i a_j \right| \Psi_0^N \right\rangle c_{ij;\lambda}; \forall m \quad (2.3.36)$$

The difference with the hh-ERPA expression, Eq. (4.4.10), is simply the use of the 2-RDM from the reference state Ψ_0^N as the metric, $M_{kl,ji}$. Due to this modification, this method only produces the double ionization energies and corresponding approximated wavefunctions for the $(N-2)$ -electron states. Following our naming convention in the previous section, this EOM variant will be labeled hole-hole extended Tamm-Dancoff approximation (hh-ETDA).

In terms of computational cost, the general formulations of hh-ERPA and hh-ETDA have formally the same scaling as ph-ERPA, depending on the sixth power of the orbital basis set size.

Taking the complex-conjugate of the hole-hole operator, Eq. (2.3.30), gives the transition operator for the process of adding two electrons to the ground state, the particle-particle operator:

$$\hat{Q}_\lambda^{+2} = \sum_{pq} c_{pq;\lambda} a_p^\dagger a_q^\dagger \quad (2.3.37)$$

which gives an approximate wavefunction for Ψ_λ^{N+2} . Taking this operator with the commutator equation Eq. (2.2.17) would lead to corresponding eigenvalue equation

to compute the double electron affinities:

$$\Delta E_n^{(N+2)} = E_n^{(N+2)} - E_0^N \quad (2.3.38)$$

This equation is equivalent to the hh-ERPA one, differing by only a minus sign.

Weitao Yang’s group has applied the pp-RPA formulation to compute improved neutral excitations energies starting from the double ionized states, $(N - 2)$ states [58, 59]. Their approach is based on rewriting the excitation energies ($\Delta E_n^N = E_n^N - E_0^N$) in terms of differences between the values of successive double electron affinities: $E_n^N - E_0^N = (E_n^N - E_0^{N-2}) - (E_0^N - E_0^{N-2})$. This technique allowed the description of excitations with double-excitation character that are typically missed by ph-RPA approaches. Furthermore, it was argued that this method provides a more balanced treatment of electronic correlation effects given that both the ground and its excited states are described at the same level. However, the accuracy of pp-RPA to compute double ionizations of molecules has been less explored and little, if anything, is known about the performance of the hh-ERPA and hh-ETDA methods introduced here.

2.4 Transition densities

Transition density (matrices) between the N -electron reference state and the (excited) state generated by an electronic transition are defined by

$$\langle \Psi_0^N | q_m^\dagger | \Psi_\lambda^{N\pm\kappa} \rangle \quad (2.4.1)$$

For the single electron removal (or attachment) EOM approaches, the transition matrix between the ionized state $\Psi_\lambda^{(N-1)}$ and the ground state Ψ_0^N , can be expressed as follows:

$$\langle \Psi_\lambda^{(N-1)} | a_p | \Psi_0^N \rangle = \langle \Psi_0^N | (\hat{Q}^{-1})_\lambda^\dagger a_p | \Psi_0^N \rangle \approx \sum_n c_{n;\lambda} \langle \Psi_0^N | a_p^\dagger a_q | \Psi_0^N \rangle$$

where the coefficients correspond to the eigenvectors of the approximated $(N - 1)$ -electron wavefunction, Eq. (2.3.22). With these transition matrices, the generalized overlap amplitudes (GOAs) or Feynman-Dyson amplitudes [44, 60, 61] can be approximated. GOAs, defined as:

$$g_\lambda = N^{1/2} \langle \Psi_\lambda^{(N-1)} | \hat{\mathbf{r}} | \Psi_0^N \rangle \quad (2.4.2)$$

where the integration runs over the coordinates of $N - 1$ -electrons. The GOAs arise, for example, when modelling the intensities of transitions observed in photoelectron spectroscopy [62, 63]. Unless the N -electron wavefunction is a Slater determinant, the GOAs are not the same as the molecular orbitals. However, as evaluated from EKT (or analogous EOM variants) they provide a similar one-electron description useful for interpretation of molecular structure and bonding. This is especially valuable for correlated electronic structure methods where the orbital picture is otherwise obscure.

For electron excitations, the oscillator strength, f_λ ,

$$f_\lambda = \frac{2}{3} (E_\lambda^N - E_0^N) | \langle \Psi_0^N | \hat{\mathbf{r}} | \Psi_\lambda^N \rangle |^2 \quad (2.4.3)$$

arises when evaluating the intensity of transitions observed in electronic absorption/emission spectroscopy. The oscillator strengths are conveniently constructed from the one-electron transition density matrices between the ground and excited states $\langle \Psi_0^N | a_p^\dagger a_q | \Psi_\lambda^N \rangle$.

These density matrices can be approximated from the eigenvectors produced by the particle-hole ERPA method (or ETDA), expressed as:

$$\langle \Psi_0^N | a_p^\dagger a_q | \Psi_\lambda^N \rangle \approx \sum_{rs} c_{rs;\lambda} \langle \Psi_0^N | [a_p^\dagger a_q, a_s^\dagger a_r] | \Psi_0^N \rangle \quad (2.4.4)$$

An alternative approximation to the oscillator strength can be derived in terms of the pairing transition density matrices $\langle \Psi_0^N | a_p^\dagger a_q^\dagger | \Psi_\lambda^{N-2} \rangle$ obtained from the particle-particle/hole-hole RPA solutions [58].

Additionally, the transition densities, together with the excitation energies, can be used to estimate the linear response function and, through it, molecular polarizability. For example, the one-electron density response function has the matrix elements

$$\chi_{pqrs} = \sum_{\lambda>0} \frac{\langle \Psi_0^N | a_p^\dagger a_q | \Psi_\lambda^{(N)} \rangle \langle \Psi_\lambda^{(N)} | a_r^\dagger a_s | \Psi_0^N \rangle}{E_0 - E_\lambda} + c.c. \quad (2.4.5)$$

where the numerator is determined by the product of the transition density matrices, and the denominator depends on the excitation energies.

2.5 Numerical illustrations

In this section the performance of the preceding EOM formulations for ionization, electron excitation, and double electron ionization are compared. To do so, a test set of second-row atoms (He, Be, C, Ne) and small molecules (NNO, NNNH, HCNO, HCNNH, H₂CNCH, HF, CO, N₂) were selected. The molecules NNO, NNNH, HCNO, HCNNH, H₂CNCH are an isoelectronic series of 22-electron 1,3-dipolar molecules that are important in cycloaddition reactions; we chose these molecules because dipolar

molecules often have both zwitterionic and diradical character, which is a chemical manifestation of nonnegligible multireference character.

The results presented for the more established approaches EKT (Eq. 2.3.4) and ph-ERPA (Eq. 2.3.24) as well as the variants IPa (Eq. 2.3.12), IPc (Eq. 2.3.12), ph-ETDA, hh-ERPA (Eq. 4.4.10) and hh-ETDA were generated using our in-house implementation of these approaches. The 1- and 2-RDMs were generated using Hartree-Fock (HF) and Heat-bath Configuration Interaction (HCI) [64] calculations, with the aug-cc-pVDZ basis set [65]. For the Hartree-Fock calculations, the PySCF electronic structure package was employed [66, 67]; we used our package PyCI [68] to obtain the correlated wavefunction and RDMs from HCI, with $\epsilon_1 = 10^{-4}$. The geometries of the molecules in the 22-electron series were optimized at the UwB97XD/def2-SVP level of theory. The geometries of the diatomic molecules were taken from the literature [39].

Our procedure to obtain the transition energies (electron excitation and ionization potentials) from the 2-RDMs is described next. For a given molecular geometry, and basis set:

1. Solve the Hartree-Fock equations to build the molecular Hamiltonian (described in terms of the one- and two-electron integrals h_{pq} and $\langle pq|rs\rangle$, respectively).
2. Use Heat-Bath Configuration Interaction problem with $\epsilon_1 = 10^{-4}$ (and no perturbative correction) for the neutral N -electron ground state using to obtain the 1- and 2-RDMs.
3. From the Hamiltonian terms and the density matrices (both expressed in the spin-orbital basis), evaluate the left-hand and right-hand matrices in the EOM equations (matrices \mathbf{A} and \mathbf{M} , respectively).

- (a) Check whether \mathbf{A} is Hermitian. Optionally symmetrize the equations (not applied in this work).
 - (b) If computing electronic excited states, check the stability of the wavefunction (verify that \mathbf{A} is positive semi-definite).
4. Solve the generalized eigenvalue problem.
- (a) Check the presence of singularities in the metric matrix. Remove components of the transition operator corresponding to singular values.

We solved the generalized eigenvalue problem in step four using NumPy. To do so, we converted the problem into a standard eigenvalue problem, which requires inverting the metric matrix, \mathbf{M} . Singularities in the metric matrix must be addressed when doing so. Such singularities, for example, arise from transitions associated with natural orbitals with near-zero occupation numbers in EKT and transitions between spin-orbitals with nearly equal occupation numbers (e.g., core-core and Rydberg-Rydberg transitions) in ph-ERPA. To address these potential singularities, the problematic components are effectively removed from the transition operator space by setting a threshold of 10^{-7} in the matrix inversion procedure. Finally, only the positive side of the spectrum is retained, and the eigenvector of the selected transition is analyzed to identify the orbitals known to participate in the transition, which is useful for labelling the states. For electronic excitations and double ionizations, we checked that the eigenvector had a positive norm with respect to the metric.

2.5.1 Lowest ionization potential

Table 2.2 presents the error in the lowest ionization potential for atoms and the 1-3 dipolar molecules, using Koopmans’ theorem (KT; Hartree-Fock reference), the extended Koopmans’ theorem (EKT; HCI reference), the anticommutator EOM form (IPa; HCI reference), and the commutator EOM form (IPc; HCI reference). The error is taken relative to the ionization potential obtained with HCI by separate computations of the N - and $N-1$ -electron ground states. The origin of the transition that produces the ion is labeled according to the main configuration from where the electron is removed (see column two). The mean absolute errors (MAEs) in the lowest ionization energies are shown separately for the atoms and the molecules in Figure 2.1.

Table 2.2: Errors in the lowest ionization potentials (in eV) computed from 1- and 2-RDMs at the aug-cc-pVDZ HF (KT) and HCI levels (EKT, IPa, IPc). The errors are evaluated as the absolute value of the deviation from HCI,

$$\Delta_{method} = |E(HCI) - E(method)|$$

	Label	Δ_{KT}	Δ_{EKT}	Δ_{IPa}^*	Δ_{IPc}^*	HCI
He	1s	0.60	0.00	0.53	2.60	24.36
Be	2s	0.87	0.00	1.67	2.60	9.29
C	2p	0.71	0.02	0.60	2.55	11.07
Ne	2p	1.72	0.00	2.18	5.55	21.49
NNO	2π	1.34	0.45	1.04	5.10	12.06
NNNH	4π	0.91	1.12	0.63	4.37	10.10
HCNO	2π	0.80	0.62	0.58	4.53	10.29
HCNNH	4π	0.61	0.29	0.34	3.90	8.93
H ₂ CNCH	4π	0.55	1.86	0.25	3.53	8.93
MAE		1.72	0.88	1.56	7.32	

* This formulation is equivalent to KT for the HF reference.

By comparing the energy errors from the third and fourth columns (KT and EKT, respectively) the importance of including electron correlation in the reference

wavefunction model becomes evident. For EKT, which uses the correlated RDMs, the agreement with the results from HCI is excellent, specially for the atomic ionization energies. For the molecules EKT accuracy deteriorates, producing ionization energies with errors ranging between 0.3 to 2.0 eV, nonetheless it is overall more accurate than the KT method. We speculate that orbital-optimized HCI wavefunctions would have better performance; it is also possible that one needs to consider smaller values for the HCI threshold, $\epsilon_1 < 10^{-4}$, to improve the description of the reference ground state by including more determinants in the CI space. Additionally, a bigger basis set (with diffuse functions) may be required to provide the flexibility necessary to describe the formation of the $N - 1$ -electron state for the molecular systems [45].

Different EOM formulations give very different results. As all these approaches use the ground state density matrices from HCI method and the simplest approximation to the ionization operator, therefore the differences are due to the form of the eigenvalue equation used. Clearly, invoking the killer condition compromises the results. Overall, for the set of species considered, IPa presents a mean average error (MAE) that is roughly twice that from EKT which has a MAE of 0.88 eV, while IPc present significantly higher errors with a MAE of 7.3 eV.

While IPa has poorer performance than EKT, this method still incorporates some correlation effects and provides some improvement over Koopmans' theorem. This can be attributed to the presence of the correlated 1-RDM in the expression of the orbital Lagrangian, Eq. 2.3.15, which accounts for fractional orbital occupations due to the multideterminant character of the wavefunction approximation. When this 1-RDM originates from the Hartree-Fock solution, IPa solutions reduce to the KT. Although for the atoms the lowest ionization energy from IPa is no better (and sometimes

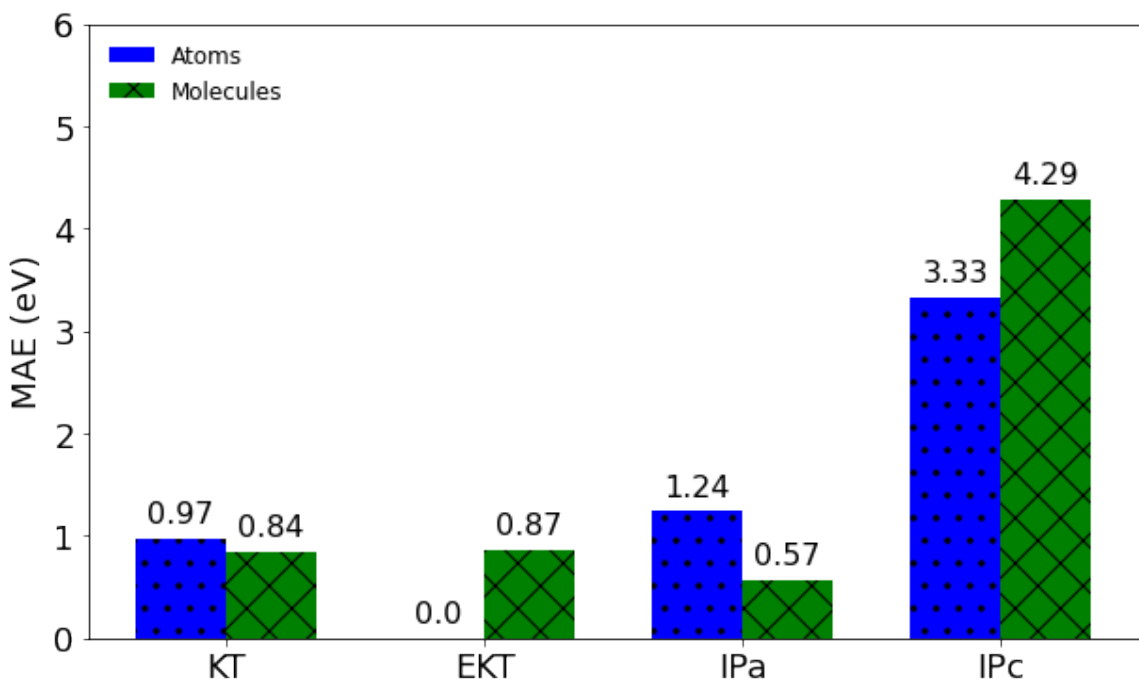


Figure 2.1: Mean absolute errors (MAE) in the lowest ionization potentials of a small test set of atoms and molecules for KT, EKT, IPa and IPc methods relative to HCI results with the aug-cc-pVDZ basis set.

worse) than EKT, for the 1,3-dipolar molecules IPa reduces the errors by about 0.3 eV. We believe that IPa is an interesting option for correlated wavefunction methods where the 1-RDM, but not the 2-RDM, is easily accessible.

2.5.2 Higher (valence) ionization potentials

The EKT, IPa, and IPc also provide predictions for excited states of the ion. Table 2.3 shows results for HF, CO, and N₂, obtained with the aug-cc-pVDZ basis set. Experimental reference values from Cioslowski et al. [39] are included in the last column. In general the trends are the same as what was observed for the lowest IPs; the ionization energies obtained from HCI RDMs with the IPa method are less

accurate than the ionization from EKT (MAE of 1.2 and 0.6 eV, respectively) but slightly better than simple Koopmans’ Theorem. Comparing the energies from the IPa method with the experimental values shows that overall it correctly reproduces the trends in the ordering of the ionized states. Notice however that for the N₂ molecule where the σ_g and π_u molecular orbitals are closer in energy (about 1 eV apart), the IPa method (like KT) incorrectly predicts that lowest ionization arises from removing an electron from the π_u orbital instead of the σ_g orbital. Interestingly, although the IPc approach (column six) greatly overestimates all ionization potentials, it does produce the correct ordering of the states for N₂.

Table 2.3: Ionization potentials (in eV) computed from 1 and 2-RDMs at the aug-cc-pVDZ HF (KT) and HCI levels (EKT, IPa, IPc). The errors are given as

$$\Delta_{method} = |E(HCI) - E(method)|.$$

	Label	KT	EKT	IPa	IPc	Exp.
HF	π	17.70	16.60	17.99	21.30	16.19
	σ	20.98	20.16	21.23	24.92	19.90
CO	σ	15.09	14.85	14.48	17.42	14.01
	π	17.45	16.28	17.32	21.47	16.85
	σ	22.00	21.39	22.05	25.03	19.78
N ₂	σ_g	17.26	16.43	16.75	19.70	15.60
	π_u	16.74	17.09	16.29	21.16	16.68
	σ_u	21.26	18.78	20.82	23.76	18.78
MAE		1.34	0.62	1.24	4.62	

Molecular geometries: $R_{HF} : 0.917\text{\AA}$; $R_{NN} : 1.098\text{\AA}$; $R_{CO} : 1.128\text{\AA}$.

2.5.3 Lowest excitation energy

Table 2.4 shows the errors in the lowest excitation energy calculated using ph-RPA, ph-ERPA and ph-ETDA for He, Be, C, Ne and the 22-electron isoelectronic series of 1,3-dipolar molecules. The error is taken as the absolute value of the difference from

the excitation energy computed directly from HCI. As explained in Section 2.3.2, all of these EOM methods approximate the excitation operator as a linear combination of particle-hole operators.

By comparing the results from ph-RPA and ph-ERPA (columns three and four, respectively) the effect of including electron correlation through the ground state can be assessed. The MAE values for particle-hole RPA and ERPA are 2.32 eV and 1.14 eV, respectively. Clearly, using the correlated RDMs from HCI considerably reduces the errors in the computed excitation energies for the atoms and molecules. For example, for the Be atom, which has static correlation arising from the near-degeneracy of the 2s and 2p orbitals, ERPA gives near-perfect valence excitation energies.

The data in Table 2.4 can be used to compare different EOM approaches. Comparison of the ERPA and ETDA methods (see columns four and five, respectively) shows that the later method, which does not have a commutator on the metric matrix (RHS), generally produces comparable results to ERPA. The ph-ETDA errors range from 0.01 to 1.6 eV, excluding the cases of nitrile oxide (HCNO) and nitrile imine (HCNNH), where ETDA yields very inaccurate excitation energies.

2.5.4 Lowest double Ionization potential

Finally the errors in the double ionization energies computed with the hh-RPA, hh-ERPA, hh-ETDA and HCI methods using the aug-cc-pVDZ basis set are compared in Table 2.5. In all cases the transition operator that generates the $(N - 2)$ -electron state from the ground state wavefunction employs a basis of two-electron removal operators.

Table 2.4: Errors in the lowest excitation energies (in eV) computed from 1 and 2-RDMs at the aug-cc-pVDZ HF (RPA) and HCI levels (ERPA, ETDA). RPA is short form for ph-RPA, ERPA for ph-ERPA and ETDA for ph-ETDA. The errors are given as $\Delta_{method} = |E(HCI) - E(method)|$.

	Label	Δ_{RPA}	Δ_{ERPA}	Δ_{ETDA}	HCI
He	$1s^2 \rightarrow 1s^1 2s^1$	0.106	0.000	0.242	20.093
Be	$2s^2 \rightarrow 2s^1 2p^1$	2.192	0.010	0.011	2.726
C	$2s^2 2p^2 \rightarrow 2s^1 2p^3$	2.440	0.114	0.105	4.011
Ne	$2s^2 2p^6 \rightarrow 2s^1 2p^5 3s^1$	1.196	0.942	0.891	18.681
NNO	$2\pi \rightarrow \sigma$	4.301	1.213	0.820	5.863
NNNH	$4\pi \rightarrow \sigma$	3.011	1.859	1.591	4.305
HCNO	$2\pi \rightarrow \sigma$	4.238	1.905	4.852	5.153
HCNNH	$4\pi \rightarrow \sigma$	0.385	1.326	2.458	2.929
H ₂ CNCH	$4\pi \rightarrow \sigma$	0.957	0.967	0.930	3.021
MAE		2.32	1.14	1.50	

Although the three EOM approaches analyzed qualitatively reproduce the trends from DIPs obtained from HCI calculations, in general, the errors are large, with MAEs of 2.44, 4.18, and 4.53 for RPA, ERPA and ETDA methods for the hole-hole operator. Alas, comparing the results from RPA (based on the uncorrelated RDMs) and ERPA (using the HCI RDMs) indicates that using the correlated ground state wavefunction does not improve the computed DIPs. The only cases where the ERPA method gives significantly better energies than the RPA one are for the He and Be. For these atoms hh-ERPA improves upon RPA by 1.42 and 0.68 eV, respectively. The results for Helium can be understood considering that the double electron removal operator in the approximated $(N - 2)$ -electron wavefunction is already exact for two electron systems. The poor performance of the three methods studied indicates that better approximations to the double ionization operator are needed by including higher-order terms (e.g., particle-hole-hole-hole terms) in the basis set expansion.

Table 2.5: Lowest double ionization potential (in eV) computed from 1 and 2-RDMs at the aug-cc-pVDZ HF (RPA) and HCI levels (ERPA, ETDA). RPA is short form for hh-RPA, ERPA for hh-ERPA and ETDA for hh-ETDA. The errors are given as

$$\Delta_{method} = |E(HCI) - E(method)|.$$

	Label	Δ_{RPA}	Δ_{ERPA}	Δ_{ETDA}	HCI
He	1s	1.45	0.03	3.80	78.63
Be	2s	1.59	0.91	1.92	27.38
C	2p	1.56	3.00	2.90	35.15
Ne	2p	8.26	10.40	9.67	61.92
NNO	2π	2.37	5.51	5.35	35.90
NNNH	4π	2.01	4.90	4.75	31.15
HCNO	2π	2.04	5.10	4.91	30.92
HCNNH	4π	1.36	4.06	3.91	27.76
H ₂ CNCH	4π	1.32	3.73	3.60	25.13
MAE		2.44	4.18	4.53	

2.6 Summary

While it is known that the equation-of-motion (EOM) approach provides a general strategy for computing electronic transition energies, the significant flexibility in how one formulates the EOM approach and how it can be applied as a post-processing tool for different wavefunctions is not always appreciated. All EOM methods take the form of a generalized eigenvalue problem, where the left-hand-side represents the operator for the transition energy and the right-hand-side represents a metric matrix, with respect to which the final (i.e., excited or ionized) states are orthogonal. In this work, we provide a (nearly complete) overview of the EOM approaches that can be formulated using the 1- and 2-electron reduced density matrices, and test these methods for very accurate RDMs computed using HCI. Under this approximation, the excitation energies can be obtained from the ground state 1- and 2-RDMs by diagonalizing a molecular system’s energy transition Hamiltonian in the basis of excited configurations generated from the reference state wavefunction.

Ionization potentials can be computed from EOM using the approximate one-electron removal operator \hat{Q}_λ^{-1} defined in Table 2.1. With no further approximation, the EKT method results. However, by invoking the killer alternative methods, both of which reduce to Koopmans’ theorem when the Hartree-Fock RDMs are used. The anticommutator EOM, IPa (Eq. 2.3.12), is especially interesting because it relies only on the 1-RDM and tends to give qualitatively useful results, although in some cases (e.g., N_2) it may give the wrong ordering for low-energy ionized states.

By contrast, EOM methods for double-electron-ionization, Eqs. (4.4.10) and (2.3.36), are often poor, and do not systematically improve the results obtained at the Hartree-Fock level except for systems that are well-approximated as two electrons outside a closed-shell core (e.g., He and Be). EOM also makes predictions for double-electron-attachment, but few neutral molecules have bound $N + 2$ -electron states, so those methods are less useful.

The ph-RPA, ph-ERPA, and ph-ETDA can be used to compute excitation energies and their associated oscillator strengths. The ph-ERPA method, which uses the correlated RDMs from HCI, provides the most accurate results, but this is still not a black-box method, as can be seen from the results for the 1,3-dipolar molecules.

Overall, our numerical results indicate that, in spite the versatility of the EOM approximations here analyzed, there is still no black-box approach to obtain accurate electronic transition energies by post-processing correlated wavefunction calculations. In most cases, qualitatively correct results are obtained, and there is significant improvements when the Hartree-Fock wavefunction is replaced by a correlated wavefunction (e.g., when Koopmans’ theorem is replaced by the extended Koopmans’ theorem, or when the random phase approximation is replaced by the extended random phase

approximation). However, the performance depends on the system and the nature of the electronic transition. So validation is be performed before application to a system of interest.

References

- [1] Mario Motta, David M. Ceperley, Garnet Kin-Lic Chan, John A. Gomez, Emanuel Gull, Sheng Guo, Carlos A. Jiménez-Hoyos, Tran Nguyen Lan, Jia Li, Fengjie Ma, Andrew J. Millis, Nikolay V. Prokof'ev, Ushnish Ray, Gustavo E. Scuseria, Sandro Sorella, Edwin M. Stoudenmire, Qiming Sun, Igor S. Tupitsyn, Steven R. White, Dominika Zgid, and Shiwei Zhang. Towards the solution of the many-electron problem in real materials: Equation of state of the hydrogen chain with state-of-the-art many-body methods. *Phys. Rev. X*, 7:031059, Sep 2017.
- [2] Nicholas H. Stair and Francesco A. Evangelista. Exploring hilbert space on a budget: Novel benchmark set and performance metric for testing electronic structure methods in the regime of strong correlation. *The Journal of Chemical Physics*, 153:104108, 9 2020. ISSN 0021-9606.
- [3] Henrik R. Larsson, Huanchen Zhai, C. J. Umrigar, and Garnet Kin-Lic Chan. The chromium dimer: Closing a chapter of quantum chemistry. *Journal of the American Chemical Society*, 144(35):15932–15937, 2022.
- [4] Gero Friesecke, Gergely Barcza, and Örs Legeza. Predicting the fci energy of large systems to chemical accuracy from restricted active space density

- matrix renormalization group calculations. *Journal of Chemical Theory and Computation*, 20(1):87–102, 2024. PMID: 38109339.
- [5] Krishnan Raghavachari, Gary W. Trucks, John A. Pople, and Martin Head-Gordon. A fifth-order perturbation comparison of electron correlation theories. *Chemical Physics Letters*, 157(6):479–483, 1989. ISSN 0009-2614.
- [6] Andrew T. B. Gilbert, Nicholas A. Besley, and Peter M. W. Gill. Self-consistent field calculations of excited states using the maximum overlap method (mom). *The Journal of Physical Chemistry A*, 112(50):13164–13171, 2008. PMID: 18729344.
- [7] Gianluca Levi, Aleksei V. Ivanov, and Hannes Jónsson. Variational calculations of excited states via direct optimization of the orbitals in dft. *Faraday Discuss.*, 224:448–466, 2020. doi: 10.1039/D0FD00064G. URL <http://dx.doi.org/10.1039/D0FD00064G>.
- [8] Antoine Marie, Fábri Kossoski, and Pierre-François Loos. Variational coupled cluster for ground and excited states. *The Journal of Chemical Physics*, 155(10):104105, 09 2021. ISSN 0021-9606.
- [9] Nicholas J. Mayhall and Krishnan Raghavachari. Multiple solutions to the single-reference ccSD equations for nih. *Journal of Chemical Theory and Computation*, 6(9):2714–2720, 2010. PMID: 26616072.
- [10] Piotr Piecuch and Karol Kowalski. *In Search of the Relationship between Multiple Solutions Characterizing Coupled-Cluster Theories*, volume 5, pages 1–104. 2000.

- [11] D. J. Rowe. Equations-of-motion method and the extended shell model. *Reviews of Modern Physics*, 40:153–166, 1968. ISSN 00346861.
- [12] Vincent McKoy. *Methods of Electronic Structure Theory*, volume 21. Springer US, 1977. ISBN 978-1-4757-0889-9.
- [13] Jack Simons and Wesley D. Smith. Theory of electron affinities of small molecules. *The Journal of Chemical Physics*, 58:4899–4907, 6 1973. ISSN 0021-9606.
- [14] Michael F. Herman, Karl F. Freed, and D. L. Yeager. *Analysis and Evaluation of Ionization Potentials, Electron Affinities, and Excitation Energies by the Equations of Motion—Green’s Function Method*, pages 1–69. John Wiley & Sons, Ltd, 1981. ISBN 9780470142684.
- [15] John F Stanton and Rodney J Bartlett. The equation of motion coupled-cluster method. a systematic biorthogonal approach to molecular excitation energies, transition probabilities, and excited state properties. *The Journal of Chemical Physics*, 98:7029–7039, 5 1993. ISSN 00219606.
- [16] Anna I. Krylov. Equation-of-motion coupled-cluster methods for open-shell and electronically excited species: The hitchhiker’s guide to fock space. *Annual Review of Physical Chemistry*, 59:433–462, 2008. ISSN 1545-1593.
- [17] Tai-Ichi Shibuya and Vincent McKoy. Higher random-phase approximation as an approximation to the equations of motion. *Phys. Rev. A*, 2:2208–2218, Dec 1970.

- [18] John F Stanton and Jürgen Gauss. Analytic energy derivatives for ionized states described by the equation-of-motion coupled cluster method. *The Journal of Chemical Physics*, 101:8938–8944, 11 1994. ISSN 0021-9606.
- [19] Marcel Nooijen and Rodney J. Bartlett. Equation of motion coupled cluster method for electron attachment. *The Journal of Chemical Physics*, 102:3629–3647, 3 1995. ISSN 0021-9606.
- [20] Rodney J. Bartlett. Coupled-cluster theory and its equation-of-motion extensions. *WIREs Computational Molecular Science*, 2(1):126–138, 2012.
- [21] Jesse J. Lutz and Piotr Piecuch. Performance of the completely renormalized equation-of-motion coupled-cluster method in calculations of excited-state potential cuts of water. *Computational and Theoretical Chemistry*, 1040-1041:20–34, 2014. ISSN 2210-271X. Excited states: From isolated molecules to complex environments.
- [22] Henrik Koch, Hans Jo/rgen Aa. Jensen, Poul Jo/rgensen, and Trygve Helgaker. Excitation energies from the coupled cluster singles and doubles linear response function (CCSDLR). Applications to Be, CH+, CO, and H2O. *The Journal of Chemical Physics*, 93(5):3345–3350, 09 1990. ISSN 0021-9606.
- [23] Bogumil Jeziorski and Hendrik J. Monkhorst. Coupled-cluster method for multideterminantal reference states. *Phys. Rev. A*, 24:1668–1681, Oct 1981.
- [24] Andreas Köhn, Matthias Hanauer, Leonie Anna Mück, Thomas-Christian Jagau, and Jürgen Gauss. State-specific multireference coupled-cluster theory. *WIREs Computational Molecular Science*, 3(2):176–197, 2013.

- [25] Koushik Chatterjee and Katarzyna Pernal. Excitation energies from extended random phase approximation employed with approximate one- and two-electron reduced density matrices. *The Journal of Chemical Physics*, 137:204109, 2012.
- [26] Darwin W. Smith and Orville W. Day. Extension of Koopmans' theorem. I. Derivation. *The Journal of Chemical Physics*, 62(1):113–114, 01 1975. ISSN 0021-9606.
- [27] Orville W. Day, Darwin W. Smith, and Robert C. Morrison. Extension of Koopmans' theorem. II. Accurate ionization energies from correlated wavefunctions for closed-shell atoms. *The Journal of Chemical Physics*, 62(1):115–119, 01 1975. ISSN 0021-9606.
- [28] Jens Oddershede, Poul Jørgensen, and Danny L. Yeager. Polarization propagator methods in atomic and molecular calculations. *Computer Physics Reports*, 2(2):33–92, 1984. ISSN 0167-7977.
- [29] Hendrik J. Monkhorst. Calculation of properties with the coupled-cluster method. *International Journal of Quantum Chemistry*, 12(S11):421–432, 1977.
- [30] Jack Simons. Chapter 17 - equations of motion methods for computing electron affinities and ionization potentials. In Clifford E. Dykstra, Gernot Frenking, Kwang S. Kim, and Gustavo E. Scuseria, editors, *Theory and Applications of Computational Chemistry*, pages 443–464. Elsevier, Amsterdam, 2005. ISBN 978-0-444-51719-7.
- [31] Loren Greenman and David A. Mazziotti. Electronic excited-state energies from

- a linear response theory based on the ground-state two-electron reduced density matrix. *The Journal of Chemical Physics*, 128, 3 2008. ISSN 0021-9606.
- [32] Johannes Tölle and Garnet Kin-Lic Chan. Exact relationships between the GW approximation and equation-of-motion coupled-cluster theories through the quasi-boson formalism. *The Journal of Chemical Physics*, 158(12):124123, 03 2023. ISSN 0021-9606.
- [33] Michael F. Herman and Karl F. Freed. Analysis of approximations and errors in equations of motion method calculations. *Chemical Physics*, 36(3):383–396, 1979. ISSN 0301-0104.
- [34] Jouni Suhonen. *From Nucleons to Nucleus*, volume 53. Springer Berlin Heidelberg, 2007. ISBN 978-3-540-48859-0.
- [35] Mark Wladyslawski and Marcel Nooijen. *The Photoelectron Spectrum of the NO₃ Radical Revisited: A Theoretical Investigation of Potential Energy Surfaces and Conical Intersections*, volume 828 of *ACS Symposium Series*, chapter 4, pages 65–92. American Chemical Society, 2002. ISBN 9780841237926.
- [36] Matthias Ruckebauer, Sebastian Mai, Philipp Marquetand, and Leticia González. Photoelectron spectra of 2-thiouracil, 4-thiouracil, and 2,4-dithiouracil. *The Journal of Chemical Physics*, 144(7):074303, 02 2016. ISSN 0021-9606.
- [37] Peter Politzer, Jane S. Murray, and Felipe A. Bulat. Average local ionization energy: A review. *Journal of Molecular Modeling*, 16(11):1731–1742, 2010. ISSN 0948-5023.

- [38] Robert C. Morrison and Guanghua Liu. Extended koopmans' theorem: Approximate ionization energies from mcsf wave functions. *Journal of Computational Chemistry*, 13(8):1004–1010, 1992.
- [39] Jerzy Cioslowski, Pawel Piskorz, and Guanghua Liu. Ionization potentials and electron affinities from the extended koopmans' theorem applied to energy-derivative density matrices: The ektmpn and ektqcisd methods. *The Journal of Chemical Physics*, 107:6804–6811, 11 . ISSN 0021-9606.
- [40] Uğur Bozkaya. The extended koopmans' theorem for orbital-optimized methods: Accurate computation of ionization potentials. *Journal of Chemical Physics*, 139, 2013. ISSN 00219606. Includes generalized fock matrix definition.
- [41] Ernest R. Davidson, Joseph Vincent Ortiz, and Viktor N. Staroverov. Complete-active-space extended koopmans theorem method. *The Journal of Chemical Physics*, 155:051102, 8 2021. ISSN 0021-9606.
- [42] James C. Ellenbogen, Orville W. Day, Darwin W. Smith, and Robert C. Morrison. Extension of Koopmans' theorem. IV. Ionization potentials from correlated wavefunctions for molecular fluorine. *The Journal of Chemical Physics*, 66(11):4795–4801, 06 1977. ISSN 0021-9606.
- [43] Dage Sundholm and Jeppe Olsen. The exactness of the extended Koopmans's theorem: A numerical study. *The Journal of Chemical Physics*, 98(5):3999–4002, 03 1993. ISSN 0021-9606.
- [44] Robert C. Morrison and Paul W. Ayers. Generalized overlap amplitudes using the extended koopmans' theorem for be. *The Journal of Chemical Physics*, 103:

- 6556–6561, 1995. ISSN 00219606. From Michael: using the DMs to transform to natural orbitals and have a diagonal problem(?).
- [45] Diederik Vanfleteren, Dimitri Van Neck, Paul W. Ayers, Robert C. Morrison, and Patrick Bultinck. Exact ionization potentials from wavefunction asymptotics: The extended koopmans’ theorem, revisited. *Journal of Chemical Physics*, 130, 2009. ISSN 00219606.
- [46] Paul W. Ayers and Junia Melin. Computing the fukui function from ab initio quantum chemistry: approaches based on the extended koopmans’ theorem. *Theoretical Chemistry Accounts*, 117(3):371–381, 2007. ISSN 1432-2234.
- [47] Dilan Yildiz and Uğur Bozkaya. Assessment of the extended koopmans’ theorem for the chemical reactivity: Accurate computations of chemical potentials, chemical hardnesses, and electrophilicity indices. *Journal of Computational Chemistry*, 37:345–353, 1 2016. ISSN 01928651.
- [48] Orville W. Day, Darwin W. Smith, and Claude Garrod. A generalization of the hartree-fock one-particle potential. *International Journal of Quantum Chemistry*, 8(S8):501–509, 1974.
- [49] Caitlin Lanssens, Paul W. Ayers, Dimitri Van Neck, Stijn De Baerdemacker, Klaas Gunst, and Patrick Bultinck. Method for making 2-electron response reduced density matrices approximately n-representable. *Journal of Chemical Physics*, 148, 7 2017.
- [50] Helen van Aggelen, Brecht Verstichel, Guillaume Acke, Matthias Degroote, Patrick Bultinck, Paul W. Ayers, and Dimitri Van Neck. Extended random

- phase approximation method for atomic excitation energies from correlated and variationally optimized second-order density matrices. *Computational and Theoretical Chemistry*, 1003:50–54, 1 2013. ISSN 2210271X.
- [51] Juan Felipe Huan Lew-Yee, Iván Alejandro Bonfil-Rivera, Mario Piris, and Jorge M. del Campo. Excited states by coupling piris natural orbital functionals with the extended random-phase approximation. *Journal of Chemical Theory and Computation*, 20(5):2140–2151, 2024. PMID: 38353418.
- [52] A. D. McLACHLAN and M. A. BALL. Time-dependent hartree—fock theory for molecules. *Reviews of Modern Physics*, 36:844–855, 7 1964. ISSN 0034-6861.
- [53] Gy Csanak. The application of the time-dependent hartree-fock method to the calculation of excited state-excited state transition densities of atoms (molecules). *Journal of Physics B: Atomic and Molecular Physics*, 8(2):337, feb 1975.
- [54] Keith Runge, David A. Micha, and Eric Q. Feng. A time-dependent molecular orbital approach to electron transfer in ion–atom collisions. *International Journal of Quantum Chemistry*, 38(S24):781–790, 1990.
- [55] Andreas Dreuw and Martin Head-Gordon. Single-reference ab initio methods for the calculation of excited states of large molecules. *Chemical Reviews*, 105: 4009–4037, 11 2005. ISSN 0009-2665.
- [56] Agisilaos Chantzis, Adèle D. Laurent, Carlo Adamo, and Denis Jacquemin. Is the tamm-dancoff approximation reliable for the calculation of absorption and

- fluorescence band shapes? *Journal of Chemical Theory and Computation*, 9(10): 4517–4525, 2013. PMID: 26589168.
- [57] Helen van Aggelen, Yang Yang, and Weitao Yang. Exchange-correlation energy from pairing matrix fluctuation and the particle-particle random-phase approximation. *Physical Review A*, 88:030501, 9 2013. ISSN 1050-2947.
- [58] Yang Yang, Helen van Aggelen, and Weitao Yang. Double, rydberg and charge transfer excitations from pairing matrix fluctuation and particle-particle random phase approximation. *The Journal of Chemical Physics*, 139:224105, 12 2013. ISSN 0021-9606.
- [59] Ye Jin, Yang Yang, Du Zhang, Degao Peng, and Weitao Yang. Excitation energies from particle-particle random phase approximation with accurate optimized effective potentials. *The Journal of Chemical Physics*, 147:134105, 10 2017. ISSN 0021-9606.
- [60] Ricardo Longo, Benoît Champagne, and Yngve Öhrn. Electron propagator theory and application. *Theoretica Chimica Acta*, 90(5):397–419, mar 1995. ISSN 1432-2234. doi: 10.1007/BF01113544. URL <https://doi.org/10.1007/BF01113544>.
- [61] J. V. Ortiz. Dyson-orbital concepts for description of electrons in molecules. *The Journal of Chemical Physics*, 153(7):070902, 08 2020. ISSN 0021-9606.
- [62] B.P. Hollebone, C.E. Brion, E.R. Davidson, and C. Boyle. Valence electron momentum distributions of the hydrogen halides. ii. comparison of ems measurements and calculations using near hartree-fock limit and configuration

- interaction wavefunctions for hydrogen chloride. *Chemical Physics*, 173(2):193–208, 1993. ISSN 0301-0104.
- [63] Michael Spanner, Serguei Patchkovskii, Congyi Zhou, Spiridoula Matsika, Marija Kotur, and Thomas C. Weinacht. Dyson norms in xuv and strong-field ionization of polyatomics: Cytosine and uracil. *Phys. Rev. A*, 86:053406, Nov 2012.
- [64] Adam A. Holmes, Norm M. Tubman, and C. J. Umrigar. Heat-bath configuration interaction: An efficient selected configuration interaction algorithm inspired by heat-bath sampling. *Journal of Chemical Theory and Computation*, 12:3674–3680, 8 2016. ISSN 1549-9618.
- [65] Jr. Dunning, Thom H. Gaussian basis sets for use in correlated molecular calculations. I. The atoms boron through neon and hydrogen. *The Journal of Chemical Physics*, 90(2):1007–1023, 01 1989. ISSN 0021-9606.
- [66] Qiming Sun, Timothy C Berkelbach, Nick S Blunt, George H Booth, Sheng Guo, Zhendong Li, Junzi Liu, James D McClain, Elvira R Sayfutyarova, Sandeep Sharma, et al. Pyscf: the python-based simulations of chemistry framework. *Wiley Interdisciplinary Reviews: Computational Molecular Science*, 8(1):e1340, 2018.
- [67] Qiming Sun, Xing Zhang, Samragni Banerjee, Peng Bao, Marc Barbry, Nick S Blunt, Nikolay A Bogdanov, George H Booth, Jia Chen, Zhi-Hao Cui, et al. Recent developments in the pyscf program package. *The Journal of Chemical Physics*, 153(2):024109, 2020.

- [68] Michelle Richer, Gabriela Sánchez-Díaz, Farnaz Heidar-Zadeh, Marco Martínez-González, Valerii Chuiko, and Paul W. Ayers. Pyci: A python-scriptable library for arbitrary determinant ci. Unpublished manuscript.

Chapter 3

Calculation of spectroscopic properties via parameterized configuration interaction methods

3.1 Introduction

Unique among the computational methods for the solution of the (time-independent, nonrelativistic) Schrödinger equation, the Full Configuration Interaction (FCI) approach simultaneously yields exact solutions for both the ground and excited states within given basis set. However, FCI's factorial scaling limits its application to small problems, rendering it impractical for most applications of chemical interest. Consequently, finding accurate and efficient solutions to the Schrödinger equation remains an active area of research in modern theoretical and computational chemistry.

The factorial cost of FCI arises because the number of wavefunction parameters grows combinatorially since there is one coefficient for each determinant. This

suggests that the curse of dimension could be broken by reexpressing the CI coefficients as functions of a limited number of parameters. This strategy is ubiquitous in electronic structure theory and includes popular approaches like coupled-cluster methods and matrix product states. The Flexible Ansatz for N-electron Configuration Interaction (FanCI) wavefunction approximation proposed by Kim et al. subsumes these methods and provides a fully general approach for parameterizing the CI coefficients [1]. FanCI provides a common framework for popular wavefunction approximations and provides a pathway for developing new wavefunction methods [2–5]. The FanCI wavefunction generalizes (selected) CI:

$$|\Psi_{FANCI}^{(N)}\rangle = \sum_{\mathbf{m} \in \mathcal{S}} f(\mathbf{m}, \mathbf{P}) |\mathbf{m}\rangle \quad (3.1.1)$$

where the coefficients of a set of N-electron Slater determinants, \mathcal{S} , specified by a bitstring representing their occupation numbers, \mathbf{m} , are written as a function of parameters \mathbf{P} . For example, for the FCI approximation, \mathcal{S} includes every N-electron determinant, $f(\mathbf{m}, \mathbf{P}) = P_{\mathbf{m}}$ is a linear function, and the parameters \mathbf{P} are merely the coefficients of the CI expansion.

The parameters of the FanCI model can be determined minimizing the energy with respect to them:

$$\min_{\mathbf{P}} E_{\lambda}(\mathbf{P}) = \min_{\mathbf{P}} \frac{\langle \Psi_{FANCI}^{(N)} | \hat{H} | \Psi_{FANCI}^{(N)} \rangle}{\langle \Psi_{FANCI}^{(N)} | \Psi_{FANCI}^{(N)} \rangle} \quad (3.1.2)$$

where \hat{H} is the Hamiltonian operator. In this form, the solutions found are guaranteed to be variational. Unfortunately, for most atomic systems of interests in chemistry, the complexity of the wavefunction approximation makes this approach computationally

intractable. Modelling excited states with the variational principle requires locating saddle points of the function $E(\mathbf{P})$, which is extremely difficult given that there are frequently thousands (or even millions) of parameters.

As an alternative to the variational principle, one can determine the system’s energy and wavefunction parameters using the projected Schrödinger equation,

$$\langle \mathbf{m} | \hat{H} | \Psi_{FANCI}^{(N)} \rangle = E_\lambda(\mathbf{P}) \langle \mathbf{m} | \Psi_{FANCI}^{(N)} \rangle \quad \forall \mathbf{m} \quad (3.1.3)$$

which results from projecting the Schrödinger equation on a set of Slater determinants, $\langle \mathbf{m} |$. (More generally, one can project against any function for which the necessary matrix elements can be efficiently computed.) Unlike the variational formulation, which tends to be intractable whenever the selected set of Slater determinants, \mathcal{S} , is large, the projected form of the Schrödinger equation is typically feasible whenever the number of parameters (which provides a lower bound on the size of the projection space) is moderate.

Equation 3.1.3 defines a system of nonlinear equations; usually the projection space is larger than the number of unknown parameters so nonlinear least squares is used. An extra equation that fixes the normalization of the wavefunction is also included. (Usually one adopts intermediate normalization, which amounts to assuming that the CI coefficient of the Hartree-Fock wavefunction is one, $f(\mathbf{m}_{HF}, \mathbf{P}) = 1$.) Overall, the computational bottleneck of this procedure is typically the cost of (iteratively) evaluating $f(\mathbf{m}, \mathbf{P})$ for every determinant in the projection space. The projection space can also be used to impose additional structure to the wavefunction, like a particular spin symmetry. If the complete set of determinants in the basis of N -electron configurations is used, the lowest energy from the nonlinear least-squares

procedure is an upper bound to the true ground-state energy, and the least-squares energy minus the least-squares error is a lower bound to the true energy. However, for a truncated projection space, this energy is not variational.

For spectroscopic applications, one can separately solve Eq. 3.1.3 for each state of interest and find “excitation” energies as their energy differences:

$$\Delta E_\lambda(\mathbf{P}) = E_\lambda(\mathbf{P}) - E_0(\mathbf{P})$$

However, the complexity of the objective/energy function, Eq. 3.1.3, a non-convex function of the parameters with multiple minima, poses a challenge for the iterative optimization algorithms commonly applied to solve it. This difficulty is exacerbated for excited states, where it is usually even more difficult to find a good initial guess for the solution. The direct approach is mainly feasible if only a few excited states, which are low in energy or have different symmetry from the ground state, are of interest. There are also some strategies for solving multiple excited states simultaneously, but the algorithms are more complicated and, thus far, have never been implemented in the context of electronic structure theory [6].

Therefore, it would be desirable, for a given FanCI approximation, to be able to simultaneously compute the full electronic spectrum, or at least a large portion thereof. To do this, we adapt the equation-of-motion (EOM) framework [7] to the FanCI framework, thereby computing multiple excitation energies in one-shot. In analogy to prior work adapting coupled-cluster theory (FanCC) [8] and many-body perturbation theory (FanPT) [9] to the FanCI framework, we call this approach FanEOM.

3.2 Excited states with FanCI: FanEOM

Let the wavefunction for the excited state $|\Psi_\lambda^{(N\pm\kappa)}\rangle$ be formulated as:

$$|\Psi_\lambda^{(N\pm\kappa)}\rangle = \hat{Q}_\lambda^{(\pm\kappa)} |\Psi_{FANCI}^{(N)}\rangle \quad (3.2.1)$$

where $|\Psi_{FANCI}^{(N)}\rangle$ is an N-electron state (typically the ground state) described by the FanCI model and $\hat{Q}_\lambda^{(\pm\kappa)}$ is an “excitation” operator that acts on the FanCI reference to create the excited state. The superscript $(N \pm \kappa)$ indicates that the electronic transition can preserve (excitation, $\kappa = 0$) or change (ionization, $\kappa \neq 0$) the number of electrons in the reference state.

This ansatz resembles the equation-of-motion coupled-cluster approach [2], however $\hat{Q}_\lambda^{(\pm\kappa)}$ is a linear operator, expanded in a basis set of excitation/transition operators $\hat{A}_{\mathbf{n}}^{(\pm\kappa)}$:

$$\hat{Q}_\lambda^{(\pm\kappa)} = \sum_{\mathbf{n}} c_{\mathbf{n},\lambda} \hat{A}_{\mathbf{n}}^{(\pm\kappa)} \quad (3.2.2)$$

In this expression, \mathbf{n} is a symbolic (multi)index that generates the basis. By appropriately selecting the basis elements $\hat{A}_{\mathbf{n}}^{(\pm\kappa)}$, one can describe electronically excited ($\kappa = 0$) or ionized ($\kappa \neq 0$) states. As an example, below we provide explicit expressions for excitation and single-electron removal:

$$\hat{Q}_\lambda^{(0)} = \sum c_{pq} a_p^\dagger a_q + \sum c_{pqrs} a_p^\dagger a_q^\dagger a_s a_r + \sum c_{pqrstu} a_p^\dagger a_q^\dagger a_r^\dagger a_u a_t a_s + \dots \quad (3.2.3)$$

$$\hat{Q}_\lambda^{(+1)} = \sum c_p a_p + \sum c_{rpq} a_r a_p^\dagger a_q + \sum c_{tpqrs} a_t a_p^\dagger a_q^\dagger a_s a_r + \dots \quad (3.2.4)$$

where, using the notation of second quantization, a_p^\dagger/a_p denotes the creation/annihilation

of an electron in the p th spin-orbital.

The coefficients in the linear expansion of the transition operator and the corresponding transition energies can be determined solving the equation:

$$\begin{aligned} \left[\hat{H}, \hat{Q}_\lambda^{(\pm\kappa)} \right] |\Psi_{FANCI}^{(N)}\rangle &= \Delta E_\lambda \hat{Q}_\lambda^{(\pm\kappa)} |\Psi_{FANCI}^{(N)}\rangle \\ \sum_{\mathbf{n}} \left[\hat{H}, \hat{A}_{\mathbf{n}}^{(\pm\kappa)} \right] |\Psi_{FANCI}^{(N)}\rangle c_{\mathbf{n},\lambda} &= \Delta E_\lambda \sum_{\mathbf{n}} \hat{A}_{\mathbf{n}}^{(\pm\kappa)} |\Psi_{FANCI}^{(N)}\rangle c_{\mathbf{n},\lambda} \end{aligned} \quad (3.2.5)$$

where in the second line the definition of $\hat{Q}_\lambda^{(\pm\kappa)}$ has been inserted, Eq. 3.2.2. This formula has a transition energy, $\Delta E_\lambda = \left(E_\lambda^{(N\pm\kappa)} - E_0^{(N)} \right)$, as a pseudo-eigenvalue of the operator $\left[\hat{H}, \hat{Q}_\lambda^{(\pm\kappa)} \right]$. For a chemical system with particle interactions described by the Hamiltonian operator:

$$\hat{H} = \sum_{pq} h_{pq} a_p^\dagger a_q + \frac{1}{2} \sum_{pqrs} \langle pq|rs\rangle a_p^\dagger a_q^\dagger a_s a_r \quad (3.2.6)$$

where h_{pq} represent the one-electron integrals in the spin-orbital basis set, and $\langle pq|rs\rangle$ the two-electron integrals, introduction of a commutator in the Equation 3.2.5 can help reduce the computational cost. Moreover, by solving directly for the transition energies rather than subtracting the energy of the (separately determined) initial and final-state energies, systematic error cancellations can occur.

Similar to the FanCI approach, satisfaction of Eq. 3.2.5 can be enforced by projecting on a complete set of $\Phi^{(N\pm\kappa)}$ states:

$$\begin{aligned} \sum_{\mathbf{n}} \left\langle \Phi^{(N\pm\kappa)} \left| \left[\hat{H}, \hat{A}_{\mathbf{n}}^{(\pm\kappa)} \right] \right| \Psi_{FANCI}^{(N)} \right\rangle c_{\mathbf{n},\lambda} \\ = \Delta E_k \sum_{\mathbf{n}} \left\langle \Phi^{(N\pm\kappa)} \left| \hat{A}_{\mathbf{n}}^{(\pm\kappa)} \right| \Psi_{FANCI}^{(N)} \right\rangle c_{\mathbf{n},\lambda} \quad \forall \Phi^{(N\pm\kappa)} \end{aligned} \quad (3.2.7)$$

defining a linear system of equations relative to the excited wavefunction parameters $c_{\mathbf{n},\lambda}$. Here, we are assuming that we know the FanCI solution from a previous calculation, otherwise Eq. (3.2.7), which implicitly depends on the FanCI model parameters \mathbf{P} , would become a non-linear system of equations. It would be feasible, albeit more challenging, to solve for the FanCI parameters \mathbf{P} and the transition-operator coefficients, $c_{\mathbf{n},\lambda}$, but the computational difficulty is compounded.

Traditionally, the “testing functions” $\Phi^{(N\pm\kappa)}$ are constructed from the basis set defining the excitation operator $\hat{Q}_\lambda^{(\pm\kappa)}$:

$$|\Phi_{\mathbf{m}}^{(N\pm\kappa)}\rangle = \hat{A}_{\mathbf{m}}^{(\pm\kappa)} |\Phi^{(N)}\rangle \quad \forall \mathbf{m} \quad (3.2.8)$$

where $\Phi^{(N)}$ is some arbitrary N-electron configuration (the FanCI model in our case). This would lead to the EOM equation in its most elementary form:

$$\begin{aligned} & \sum_{\mathbf{n}} \left\langle \Phi^{(N)} \left| \left(\hat{A}_{\mathbf{m}}^{(\pm\kappa)} \right)^\dagger \left[\hat{H}, \hat{A}_{\mathbf{n}}^{(\pm\kappa)} \right] \right| \Psi_{FANCI}^{(N)} \right\rangle c_{\mathbf{n},\lambda} \\ & = \Delta E_k \sum_{\mathbf{n}} \left\langle \Phi^{(N)} \left| \left(\hat{A}_{\mathbf{m}}^{(\pm\kappa)} \right)^\dagger \hat{A}_{\mathbf{n}}^{(\pm\kappa)} \right| \Psi_{FANCI}^{(N)} \right\rangle c_{\mathbf{n},\lambda} \quad \forall \mathbf{m} \end{aligned} \quad (3.2.9)$$

However, in our case, because the wavefunctions in the bra are not eigenstates of the Hamiltonian, the standard tricks to build higher-order commutators [10–12], such as:

$$\left[\left(\hat{A}_{\mathbf{m}}^{(\pm\kappa)} \right)^\dagger, \left[\hat{H}, \hat{A}_{\mathbf{m}}^{(\pm\kappa)} \right] \right] \quad (3.2.10)$$

or even the more symmetric one:

$$\frac{1}{2} \left(\left[\left(\hat{A}_{\mathbf{m}}^{(\pm\kappa)} \right)^\dagger, \left[\hat{H}, \hat{A}_{\mathbf{n}}^{(\pm\kappa)} \right] \right] + \left[\left[\left(\hat{A}_{\mathbf{m}}^{(\pm\kappa)} \right)^\dagger, \hat{H} \right], \hat{A}_{\mathbf{n}}^{(\pm\kappa)} \right] \right) \quad (3.2.11)$$

do not work.

Any set of test functions can be used, and it is possible that the set in Eq. (3.2.8) is not the most convenient choice. We choose to use directly Eq. (3.2.7) and select Slater determinants with $(N \pm \kappa)$ electrons, $\Phi_{\mathbf{m}}^{(N \pm \kappa)}$, as the projection space:

$$\begin{aligned} & \sum_{\mathbf{n}} \left\langle \Phi_{\mathbf{m}}^{(N \pm \kappa)} \left| \left[\hat{H}, \hat{A}_{\mathbf{n}}^{(\pm \kappa)} \right] \right| \Psi_{FANCI}^{(N)} \right\rangle c_{\mathbf{n}, \lambda} \\ & = \Delta E_k \sum_{\mathbf{n}} \left\langle \Phi_{\mathbf{m}}^{(N \pm \kappa)} \left| \hat{A}_{\mathbf{n}}^{(\pm \kappa)} \right| \Psi_{FANCI}^{(N)} \right\rangle c_{\mathbf{n}, \lambda} \quad \forall \mathbf{m} \end{aligned} \quad (3.2.12)$$

The great advantage to this more general approach is that one can use more test functions than there are unknowns, which helps resolve singularities and can provide statistical information/errors for the solutions of Eq. (3.2.12). One could also add additional equations corresponding to the “killer condition”,

$$\left(\hat{Q}_{\lambda}^{(\pm \kappa)} \right)^{\dagger} \left| \Psi_{FANCI}^{(N)} \right\rangle = 0 \quad (3.2.13)$$

E.g., one can require that:

$$\sum_{\mathbf{n}} \left\langle \Phi_{\mathbf{m}}^{(N)} \left| \hat{A}_{\mathbf{m}}^{(\pm \kappa)} \left(\hat{A}_{\mathbf{n}}^{(\pm \kappa)} \right)^{\dagger} \right| \Psi_{FANCI}^{(N)} \right\rangle c_{\mathbf{n}, \lambda}^* = 0 \quad \forall \mathbf{m} \quad (3.2.14)$$

$$\sum_{\mathbf{n}} \left\langle \Phi_{\mathbf{j}}^{(N \pm \kappa)} \left| \hat{A}_{\mathbf{k}}^{(\pm \kappa)} \hat{A}_{\mathbf{l}}^{(\pm \kappa)} \left(\hat{A}_{\mathbf{n}}^{(\pm \kappa)} \right)^{\dagger} \right| \Psi_{FANCI}^{(N)} \right\rangle c_{\mathbf{n}, \lambda}^* = 0 \quad \forall \mathbf{j}, \mathbf{k}, \mathbf{l} \quad (3.2.15)$$

Note, however, that these equations, which are satisfied by the exact solution, are not used in the derivation of Eqs. (3.2.9) and (3.2.12) and thus, unlike traditional EOM and extended random phase approximation methods, do not need to be imposed in our approach.

The formulation introduced thus far is exact if the reference wavefunction is exact and the transition operator is expanded in a complete basis. However, for practical applications of the FanEOM framework, we are mainly interested in cases where the operator $\left[\hat{H}, \hat{A}_{\mathbf{n}}^{(\pm\kappa)}\right]$ has four or fewer creation/annihilation operators, so that only the one- and two-electron transition reduced density matrices of the FanCI wavefunction are needed. Hence, the most interesting cases are:

$$\hat{A}_n^{(+1)} = a_n^\dagger \quad (3.2.16)$$

$$\hat{A}_n^{(-1)} = a_n \quad (3.2.17)$$

$$\hat{A}_{n_1 n_2}^{(0)} = a_{n_1}^\dagger a_{n_2} \quad (3.2.18)$$

corresponding to single electron attachment, single electron removal, and excitation respectively.

3.3 Linear response function

In atomic systems, several important physicochemical properties (e.g. density-related properties like the polarizability) can be described using response functions. In this section we show that is also possible to evaluate the linear response functions within our formulation.

The general expression for the linear response function in the frequency domain is given by:

$$\langle A, B \rangle_\omega = \sum_{\lambda > 0} \frac{\langle \Psi_0 | \hat{A} | \Psi_\lambda \rangle \langle \Psi_\lambda | \hat{B} | \Psi_0 \rangle}{\hbar\omega + i\eta + (E_0 - E_\lambda)} - \frac{\langle \Psi_0 | \hat{B} | \Psi_\lambda \rangle \langle \Psi_\lambda | \hat{A} | \Psi_0 \rangle}{\hbar\omega + i\eta - (E_0 - E_\lambda)} \quad (3.3.1)$$

where \hat{A} is the operator for some observable property and \hat{B} is the operator associated with the perturbation to the system. The poles, the energy differences ($E_0 - E_\lambda$) in the denominator, correspond to transition energies while the residues, $\langle \Psi_0 | \hat{A} | \Psi_\lambda \rangle$, are transition matrix elements between the ground and excited states. For example, for a one body perturbation \hat{B} (e.g. an electromagnetic field), the linear response takes the form:

$$\langle A \rangle_\omega = \sum_{\lambda > 0} \frac{\langle \Psi_{FANCI}^{(N)} | \hat{A} | \Psi_\lambda^{(N)} \rangle \langle \Psi_\lambda^{(N)} | a_p^\dagger a_q | \Psi_{FANCI}^{(N)} \rangle}{\hbar\omega + i\eta + E_0^{(N)} - E_\lambda^{(N)}} + c.c. \quad (3.3.2)$$

where we have considered the ground state described by the FanCI model.

These type of expressions can be evaluated based on the solutions to the FanEOM equations (Eq. (3.2.9) or (3.2.12)). However, due to the asymmetric nature of the FanEOM approach, we cannot directly compute the transition matrices between the ground and excited states:

$$\langle \Psi_{FANCI}^{(N)} | a_p^\dagger a_q | \sum_{n_1 n_2} c_{n_1 n_2; \lambda} \hat{A}_{n_1 n_2}^{(0)} | \Psi_{FANCI}^{(N)} \rangle \quad (3.3.3)$$

where we have inserted the definition of the excited state wavefunction (cf. Eqs. 3.2.1 and 3.2.18). Evaluating these terms require the one- and two-electron density matrices of the FanCI ansatz, which are not easily obtained.

One obvious thing to do is to use the approximate resolution of the identity defined by the projection space to estimate Eq. (3.3.3). This leads to an expression for the linear response function that involves only the transition reduced density matrices:

$$\sum_{\mathbf{m}} \langle \Psi_{FANCI}^{(N)} | a_p^\dagger a_q | \Phi_{\mathbf{m}}^{(N)} \rangle \langle \Phi_{\mathbf{m}}^{(N)} | \sum_{n_1 n_2} c_{n_1 n_2; \lambda} \hat{A}_{n_1 n_2}^{(0)} | \Psi_{FANCI}^{(N)} \rangle \quad (3.3.4)$$

3.3.1 Solving the FanEOM problem

The FanEOM system of equations (Eqs. (3.2.9) or (3.2.12)) is a rectangular generalized eigenvalue problem (GEVP):

$$\begin{aligned} \mathbf{A}\mathbf{C} &= \Delta E_\lambda \mathbf{M}\mathbf{C} & (3.3.5) \\ \mathbf{A} &= \left\langle \Phi_{\mathbf{m}}^{(N\pm\kappa)} \left| \left[\hat{H}, \hat{A}_{\mathbf{n}}^{(\pm\kappa)} \right] \right| \Psi_{FANCI}^{(N)} \right\rangle \\ \mathbf{M} &= \left\langle \Phi_{\mathbf{m}}^{(N\pm\kappa)} \left| \hat{A}_{\mathbf{n}}^{(\pm\kappa)} \right| \Psi_{FANCI}^{(N)} \right\rangle \end{aligned}$$

where \mathbf{A} and \mathbf{M} are $m \times n$ matrices with $m > n$. This means that standard approaches where the spectrum is found based on diagonalization of a matrix ($\mathbf{M}^{-1}\mathbf{A}$) are not applicable.

The first method we considered was the minimal perturbation approach (MPA) procedure devised by Ito and Murota to find solutions to non-square matrix pencils like our eigenvalue problem [13]. This method consists of the following steps:

1. Define the matrix $[\mathbf{M}|\mathbf{A}]$ as the $m \times 2n$ matrix obtained by appending \mathbf{A} to \mathbf{M} .
2. Perform a singular value decomposition of $[\mathbf{M}|\mathbf{A}]$:

$$[\mathbf{M}|\mathbf{A}] = \mathbf{U}\mathbf{\Sigma}\mathbf{V}^\dagger \quad (3.3.6)$$

where $\mathbf{\Sigma}$ is the diagonal matrix of singular values, \mathbf{U} and \mathbf{V} are (complex) unitary matrices, and \mathbf{V}^\dagger is the conjugate transpose of \mathbf{V} . It is important to note that if the number of nonzero singular values is less than n it implies the FanEOM system of equations is underdetermined and can not be solved. (I.e., the projection space is too small and should be extended.)

3. Perform the partitioning:

$$\mathbf{U} = \begin{bmatrix} U_1 & U_2 \end{bmatrix}, \mathbf{V} = \begin{bmatrix} V_{11} & V_{12} \\ V_{21} & V_{22} \end{bmatrix}, \mathbf{\Sigma} = \begin{bmatrix} \Sigma_1 & 0 \\ 0 & \Sigma_2 \end{bmatrix} \quad (3.3.7)$$

where Σ_1 , V_{11} , V_{12} , V_{21} , and V_{22} are all $n \times n$ matrices; U_1 is an $m \times n$ matrix, U_2 is a $m \times m - n$ matrix and Σ_2 is an $m - n \times n$ matrix. Σ_1 and Σ_2 are diagonal matrices of singular values.

4. Finally, the desired eigenvalues and eigenvectors come from the solution to the square generalized eigenvalue problem,

$$V_{21}^\dagger \mathbf{C} = \Delta E_\lambda V_{11}^\dagger \mathbf{C} \quad (3.3.8)$$

The second approach, which we will label as BDagger method, consists of multiplying Eq. (5.4.2) on the left by a matrix to make it square. This can be an arbitrary $m \times n$ matrix, but the simplest choice is to consider the transpose of the metric \mathbf{M} , which results in:

$$\mathbf{M}^\dagger \mathbf{A} \mathbf{C} = \Delta E_\lambda \mathbf{M}^\dagger \mathbf{M} \mathbf{C} \quad (3.3.9)$$

This technique resembles the collocation method for numerical integration that has been used to obtain approximate solutions of the Schrödinger equation and other chemical physics problems [14, 15].

Finally, we examine the minimization of the least-squares solution with respect to the transition operator coefficients and energy:

$$\min_{\mathbf{C}, \Delta E_\lambda} \mathbf{C}^\dagger (\mathbf{A} + \Delta E_\lambda \mathbf{M})^\dagger (\mathbf{A} + \Delta E_\lambda \mathbf{M}) \mathbf{C} \quad (3.3.10)$$

which results in a square, symmetric, generalized eigenvalue problem:

$$\frac{(\mathbf{A}^\dagger \mathbf{M} + \mathbf{M}^\dagger \mathbf{A})}{2} \mathbf{C} = \Delta E_\lambda \mathbf{M}^\dagger \mathbf{M} \mathbf{C} \quad (3.3.11)$$

Among the strategies we consider, only the least-squares method gives a symmetric eigenproblem.

3.4 Computational considerations

To test the accuracy of the FanEOM framework previously described we studied the ionization and excitation energies of Beryllium and LiH systems using the 6-31G basis set [16–18]. These are small model systems for which accurate full configuration interaction (FCI) computations can be performed.

All excited state calculations were performed with our implementation of the FanEOM equations. The FCI ground state was obtained with our in-house package PyCI implementing the CI and FanCI problems [19]. The initial one- and two-electron integrals needed for the FanCI and FanEOM methods were generated from restricted Hartree-Fock calculations using PySCF [20, 21]. For comparison we used the ionization potentials and excitation energies obtained from our implementations of the extended Koopmans’ Theorem (EKT) and particle-hole extended random phase approximation (ERPA) methods, respectively, at the same level of theory.

Our procedure to solve the FanEOM equations for the ionized and excited states is as follows:

- Select the projection space. For the ionized states, the $(N - 1)$ configurations were generated applying the one-electron removal operators defining $\hat{Q}_\lambda^{(+1)}$,

Eq. 3.2.16, to a set of N -electron Slater determinants. This is in line with the usual approach used in EKT. For the excited states, single determinant N -electron configurations were generated as n th order excitations on top of the Hartree-Fock reference.

- Evaluate the matrices \mathbf{A} and \mathbf{M} defining the rectangular eigenvalue problem Eq. 5.4.2 using Eq. 3.2.9 for the $(N - 1)$ ionized states and Eq. 3.2.12 for the excited states. In the case of excited states, to facilitate numerical evaluation, the commutator operator in the left-hand-side matrix, \mathbf{A} , is expanded, and a resolution of the identity in the space of test functions, $\sum_{n \in P} |\Phi_n^N\rangle \langle \Phi_n^N|$, is introduced. This results in the following formula for the elements of \mathbf{A} :

$$\begin{aligned} A_{m,pq} &= \langle \Phi_m^N | \hat{H} a_p^\dagger a_q | \Psi_0^N \rangle - \langle \Phi_m^N | a_p^\dagger a_q \hat{H} | \Psi_0^N \rangle \\ &= \sum_{n \in P} \langle \Phi_m^N | \hat{H} | \Phi_n^N \rangle \langle \Phi_n^N | a_p^\dagger a_q | \Psi_0^N \rangle - E_0^N \langle \Phi_m^N | a_p^\dagger a_q | \Psi_0^N \rangle \end{aligned}$$

which depends on the Hamiltonian matrix elements between the determinants in the projection space and the one-electron transition density matrices (1-TDMs).

- Remove configurations from the projection space that have negligible transition matrix elements with the FanCI model as they can cause singularities in the metric matrix \mathbf{M} . To do so find the rows from matrix \mathbf{M} with magnitude below a cut-off value and eliminate them from \mathbf{A} and \mathbf{M} .
- For the ionized states, the procedure to generate test functions can result in duplicate Slater determinants being included; for example, a configuration with an electron removed from orbital i , $\Phi_i^{(N-1)}$, can be generated from the Hartree-Fock determinant as $a_i \Phi_0$ or from the excited determinant $\Phi_i^a = a_a^\dagger a_i \Phi_0$ as $a_a^\dagger \Phi_i^a$.

We remove these redundant elements from the projection space.

- Solve the rectangular eigenvalue problem using the BDagger, LS, or MPA method.

In the present work, a tolerance value of 10^{-7} was used with the BDagger and LS methods for the rectangular eigenvalue problem (Eq. 5.4.2). The same cut-off value was used when solving the EKT and ERPA equations. However, one must keep in mind that this value has different interpretation in the context of EKT versus the solution procedures in FanEOM. For instance, for EKT one removes eigenvectors of the 1-RDM with small eigenvalues; in the LS and BDagger approaches to FanEOM one removes right-eigenvectors of the transition-1RDM with small eigenvalues.

Similar to conventional EOM approaches with coupled cluster wavefunction models, FanEOM can suffer from spurious solutions, which can be difficult to identify. We identify these solutions by searching for transitions that are stable for different methods and different projection spaces.

3.5 Numerical illustrations

3.5.1 Ionization potentials

Tables 3.1 and 3.3 present ionization potentials for Beryllium and LiH obtained with the FanEOM approach as described in the previous sections. The aim is to illustrate the accuracy of the proposed method and to compare the three approaches to solve the FanEOM rectangular eigenvalue problem (MPA, BDagger, and LS). The showcased values correspond to the eigenstates found by using as test functions the

(N-1)-electron configurations generated from CISD. The EKT values at the same level of theory are also shown and taken as the accurate reference.

Table 3.1: Be ionization potentials (in Hartree) from FanEOM and EKT at the FCI/6-31G level of theory. The FanEOM projection space includes all unique one-electron removed configurations from the N-electron CISD model. Three procedures to solve the non-square matrix problem are compared, BDagger, LS and MPA. The transitions are labeled according to the main configuration from where the electron is removed

Label		1s2 2s1	1s2 2p1	1s2 3s1	1s1 2s2	MAE
FanEOM	BDagger	0.3375	0.4880	0.9283	4.6946	0.0023
	LS	0.3372	0.4879	0.9283	4.5298	0.0435
	MPA	–	0.4893	–	4.6574	0.0193
EKT		0.3376	0.4880	0.9373	4.6946	

Beryllium is a small system amenable to description at the FCI level while presenting important static correlation effects due to the near degeneracy of its 2s and 2p atomic orbitals. Furthermore, its ionized states are well characterized, making it an ideal test of the proposed framework. Table 3.1 displays its ionized states involving up to the 3s atomic orbital. As seen from this table, the correspondence between the FanEOM and EKT results is extremely good for this set of states, with the lowest mean absolute errors (MAEs) obtained using the BDagger procedure. In particular, the lowest IP described by BDagger and LS procedures, corresponding to an electron removed from the 2s orbital, matches EKT. Moreover, even for higher IPs, BDagger results reproduce those of EKT, except for the 1s2 3s IP where it underestimates its energy by about 0.01 Hartree. However, it is worth mentioning that transitions involving the 3s and 3p atomic orbitals are expected to be poorly described due to the limitations of the basis set being used. For the 3s orbital (third column in the table), the experimental ionization potential is 0.7446 Hartree [22], which is poorly

estimated even by EKT. On the other hand, all methods were found to miss the $1s2\ 3p1$ IP. It is also interesting to notice that, excluding the IP value for Beryllium $1s$ orbital (fourth column in the table), for which LS deviates about 0.2 Hartree from EKT, the LS method is as accurate as BDagger. On the other hand, the MPA procedure did not perform well, as it misses the lowest and the $1s2\ 3s1$ transitions. It is possible that one needs to project the eigenvalue problem using a threshold prior to implementing the MPA approach and it is also possible that the mathematical assumptions used when deriving the MPA approach are not valid for this generalized rectangular eigenproblem.

An important factor to consider for the FanEOM procedures is the influence of the selected test functions on the quality of the results. To analyze this aspect, we present the convergence of selected IPs for Be atom with the size of the projection space in Table 3.2. Convergence is assessed relative to results for projection on all $(N-1)$ -electron determinants. The results from the BDagger procedure are presented.

Table 3.2: Convergence with size of projection space (PSpace) of Be ionization potentials (in Hartree) from FanEOM at the FCI/6-31G level of theory. The eigenstates from BDagger procedure are shown. The MAE is given relative to the projection on the full space of $(N-1)$ -electron determinants. The transitions are labeled according to the main configuration from where the electron is removed

PSpace	Label				MAE
	1s2 2s1	1s2 2p1	1s2 3s1	1s1 2s2	
HF	0.3462			4.7016	0.0078
CIS	0.3374	0.4880	0.9201	4.6960	0.0047
CISD	0.3375	0.4880	0.9283	4.6946	0.0023
CISDT	0.3376	0.4880	0.9373	4.6946	0.0000
FCI	0.3376	0.4880	0.9373	4.6946	

The rows in Table 3.2 correspond to the projection space as determined by the

order of excitation in the CI expansion. In each case, single-electron-removed configurations are generated from the listed N -electron projection spaces. As one can see, at the triplet excitation order, all IPs agree with the corresponding FCI results. Evidently, the higher the number of test functions included the higher the computational cost of the method, and ideally one would like to reach a compromise between accuracy and the size of the projection space. Taking this fact into consideration, the spectrum from the CISD space can be considered as good as that from the triplet space with an overall MAE of 2.3 mHartree, with the main difference due to the $1s2\ 3s1$ ionization. Moreover, if only the lowest IP were of interest, even the test functions from CIS would suffice. As seen, for the $(N - 1)$ -electron test functions from Hartree-Fock, the spectrum resembles that of Koopmans' theorem, where only the $1s2\ 2s1$ and $1s1\ 2s2$ IPs are found. From this analysis we conclude that the CISD projections space produces good IP results, and we will use this projection space henceforth.

To evaluate the performance of the method in a molecular system, we study LiH. The five lowest ionization potentials of LiH, determined by FanEOM and EKT, are presented in Table 3.3. The transitions are labeled based on the symmetry of the molecular orbitals with the greatest contribution to the excited state. The ionization potentials of LiH are also properly described with FanEOM. Similar to the Beryllium system, both the BDagger and LS procedures show excellent agreement with EKT with differences less than 1 mHartree. The lowest ionization potential, associated with an electron removed from the 2σ molecular orbital (first column of values in the table), is accurately reproduced using the projection space based on CISD. Conversely, the MPA procedure provides a qualitative correct spectrum, capturing the first IP, but missing all other transitions below 1.3 Hartree. Interestingly, the

BDagger solution method fails to capture the ionization at 0.76 Hartree, which is associated with removing an electron from a 1π orbital.

Table 3.3: LiH ionization potentials (in Hartree) from FanEOM and EKT at the FCI/6-31G level of theory. The FanEOM projection space includes all unique one-electron removed configurations from CISD. Three procedures to solve the non-square matrix problem are compared, BDagger, LS and MPA. The transitions are labeled according to the symmetry of the orbital from where the electron is removed.

Label		2σ	3σ	1π	σ	σ
FanEOM	BDagger	0.2788	0.7435	–	0.9183	1.3902
	LS	0.2788	0.7435	0.7681	0.9183	1.3902
	MPA	0.2796	–	–	–	1.3738
EKT		0.2788	0.7435	0.7681	0.9185	1.3904

In summary, we find the proposed FanEOM framework, when combined with either the BDagger or LS solver methods, to be promising for evaluating IPs. In the next section, we will explore its potential application to excited states.

3.5.2 Excitation energies

FanEOM results for excited states also appear promising. Tables 3.4 and 3.5 show the lowest four and six excitation energies of Beryllium and LiH, respectively, obtained by solving the FCI problem with the 6-31G basis set (last row on the tables) and the corresponding values from the FanEOM and ERPA. The results from FanEOM with the BDagger and LS approaches correspond to the excitation energies found using a projection space truncated at the CISDT level. For the Be atom and LiH systems, the small size of the basis set means that when the CISD determinants are used, the system of equations is only slightly over-determined. Both FanEOM and ERPA use FCI ground state as the reference in the excited state wavefunction ansatz.

Table 3.4: Be excitation energies (in Hartree) from FanEOM, ERPA and FCI with 6-31G levels of theory. The FanEOM projection space is CISDT. The transitions are labeled by the leading configuration in the FCI solution and the multiplicity of the state indicated by the spin (S=0, singlet or S=1, triplet).

Label		S=1		S=0	
		1s2 2s 2p	1s2 2s 2p	1s2 2p2	1s2 2p2
FanEOM	BDagger	0.1053	0.2420	0.2852	0.3212
	LS	0.1053	0.2420	0.2852	0.3212
ERPA		0.1055	0.2429	–	–
FCI		0.1052	0.2417	0.2818	0.3169

Table 3.5: LiH excitation energies (in Hartree) from FanEOM, ERPA and FCI with 6-31G levels of theory. The FanEOM projection space is CISDT. The transitions are labeled by the symmetry of the orbitals in the leading FCI configuration and the multiplicity of the state indicated by the spin (S=0, singlet or S=1, triplet).

Label		S=1		S=0		S=1		S=0	
		$2\sigma^1 3\sigma^1$	$2\sigma^1 3\sigma^1$	$2\sigma^1 1\pi^1$	$2\sigma^1 1\pi^1$	$2\sigma^1 4\sigma^1$	$2\sigma^1 4\sigma^1$	$2\sigma^1 4\sigma^1$	$2\sigma^1 4\sigma^1$
FanEOM	Boys	0.1165	0.1433	–	–	–	–	–	0.2674
	LS	0.1165	0.1433	–	–	–	–	–	0.2674
ERPA		0.1041	0.1398	0.1481	0.1601	0.2174	0.2731	0.2731	0.2731
FCI		0.1037	0.1208	0.1473	0.1591	0.2174	0.2591	0.2591	0.2591

At the level of the basis set used in these numerical examples, Beryllium’s electronic transitions (Table 3.4) only involve up to the 3p shell of atomic orbitals. The lowest excited state predicted by the FanEOM method, corresponding to the triplet transition from the 2s to 2p orbital, closely matches the FCI result (see first column of values), with an absolute error of approximately 10^{-4} Hartree. The subsequent three higher excitation energies, ranging between 0.2 and 0.3 Hartree, are also qualitatively well-described. In contrast to the FanEOM results for IPs, the BDagger and LS strategies yield equivalent results in this case. Interestingly, the last two excitation energies above 0.24 Hartree were reproduced by the FanEOM method but not by ERPA. These higher energy transitions have double excitation character and, as can

be seen in the convergence Table 3.6, they are FanEOM solutions with all projection spaces.

Table 3.6: Convergence of Be excitation energies (in Hartree) with size of projection space (PSpace) computed with FanEOM at the FCI/6-31G level of theory. The eigenstates from BDagger method are shown. The transitions are labeled by the leading configuration in the FCI solution and the multiplicity of the state indicated by the spin (S=0, singlet or S=1, triplet).

PSpace	Label			
	S=1		S=0	
	1s2 2s 2p	1s2 2s 2p	1s2 2p2	1s2 2p2
CISD	0.1058	0.2427	0.2854	0.3214
CISDT	0.1053	0.2420	0.2852	0.3212
FCI	0.1053	0.2420	0.2850	0.3210

Our FanEOM approach can also produce good excitation energies for molecules, as illustrated in Table 3.5 for LiH. Similar to the Beryllium system, truncating the projection space at the CISDT level produces good agreement with the Full CI (or ERPA) results. However, the overall accuracy of the spectrum does deteriorates relative to Beryllium: for LiH the excitation energies relative to FCI are overestimated by about 0.01 Hartree. Additionally, a few intermediate energy transitions between 0.12 and 0.25 Hartree are missing with either the BDagger or LS solution algorithms.

3.6 Summary

We have presented an equation-of-motion (EOM) framework suitable for the FanCI ansatz (FanEOM) that extends its application to excited states properties. It involves the solution of a rectangular generalized eigenvalue problem, for which we proposed three solution algorithms, including an approach based on matrix pencils (MPA), an approach based on left-multiplying by the Hermitian conjugate of the metric

matrix (Bdagger), and least-squares solution of the eigenproblem (LS). Based on the performance assessment for the solution of the ionization and excited state FanEOM problems for Be and LiH, the BDagger and LS procedures work best. The LS rectangular eigenvalue problem solution method, has the added advantage that the final eigenvalue problem is symmetric. One advantage of FanEOM over traditional EOM and extended random phase approximation (ERPA) methods is that no killer condition is invoked; this may explain why FanEOM give slightly better excitations energies than ERPA in some cases. The killer condition could be imposed as additional constraint, which might improve the results further. The next step, however, would be to compare ERPA and FanEOM for approximate FanCI wavefunctions (e.g., antisymmetrized geminal products) and to explore whether there is an advantage to optimizing the FanCI parameters and the FanEOM coefficients simultaneously, as opposed to the current approach of using FanEOM as a post-processing step for FanCI calculations.

References

- [1] Taewon D Kim, Ramón Alain Miranda-Quintana, Michael Richer, and Paul W Ayers. Flexible ansatz for N -body configuration interaction. *Computational and Theoretical Chemistry*, 1202:113187, 2021.
- [2] Dmitry I. Lyakh, Monika Musiał, Victor F. Lotrich, and Rodney J. Bartlett. Multireference nature of chemistry: The coupled-cluster view. *Chemical Reviews*, 112(1):182–243, 2012. PMID: 22220988.
- [3] Peter A. Limacher, Paul W. Ayers, Paul A. Johnson, Stijn De Baerdemacker, Dimitri Van Neck, and Patrick Bultinck. A new mean-field method suitable for strongly correlated electrons: Computationally facile antisymmetric products of nonorthogonal geminals. *Journal of Chemical Theory and Computation*, 9:1394–1401, 2013. ISSN 15499618.
- [4] Peter A. Limacher. A new wavefunction hierarchy for interacting geminals. *The Journal of Chemical Physics*, 145:194102, 11 2016. ISSN 0021-9606.
- [5] Steven R. White. Density matrix formulation for quantum renormalization groups. *Physical Review Letters*, 69:2863–2866, 11 1992. ISSN 0031-9007.
- [6] Paul A. Johnson, Peter A. Limacher, Taewon D. Kim, Michael Richer,

- Ramón Alain Miranda-Quintana, Farnaz Heidar-Zadeh, Paul W. Ayers, Patrick Bultinck, Stijn De Baerdemacker, and Dimitri Van Neck. Strategies for extending geminal-based wavefunctions: Open shells and beyond. *Computational and Theoretical Chemistry*, 1116:207–219, 2017. ISSN 2210-271X. Understanding Chemistry and Biochemistry Using Computational Valence Bond Theory.
- [7] D. J. Rowe. Equations-of-motion method and the extended shell model. *Reviews of Modern Physics*, 40:153–166, 1968. ISSN 00346861.
- [8] Pratiksha B. Gaikwad, Taewon D. Kim, M. Richer, Rugwed A. Lokhande, Gabriela Sánchez-Díaz, Peter A. Limacher, Paul W. Ayers, and Ramón Alain Miranda-Quintana. Coupled cluster-inspired geminal wavefunctions. *The Journal of Chemical Physics*, 160(14):144108, 04 2024. ISSN 0021-9606.
- [9] Ramón Alain Miranda-Quintana, Taewon D. Kim, Rugwed A. Lokhande, M. Richer, Gabriela Sánchez-Díaz, Pratiksha B. Gaikwad, and Paul W. Ayers. Flexible ansatz for n-body perturbation theory. *The Journal of Physical Chemistry A*, 128(17):3458–3467, 2024. PMID: 38651558.
- [10] Vincent McKoy. *Methods of Electronic Structure Theory*, volume 21. Springer US, 1977. ISBN 978-1-4757-0889-9.
- [11] Koushik Chatterjee and Katarzyna Pernal. Excitation energies from extended random phase approximation employed with approximate one- and two-electron reduced density matrices. *The Journal of Chemical Physics*, 137:204109, 2012.
- [12] Yang Yang, Helen van Aggelen, and Weitao Yang. Double, rydberg and charge transfer excitations from pairing matrix fluctuation and particle-particle random

- phase approximation. *The Journal of Chemical Physics*, 139:224105, 12 2013. ISSN 0021-9606.
- [13] Shinji Ito and Kazuo Murota. An algorithm for the generalized eigenvalue problem for nonsquare matrix pencils by minimal perturbation approach. *SIAM Journal on Matrix Analysis and Applications*, 37:409–419, 1 2016. ISSN 0895-4798.
- [14] Samuel Francis Boys and John Wilfrid Linnett. Some bilinear convergence characteristics of the solutions of dissymmetric secular equations. *Proceedings of the Royal Society of London. A. Mathematical and Physical Sciences*, 309 (1497):195–208, 1969.
- [15] Sergei Manzhos, Manabu Ihara, and Tucker Carrington. Using collocation to solve the schrödinger equation. *Journal of Chemical Theory and Computation*, 19(6):1641–1656, 2023. PMID: 36974479.
- [16] R. Ditchfield, W. J. Hehre, and J. A. Pople. Self-Consistent Molecular-Orbital Methods. IX. An Extended Gaussian-Type Basis for Molecular-Orbital Studies of Organic Molecules. *The Journal of Chemical Physics*, 54(2):724–728, 01 1971. ISSN 0021-9606.
- [17] James D. Dill and John A. Pople. Self-consistent molecular orbital methods. XV. Extended Gaussian-type basis sets for lithium, beryllium, and boron. *The Journal of Chemical Physics*, 62(7):2921–2923, 04 1975. ISSN 0021-9606.
- [18] J. Stephen Binkley and John A. Pople. Self-consistent molecular orbital methods.

- XIX. Split-valence Gaussian-type basis sets for beryllium. *The Journal of Chemical Physics*, 66(2):879–880, 01 1977. ISSN 0021-9606.
- [19] Michelle Richer, Gabriela Sánchez-Díaz, Farnaz Heidar-Zadeh, Marco Martínez-González, Valerii Chuiko, and Paul W. Ayers. Pyci: A python-scriptable library for arbitrary determinant ci. Unpublished manuscript.
- [20] Qiming Sun, Timothy C Berkelbach, Nick S Blunt, George H Booth, Sheng Guo, Zhendong Li, Junzi Liu, James D McClain, Elvira R Sayfutyarova, Sandeep Sharma, et al. Pyscf: the python-based simulations of chemistry framework. *Wiley Interdisciplinary Reviews: Computational Molecular Science*, 8(1):e1340, 2018.
- [21] Qiming Sun, Xing Zhang, Samragni Banerjee, Peng Bao, Marc Barbry, Nick S Blunt, Nikolay A Bogdanov, George H Booth, Jia Chen, Zhi-Hao Cui, et al. Recent developments in the pyscf program package. *The Journal of Chemical Physics*, 153(2):024109, 2020.
- [22] A. Kramida, Yu. Ralchenko, J. Reader, and NIST ASD Team. Nist atomic spectra database (version 5.10), 2022. URL <http://physics.nist.gov/asd>.

Chapter 4

Dynamic correlation energy from extended random phase approximation approaches

4.1 Introduction

Accurate determination of electronic correlation energy is a cornerstone in the field of quantum chemistry. The challenge lies in the need to effectively account for both dynamic and static (multiconfiguration) electron correlations. Strong (or static) electron correlation is pervasive in next-generation materials (e.g., high-temperature superconductors and nonlinear optical materials, both of which typically include rare earth elements) and industrially important molecules like transition-metal catalysts [1–5]. For substances like these, the single reference wavefunction methods used in standard *ab initio* computational packages fail catastrophically. Therefore, their description requires the development of new/unconventional wavefunction forms such

as truncated or selected Configuration Interaction (CI) [6–8], geminal-based wavefunctions [9, 10], and matrix product states [11, 12]. However, while these models work well for strong electron correlation, they tend to miss the weak (dynamic) correlation that is required to make *quantitative* predictions for quantities like the critical temperature in a superconductor or the Curie temperature in a molecular magnet.

Recently, a promising approach for recovering dynamic correlation has emerged, based on the extension of the adiabatic connection (AC) framework to correlated wavefunction models [13]. This formulation allows interpolation between a non- or partially-interacting system described by a multireference approximation and the real, fully interacting, system. Historically, the AC formulation has been used by the density functional theory (DFT) community to develop exchange-correlation functionals. In DFT a non-interacting system is described by Kohn-Sham DFT and one interpolates with respect to increasing electron-electron interaction strength, at constant electron density, until the physical fully-interacting system is reached.[14, 15].

AC facilitates the derivation of analytic expressions for the correlation energy. The main ingredient in any AC formulation is the response function (or equivalently, the transition density matrices), which can be obtained by solving the (extended) random phase approximation equation ((E)RPA). This has paved the way for developing AC-ERPA based methods for adding dynamic correlation to the ground state of general multireference models such as the generalized valence bond, complete active space and matrix product states wavefunction ansätze [16–20]. Since AC-ERPA methods require only the one- and two-electron reduced density matrices (RDMs) for the reference system, its cost is comparable to other dynamic correlation techniques such

as those based on second-order perturbation theory [21, 22]. However, as AC-ERPA is nonperturbative, it is potentially more accurate.

The above-mentioned ERPA approach corresponds to the particle-hole ERPA (ph-ERPA). The ph-ERPA methodology is an extension of the particle-hole random phase approximation (ph-RPA) [23–25], where correlation effects are described in terms of density fluctuations resulting from particle-hole pair excitations. Based on Rowe’s equation-of-motion formalism (EOM), Chatterjee and Pernal developed ERPA for correlated wavefunction approximations [26]. Analogous to ph-RPA, ERPA has a dual role as cost-effective electronic structure method for predicting excited state properties of molecules [26, 27] and a ground state electron correlation method.

Despite its utility, the particle-hole channel is not the sole avenue for approximating the correlation energy. Other channels, such as hole-hole (hh, corresponding to two-electron removal) and particle-particle (pp, corresponding to two-electron addition), have also been explored, albeit solely within the Hartree-Fock (HF) and DFT approximations. In these cases, the creation of two holes (or two electrons) results in pairing density matrix fluctuations from which the correlation energy can be derived. Yang and collaborators developed an AC formalism in the traditional single-reference theory based on these variants, denominated pp-RPA [28]. Their method overcame limitations present in the particle-hole RPA approach, such as the one-electron self-interaction energy, yielding promising results in the description of thermodynamic properties and molecular non-bonded interactions.[29]

Nothing is known about the accuracy of the hole-hole and particle-particle approximations in the AC approach to dynamic correlation. Thus, in this work, an analogous multireference AC for the hh/pp channel is formulated following the ideas in the

original AC-ERPA works. Like the current AC-ERPA methods the new ones should require only low-order reduced density matrices from the reference system.

The chapter is structured as follows: Section 4.2 revisits the derivation of the correlation energy correction using the adiabatic connection approach and discusses various factorizations of the 2-RDM. Following this, Section 4.4 presents the formulations of ERPA for both particle-hole and hole-hole/particle-particle channels, expressed in terms of reduced density matrices. Section 4.6 gives more specific AC formulas for Hartree-Fock and double occupied configuration interaction (DOCI) methods. Finally, Section 4.8 presents illustrative numerical results for the hh/pp-AC-ERPA methods' performance and highlights some of the differences relative to AC-ERPA in the particle-hole channel.

4.2 Correlation energy from the adiabatic connection

Assume we know the exact wavefunction $|\Phi_\nu\rangle$ and energy E_ν^0 of some (model) Hamiltonian \hat{H}^0 for a non-interacting or partially interacting reference system:

$$\hat{H}^0 |\Phi_\nu\rangle = E_\nu^0 |\Phi_\nu\rangle \quad (4.2.1)$$

We assume that the targeted reference state is a good approximation to the eigenstate of interest, $|\Psi_\nu\rangle$, for the exact Hamiltonian for the system, \hat{H} , for which:

$$\hat{H} |\Psi_\nu\rangle = E_\nu |\Psi_\nu\rangle \quad (4.2.2)$$

For example, $|\Phi_\nu\rangle$ could come from the Hartree-Fock (HF) or a post HF wavefunction model. We will mainly be interested in the ground-state, $\nu = 0$, but this formulation

is equally applicable to excited states, although technical nuances arise [30–32].

Our goal is to add the electron correlation effects that $|\Phi_\nu\rangle$ lacks because of the missing terms in \hat{H}^0 and, specifically, to determine the residual correlation energy, $\Delta E_\nu = E_\nu - E_\nu^0$. To achieve this, we take inspiration from perturbation theory and define a Hamiltonian that depends on a parameter, λ , which interpolates between the model Hamiltonian and the real/fully interacting one as the parameter smoothly increases from 0 to 1. Specifically,

$$\hat{H}^\lambda = \sum_{pq} h_{pq}^\lambda a_p^\dagger a_q + \frac{1}{2} \sum_{pqrs} g_{pqrs}^\lambda a_p^\dagger a_q^\dagger a_s a_r \quad (4.2.3)$$

where h_{pq}^λ and g_{pqrs}^λ are the one- and two-electron integrals at a given λ ; a_p^\dagger and a_q are the fermionic creation and annihilation operators, and the indexes p, q, r, s label an arbitrary spin-orbital. For simplicity, we decided to let the Hamiltonian's matrix elements depend linearly on λ :

$$\begin{aligned} h_{pq}^\lambda &= h_{pq}^{\lambda=0} + \lambda(h_{pq}^{\lambda=1} - h_{pq}^{\lambda=0}) \\ g_{pqrs}^\lambda &= g_{pqrs}^{\lambda=0} + \lambda(g_{pqrs}^{\lambda=1} - g_{pqrs}^{\lambda=0}) \end{aligned} \quad (4.2.4)$$

where the two-electron integrals $g_{pqrs}^{\lambda=1}$ are defined in physicist's notation as:

$$g_{pqrs}^{\lambda=1} = g_{pqrs} = \langle pq|rs\rangle$$

At $\lambda = 0$ we have the eigenstate of the non- or partially-interacting system, $\Psi_0^{\lambda=0} = \Phi_0$, with energy $E_0^{\lambda=0} = E_0^0$, and at $\lambda = 1$, we have a (necessarily approximate) eigenstate of the fully correlated one, $\Psi_0^{\lambda=1} = \Psi_0$, with $E_0^{\lambda=1} = E_0$.

The ground state energy of \hat{H}^λ can be expressed as a functional of the one- and two-electron reduced density matrices, γ^λ (1-RDM) and Γ^λ (2-RDM), respectively:

$$E_0^\lambda = \langle \Psi_0^\lambda | \hat{H}^\lambda | \Psi_0^\lambda \rangle = \sum_{pq} h_{pq}^\lambda \gamma_{pq}^\lambda + \frac{1}{2} \sum_{pqrs} g_{pqrs}^\lambda \Gamma_{pqrs}^\lambda \quad (4.2.5)$$

where the matrix elements γ_{pq}^λ and Γ_{pqrs}^λ have the usual definitions:

$$\gamma_{pq}^\lambda = \langle \Psi_0^\lambda | a_p^\dagger a_q | \Psi_0^\lambda \rangle \quad (4.2.6)$$

$$\Gamma_{pqrs}^\lambda = \langle \Psi_0^\lambda | a_p^\dagger a_q^\dagger a_s a_r | \Psi_0^\lambda \rangle \quad (4.2.7)$$

Then, using the Hellmann-Feynman theorem, $\frac{\partial E_0^\lambda}{\partial \lambda} = \langle \Psi_0^\lambda | \frac{\partial \hat{H}^\lambda}{\partial \lambda} | \Psi_0^\lambda \rangle$, we obtain an expression for the correction to the ground state energy of the model system:

$$\begin{aligned} E_0^{\lambda=1} - E_0^{\lambda=0} &= \int_0^1 \frac{\partial E_0^\lambda}{\partial \lambda} d\lambda \\ &= \int_0^1 d\lambda \sum_{pq} \frac{dh_{pq}^\lambda}{d\lambda} \gamma_{pq}^\lambda + \frac{1}{2} \int_0^1 d\lambda \sum_{pqrs} \frac{dg_{pqrs}^\lambda}{d\lambda} \Gamma_{pqrs}^\lambda \end{aligned} \quad (4.2.8)$$

$$= \sum_{pq} (h_{pq}^{\lambda=1} - h_{pq}^{\lambda=0}) \int_0^1 \gamma_{pq}^\lambda d\lambda + \frac{1}{2} \sum_{pqrs} \int_0^1 (g_{pqrs}^{\lambda=1} - g_{pqrs}^{\lambda=0}) \Gamma_{pqrs}^\lambda d\lambda \quad (4.2.9)$$

where in the last line, the definition of the AC Hamiltonian electron integrals, Eq. (4.2.4), was used.

To make further progress, we introduce the assumption that the zeroth order wavefunction, $\Psi_0^{\lambda=0}$, is a good model for static correlation. Therefore, the 1-RDM already has the correct structure and can be assumed to remain (nearly) constant along the adiabatic connection path. The *assumption* that $\gamma^\lambda = \gamma^{\lambda=0}$ in the interval $0 \leq \lambda \leq 1$ is the first approximation in the derivation of the AC-ERPA approach.

With this approximation, the expression for the ground state energy of the fully interacting system simplifies to:

$$E_0^{\lambda=1} = E_0^{\lambda=0} + \sum_{pq} (h_{pq}^{\lambda=1} - h_{pq}^{\lambda=0}) \gamma_{pq}^{\lambda=0} + \frac{1}{2} \sum_{pqrs} \int_0^1 (g_{pqrs}^{\lambda=1} - g_{pqrs}^{\lambda=0}) \Gamma_{pqrs}^{\lambda} d\lambda \quad (4.2.10)$$

Alternatively, we can write an explicit expression for the correlation energy:

$$E_c = E_0^{\lambda=1} - \langle \Psi_0^{\lambda=0} | \hat{H}^{\lambda=1} | \Psi_0^{\lambda=0} \rangle = \frac{1}{2} \sum_{pqrs} \int_0^1 (g_{pqrs}^{\lambda=1} - g_{pqrs}^{\lambda=0}) (\Gamma_{pqrs}^{\lambda} - \Gamma_{pqrs}^{\lambda=0}) d\lambda \quad (4.2.11)$$

To derive this expression, we use the equation for the expectation value of the real Hamiltonian using the (partially) non-interacting reference wavefunction $\Psi_0^{\lambda=0}$. The last term in parenthesis in Eq. (4.2.11) is the correlation part of the 2-RDM; had we not assumed that the 1-RDM was constant along the adiabatic connection pathway there would be a second, similar, term corresponding to the correlation part of the 1-RDM, $(\gamma_{pq}^{\lambda} - \gamma_{pq}^{\lambda=0})$. For simplicity, hereon, the notation γ_{pq} will be used instead of $\gamma_{pq}^{\lambda=0}$.

Eq. (4.2.11) (or equivalently (4.2.10)) is the main equation of the AC method. It provides an explicit expression for the correlation energy of the ground state as a function of a λ -dependent 2-RDM. So far, the only approximation is the assumption that the 1-RDM remains constant along λ integration path. While this expression for the correlation energy is not exact, it will provide very accurate correlation energies provided the Γ^{λ} at every λ are known. However, approximating this density matrix is challenging. As we shall see in the next section, the need to approximate a four index operator matrix can be circumvented by introducing a resolution of the identity into the definition of the 2-RDM.

4.3 Exact two-electron reduced density matrix formulas

In the previous section, the AC approach was used to add the (dynamic) electron correlation that is missed when an approximate Hamiltonian is used, see (Eq. (4.2.11)). The resulting expression is only computationally practical if one can efficiently evaluate, yet accurately, approximate the interaction-strength dependent 2-RDM. In this section, we present three distinct ways to achieve this, based on different factorizations of the 2-RDM.

Before delving into the derivations, we note that the 2-RDM expressions presented here can also be obtained starting from the polarization propagator [33, 34] and the particle-particle propagator [28] via the fluctuation dissipation theorem. However, we prefer the following approach, where exact expressions for the 2-RDM are obtained from the 1-RDM and transition RDMs, using only the commutation laws for the fermionic creation and annihilation operators and the completeness of the eigenfunctions of a Hermitian operator, which we choose to be the Hamiltonian.

Using the fundamental anticommutation properties of the spin-orbital creation and annihilation operators:

$$\{a_p a_q + a_q a_p\} = 0 \quad (4.3.1)$$

and

$$\{a_p^\dagger a_q + a_q a_p^\dagger\} = \delta_{pq} \quad (4.3.2)$$

the 2-RDM, Eq. (4.2.7), can be rewritten in terms of the two-electron G-matrix, with

elements $\langle \Psi_0 | a_p^\dagger a_r a_s^\dagger a_q | \Psi_0 \rangle$:

$$\Gamma_{pqrs} = -\Gamma_{pqsr} = \langle \Psi_0 | a_p^\dagger a_r a_s^\dagger a_q | \Psi_0 \rangle - \delta_{ps} \gamma_{qr} \quad (4.3.3)$$

From here, the McLachlan and Ball formula for the 2-RDM [33] can be derived introducing a resolution of the identity in the space of N-electron states, $\hat{\mathbf{1}} = \sum_n |\Psi_n^\lambda\rangle \langle \Psi_n^\lambda|$:

$$\begin{aligned} \Gamma_{pqrs}^{ph;\lambda} &= \sum_n^\infty \langle \Psi_0^\lambda | a_p^\dagger a_r | \Psi_n^\lambda \rangle \langle \Psi_n^\lambda | a_s^\dagger a_q | \Psi_0^\lambda \rangle - \delta_{ps} \gamma_{qr} \\ &= \sum_{n \neq 0}^\infty \langle \Psi_0^\lambda | a_p^\dagger a_r | \Psi_n^\lambda \rangle \langle \Psi_n^\lambda | a_s^\dagger a_q | \Psi_0^\lambda \rangle + \gamma_{pr} \gamma_{qs} - \delta_{ps} \gamma_{qr} \end{aligned} \quad (4.3.4)$$

Notice that in the second line of this equation, the sum runs over all but the ground state. The matrix elements $\langle \Psi_0^\lambda | a_p^\dagger a_q | \Psi_n^\lambda \rangle$, correspond to the one-electron transition density matrices (1-TDM) and represent the transition probabilities between the ground state, $|\Psi_0^\lambda\rangle$, and *all* the excited states, $|\Psi_n^\lambda\rangle$. Given that the 2-RDM is being factorized in terms of two-index operators of the form $a_p^\dagger a_q$, corresponding to removing and adding one electron from the ground state, this formula is labeled as the particle-hole resolution, $\Gamma_{pqrs}^{ph;\lambda}$.

However, the previous partitioning of the 2-RDM is not the only choice. An alternative expression can be derived in terms of transition matrix elements between the ground and double ionized states $|\Psi_{N-2;n}^\lambda\rangle$:

$$\langle \Psi_0^\lambda | a_p^\dagger a_q^\dagger | \Psi_{N-2;n}^\lambda \rangle = (\langle \Psi_{N-2;n}^\lambda | a_q a_p | \Psi_0^\lambda \rangle)^\dagger \quad (4.3.5)$$

Starting from the definition of the 2-RDM and applying a resolution of the identity in the space of two-electron removed states, $\hat{\mathbf{1}} = \sum_n |\Psi_{N-2;n}^\lambda\rangle \langle \Psi_{N-2;n}^\lambda|$, results in the

equation:

$$\Gamma_{pqrs}^{hh;\lambda} = \langle \Psi_0^\lambda | a_p^\dagger a_q^\dagger a_s a_r | \Psi_0^\lambda \rangle = \sum_{n=0}^{\infty} \langle \Psi_0^\lambda | a_p^\dagger a_q^\dagger | \Psi_{N-2;n}^\lambda \rangle \langle \Psi_{N-2;n}^\lambda | a_s a_r | \Psi_0^\lambda \rangle \quad (4.3.6)$$

This 2-RDM decomposition is labeled as the hole-hole resolution, $\Gamma_{pqrs}^{hh,\lambda}$, given that the lower order matrices have two-index operators of the form $a_p a_q$, corresponding to removing two electrons from the ground state.

Another formulation is based on the linear relation between the 2-RDM and the Q-matrix, $\langle \Psi_0 | a_p a_q a_s^\dagger a_r^\dagger | \Psi_0 \rangle$:

$$\begin{aligned} \Gamma_{pqrs} &= \Gamma_{srqp} \\ &= \langle \Psi_0 | a_s^\dagger a_r^\dagger a_p a_q | \Psi_0 \rangle \\ &= \langle \Psi_0 | a_p a_q a_s^\dagger a_r^\dagger | \Psi_0 \rangle + \delta_{pr} \gamma_{qs} + \delta_{qs} \gamma_{pr} - \delta_{ps} \gamma_{qr} - \delta_{qr} \gamma_{ps} - \delta_{pr} \delta_{qs} + \delta_{ps} \delta_{qr} \end{aligned} \quad (4.3.7)$$

where the 2-RDM permutation symmetries and the anticommutation rules in Eq. (4.3.1) and (4.3.2) were used. Then, starting from the third line in above expression and applying a resolution of identity in the basis of $(N+2)$ -electron states, $\hat{\mathbf{1}} = \sum_n |\Psi_{N+2;n}^\lambda\rangle \langle \Psi_{N+2;n}^\lambda|$, the 2-RDM can be written in terms of the transition matrices of the form $\langle \Psi_0^\lambda | a_p a_q | \Psi_{N+2;n}^\lambda \rangle$:

$$\begin{aligned} \Gamma_{pqrs}^{pp,\lambda} &= \sum_{n=0}^{\infty} \langle \Psi_0^\lambda | a_p a_q | \Psi_{N+2;n}^\lambda \rangle \langle \Psi_{N+2;n}^\lambda | a_s^\dagger a_r^\dagger | \Psi_0^\lambda \rangle \\ &\quad + \delta_{pr} \gamma_{qs} + \delta_{qs} \gamma_{pr} - \delta_{ps} \gamma_{qr} - \delta_{qr} \gamma_{ps} - \delta_{pr} \delta_{qs} + \delta_{ps} \delta_{qr} \end{aligned} \quad (4.3.8)$$

Consistent with the notation for the other 2-RDM partitioning, this 2-RDM equation is labeled as the particle-particle resolution, $\Gamma_{pqrs}^{pp,\lambda}$, since the transition matrices that

appear have two-index operators of the form $a_p^\dagger a_q^\dagger$, corresponding to adding two electrons to the ground state.

Thus, the evaluation of the two-electron density matrix, $\mathbf{\Gamma}^\lambda$, that enters the AC expression, Eq. (4.2.11), can be factorized in terms of lower-rank transition density matrices for excitation (transition-1RDM) and double ionization. The three formulas, Eq. (4.3.4), (4.3.6) and (4.3.8), are exact and equivalent provided the TDMs in the equations are known exactly. The problem becomes the ability to obtain the TDMs for the complete set of excited states.

4.4 ERPA approximated 2-RDMs

Using these 2-RDM expressions to evaluate the correlation energy via the adiabatic connection requires computing the appropriate transition density matrices for *all* excited states along the *entire* adiabatic connection path. Traditionally, the RPA equations have been used for this purpose, providing first-order approximations to the TDMs for HF and DFT methods. Here we focus on how these methods can be extended to correlation wavefunction models.

4.4.1 Particle-hole ERPA

To find the one-electron transition density matrices, $\langle \Psi_0^\lambda | a_p^\dagger a_q | \Psi_n^\lambda \rangle$, that enter Eq. (4.3.4) for the 2-RDM, one needs to model N -electron excited states. This can be achieved using the equation of motion (EOM) approach and, specifically, the particle-hole ERPA equations. This approach is approximate because (a) the excited states are computed only approximately, because the transition operator is truncated at the

particle-hole level, (b) the killer condition is assumed to hold, and (c) the 1-RDM and 2-RDM of the reference (non)interacting system are used to model excited states along the AC path. When the reference is the (noninteracting) Hartree-Fock method, this approach reduces to ph-RPA. When a correlated wavefunction is used, one obtains the λ -dependent ph-ERPA equation introduced by Pernal [13].

Like the original ph-ERPA formulation [26], the derivation of the perturbation strength dependent ph-ERPA equation follows from Rowe’s Equation-of-Motion method [35], whereby the n th electronic excited state, $|\Psi_n^\lambda\rangle$, can be generated from all possible single electron excitations from the ground state:

$$|\Psi_n^\lambda\rangle = \sum_{pq} c_{pq;n}^\lambda a_p^\dagger a_q |\Psi_0^\lambda\rangle \quad (4.4.1)$$

where the excited state dependence in the coupling parameter is being included through the reference state, $|\Psi_0^\lambda\rangle$. The transition amplitudes, $c_{pq;n}^\lambda$, are then determined solving an eigenvalue problem of the form:

$$\mathbf{A}^\lambda \mathbf{C}_n^\lambda = \omega_n^\lambda \mathbf{M}^\lambda \mathbf{C}_n^\lambda \quad (4.4.2)$$

where the elements of the left-hand-side matrix \mathbf{A}^λ and metric matrix \mathbf{M}^λ are defined as:

$$\begin{aligned} A_{pqrs}^\lambda &= \langle \Psi_0^\lambda | [a_p^\dagger a_q, [\hat{H}^\lambda, a_s^\dagger a_r]] | \Psi_0^\lambda \rangle \\ M_{pqrs}^\lambda &= \langle \Psi_0^\lambda | [a_p^\dagger a_q, a_s^\dagger a_r] | \Psi_0^\lambda \rangle \end{aligned} \quad (4.4.3)$$

Notice that in the nested commutator matrix \mathbf{A}^λ , the real Hamiltonian is replaced by

the AC one H^λ . The solutions to this matrix equation, ω_n^λ , come in (mirrored) pairs with energies equal in magnitude but with opposite sign; positive transitions, $\omega_n^\lambda > 0$ with eigenvectors \mathbf{C}_n^λ correspond to single electron excitations, $\omega_n^\lambda = E_n^\lambda - E_0^\lambda$, and negative ones, $\omega_{-n}^\lambda < 0$, with \mathbf{C}_{-n}^λ , to de-excitations, $\omega_{-n}^\lambda = -\omega_n^\lambda$.

The matrices \mathbf{A}^λ and \mathbf{M}^λ can be expressed entirely in terms of the Hamiltonian electron integrals and the 1- and 2-RDMs [26]. For clarity, here we provide the formula for the matrix elements of \mathbf{M}^λ as illustration:

$$M_{pq,rs}^\lambda = \delta_{qs} \gamma_{pr}^\lambda - \delta_{pr} \gamma_{qs}^\lambda \quad (4.4.4)$$

Equation (4.4.2) then provides a general formulation applicable to multideterminant wavefunction methods without making explicit reference to an occupied-virtual orbital picture; this extends particle-hole RPA approaches beyond the Slater determinant wavefunctions [36].

However, at every λ value along the AC path, evaluating the λ -dependent ERPA matrix elements, Eq. (4.4.3), requires knowledge of the 1- and 2-RDMs. However, only the RDMs for the model system (at $\lambda = 0$) are known exactly. For practical reasons, we assume that it is sufficient to include only the Hamiltonian needs to depend on the coupling parameter, while the reference system's wavefunction can be used in Eq. (4.4.3) (i.e. $|\Psi_0^\lambda\rangle = |\Psi_0^{\lambda=0}\rangle \quad \forall \lambda$).

Then, from the solutions to the ph-ERPA eigenvalue problem, Eq. (4.4.2), the desired 1-TDMs at a given λ can be obtained as:

$$\langle \Psi_0^\lambda | a_p^\dagger a_r | \Psi_n^\lambda \rangle \approx \sum_{ij} c_{ij;n}^\lambda \langle \Psi_0^{\lambda=0} | [a_p^\dagger a_r, a_j^\dagger a_i] | \Psi_0^{\lambda=0} \rangle = \sum_{ij} c_{ij;n}^\lambda M_{pr,ij}^{\lambda=0} \quad (4.4.5)$$

where the EOM definition of the excited state, Eq. (4.4.1), is considered and the elements of the metric matrix $\mathbf{M}^{\lambda=0}$ are given by Eq. (4.4.4). Consistent with the orthogonality between the ground and excited states, the diagonal elements of this transition matrix, $\langle \Psi_0^\lambda | a_p^\dagger a_p | \Psi_n^\lambda \rangle$, will be zero. From Eq. (4.4.4) it follows that the metric matrix does not change with λ , hence, for simplicity, \mathbf{M} will be used instead of $\mathbf{M}^{\lambda=0}$ hereon.

Inserting the 1-TDM, Eq.(4.4.5), into Eq.(4.3.4) for the 2-RDM, and considering the transition matrix elements given by:

$$(\langle \Psi_0^\lambda | a_p^\dagger a_r | \Psi_n^\lambda \rangle)^\dagger = \langle \Psi_n^\lambda | a_r^\dagger a_p | \Psi_0^\lambda \rangle \quad (4.4.6)$$

leads to an explicit formula in terms of the excited state coefficients and the natural-spin-orbital occupation numbers in the reference state $|\Psi_0^{\lambda=0}\rangle$:

$$\Gamma_{pqrs}^{phERP A;\lambda} = \sum_{n \neq 0} (n_p - n_r)(n_q - n_s) c_{pr;n}^\lambda c_{qs;n}^\lambda + n_p n_q \delta_{pr} \delta_{qs} - n_q \delta_{ps} \delta_{qr} \quad (4.4.7)$$

Here, for convenience, the natural spin-orbital basis in which the 1-RDM is diagonal was used, as it simplifies the final expression. As can be seen from this expression for the 2-RDM expression, the transitions that contribute to the sum in the first term are those involving (partially) occupied to (partially) virtual orbitals, (e.g., $(n_p - n_q) \neq 0$, with $n_p \approx 1$ and $n_q \approx 0$). It is important to note that only solutions from the positive side of the spectrum (excitations) enter the sum in this equation. Furthermore, these solutions must be orthonormal, satisfying the condition $\mathbf{C}_n^\lambda \mathbf{M} \mathbf{C}_n^\lambda = \mathbf{I}$. Additionally, although the 2-RDMs obtained through this approach have the right norm for the number of electron pairs ($\sum_{pq} \Gamma_{pqpq} = N(N-1)$), they do not have the right symmetry

properties, and therefore they are not N-representable.

To close this section we reiterate the main approximations that were introduced, namely, (a) the 1-RDM is constant along the adiabatic connection pathway, (b) excitation operators of only first order are enough to adequately approximate the sum over excited states $|\Psi_n^\lambda\rangle$, Eq. (4.4.1), and (c) the ERPA equations evaluated with the 1-RDM and 2-RDM at $\lambda = 0$ are good enough to determine the transition 1-RDMs for interacting systems. As we shall now see, analogous approximations can be made for the hole-hole and particle-particle channels of (extended) RPA.

4.4.2 Hole-hole ERPA

Instead of using particle-hole ERPA to approximate the 2-RDM, one can use the hole-hole ERPA method to estimate the pair-removal transition density matrix elements at every λ value, $\langle\Psi_0^\lambda|a_p^\dagger a_q^\dagger|\Psi_{N-2;n}^\lambda\rangle$, then evaluate the 2-RDM using Eq. (4.3.6). Similar to ph-ERPA, if the Hartree-Fock reference wavefunction is used, the pp-RPA method is recovered.

The hh-ERPA equation as a function of λ can be derived via the EOM approach assuming the double ionized states, $|\Psi_{N-2;n}^\lambda\rangle$, can be generated from the ground state, $|\Psi_0^\lambda\rangle$, by a linear combination of two-electron removing operators:

$$|\Psi_{N-2;n}^\lambda\rangle = \sum_{pq} c_{pq;n}^\lambda a_p a_q |\Psi_0^\lambda\rangle \quad (4.4.8)$$

The complex conjugate of this operator, $(\hat{Q}_n^\lambda)^\dagger$, gives instead the double electron

attached states $|\Psi_{N+2;n}^\lambda\rangle$:

$$|\Psi_{N+2;n}^\lambda\rangle = \sum_{pq} c_{pq;n}^\lambda a_p^\dagger a_q^\dagger |\Psi_0^\lambda\rangle \quad (4.4.9)$$

The corresponding hh-ERPA eigenvalue equation at a given λ value is expressed as:

$$\mathbf{A}^\lambda \mathbf{C}_n^\lambda = \omega_n^\lambda \mathbf{M} \mathbf{C}_n^\lambda \quad (4.4.10)$$

where the elements of the left-hand-side matrix \mathbf{A}^λ and the metric matrix \mathbf{M} are given by:

$$\begin{aligned} A_{pqrs}^\lambda &= \langle \Psi_0^{\lambda=0} | [a_p^\dagger a_q^\dagger, [\hat{H}^\lambda, a_s a_r]] | \Psi_0^{\lambda=0} \rangle \\ M_{pqrs} &= \langle \Psi_0^{\lambda=0} | [a_p^\dagger a_q^\dagger, a_s a_r] | \Psi_0^{\lambda=0} \rangle \end{aligned} \quad (4.4.11)$$

Here, the indices p, q, r, s label arbitrary spin-orbitals. As with ph-ERPA, the AC Hamiltonian, \hat{H}^λ , and the zeroth-order ground state approximation, $|\Psi_0^{\lambda=0}\rangle$, are used instead of the actual Hamiltonian and ground state wavefunction. Thus the dependence on the perturbation strength is modelled only through the Hamiltonian operator.

As with the particle-hole counterpart, the matrices \mathbf{A}^λ and \mathbf{M} can be approximated

as functions of the 1- and 2-RDMs of the reference state:

$$\begin{aligned}
A_{pqrs}^\lambda &= 2(-h_{rq}^\lambda \delta_{sp} + h_{rp}^\lambda \delta_{sq} + h_{sp}^\lambda \gamma_{qr} - h_{sq}^\lambda \gamma_{pr}) + 2 \sum_t h_{rt}^\lambda (\delta_{sp} \gamma_{qt} - \delta_{sq} \gamma_{pt}) \\
&+ v_{rspq}^\lambda + \sum_t (v_{rsqt}^\lambda \gamma_{pt} - v_{rspt}^\lambda \gamma_{qt}) + 2 \sum_t v_{trpq}^\lambda \gamma_{ts} + 2 \sum_{tu} (v_{stup}^\lambda \delta_{qr} + v_{stqu}^\lambda \delta_{pr}) \gamma_{tu} \\
&+ 2 \sum_{tu} (v_{rtup}^\lambda \Gamma_{tqus}^{\lambda=0} + v_{rtqu}^\lambda \Gamma_{tpus}^{\lambda=0}) + \sum_{tuv} v_{truv}^\lambda (\delta_{ps} \Gamma_{tquv}^{\lambda=0} - \delta_{qs} \Gamma_{tpuv}^{\lambda=0}) \\
M_{pqrs} &= \delta_{sp} (\delta_{rq} - \gamma_{qr}) - \delta_{sq} (\delta_{rp} - \gamma_{pr}) - \delta_{rq} \gamma_{ps} + \delta_{rp} \gamma_{qs}
\end{aligned} \tag{4.4.12}$$

where the elements $v_{pqrs}^\lambda = g_{pqrs}^\lambda - g_{pqsr}^\lambda$, are antisymmetrized two electron integrals and, for simplicity of notation, we have taken $\gamma_{pq}^{\lambda=0} = \gamma_{pq}$, omitting the 1-RDM dependence on the coupling parameter. For hh-ERPA the matrix \mathbf{A}^λ represents the stability of the wavefunction with respect to double electron removal (or addition) and for molecular systems will be positive semi-definite, guaranteeing real solutions [29]. This is in contrast with ph-ERPA where orbital rotation instabilities can frequently emerge (e.g., due to orbital near-degeneracies).

The eigenvalues obtained from Eq. (4.4.10) form two sets depending on their sign; positive solutions $\omega_n^\lambda > 0$ are double ionization energies producing $(N - 2)$ states, $\omega_n^\lambda = E_n^{(N-2);\lambda} - E_0^{\lambda=0}$, while negative ones $\omega_{-n}^\lambda < 0$ correspond to double electron additions for the $(N + 2)$ states, $\omega_{-n}^\lambda = -(E_n^{(N+2);\lambda} - E_0^{\lambda=0})$. Their corresponding eigenvectors satisfy the orthonormality conditions $\mathbf{C}_n^\lambda \mathbf{M} \mathbf{C}_n^\lambda = \mathbf{I}$ and $\mathbf{C}_{-n}^\lambda \mathbf{M} \mathbf{C}_{-n}^\lambda = -\mathbf{I}$.

Then, the transition pairing matrix elements can be approximated as:

$$\langle \Psi_0^\lambda | a_p^\dagger a_q^\dagger | \Psi_{N-2;n}^\lambda \rangle \approx \sum_{rs} c_{rs;n}^\lambda \langle \Psi_0^{\lambda=0} | [a_p^\dagger a_q^\dagger, a_s a_r] | \Psi_0^{\lambda=0} \rangle \tag{4.4.13}$$

with complex conjugate components given by:

$$(\langle \Psi_0^\lambda | a_p^\dagger a_q^\dagger | \Psi_{N-2;n}^\lambda \rangle)^\dagger = \langle \Psi_{N-2;n}^\lambda | a_q a_p | \Psi_0^\lambda \rangle \quad (4.4.14)$$

Inserting these expression into Eq. (4.3.6) results in the following explicit formula for the 2-RDM matrix elements based on the hh-ERPA approximation to the TDMs:

$$\Gamma_{pqrs}^{hhERPA;\lambda} = \sum_n (n_p + n_q - 1)(n_r + n_s - 1)(c_{pq;n}^\lambda - c_{qp;n}^\lambda)(c_{rs;n}^\lambda - c_{sr;n}^\lambda) \quad (4.4.15)$$

where the sum runs over all eigenvectors for $(N - 2)$ transitions, and it has been assumed that the 1-RDMs are expressed in the natural spin-orbital basis. Like the 2-RDM obtained from ph-ERPA, $\Gamma_{pqrs}^{ph;\lambda}$, the 2-RDM derived here in Eq. (4.4.15) is not N-representable. Unlike the 2-RDM from ph-ERPA, the hh-ERPA 2-RDM does not give the right normalization for the number of electron pairs, although it possess the correct permutational (anti)symmetry properties.

Finally, the 2-RDM terms based on the particle-particle resolution, $\Gamma_{pqrs}^{pp;\lambda}$, given by Eq. (4.3.8), can be approximated from the solutions to ERPA equations formulated for the double-electron-attachment states, Eq. (4.4.9). Alternatively, this 2-RDM can also be obtained from (the negative of) the $N + 2$ solutions from hh-ERPA. Notice, for example, that the metric matrix for hh-ERPA, Eq. (4.4.11), is the negative of that used in pp-ERPA:

$$\langle \Psi_0^{\lambda=0} | [a_p^\dagger a_q^\dagger, a_s a_r] | \Psi_0^{\lambda=0} \rangle = - \langle \Psi_0^{\lambda=0} | [a_s a_r, a_p^\dagger a_q^\dagger] | \Psi_0^{\lambda=0} \rangle \quad (4.4.16)$$

The approximated 2-RDM for the particle-particle resolution then reads:

$$\begin{aligned} \Gamma_{pqrs}^{ppERPA;\lambda} = & \sum_n (1 - n_p - n_q)(1 - n_r - n_s)(c_{pq;-n}^\lambda - c_{qp;-n}^\lambda)(c_{rs;-n}^\lambda - c_{sr;-n}^\lambda) \\ & + \delta_{pr}\gamma_{qs} + \delta_{qs}\gamma_{pr} - \delta_{ps}\gamma_{qr} - \delta_{qr}\gamma_{ps} - \delta_{pr}\delta_{qs} + \delta_{ps}\delta_{qr} \end{aligned} \quad (4.4.17)$$

4.5 AC-ERPA correlation energy

Substituting the three alternative formulas for the 2-RDM approximated via ERPA (Eqs. (4.4.7), (4.4.15), and (4.4.17)) into Eq. (4.2.11) for the correlation energy, three expressions are obtained:

$$E_c^{phERPA} = \frac{1}{2} \int_0^1 \sum_{pqrs} (g_{pqrs}^{\lambda=1} - g_{pqrs}^{\lambda=0}) (\Gamma_{pqrs}^{phERPA,\lambda} - \Gamma_{pqrs}^{\lambda=0}) \quad (4.5.1)$$

$$E_c^{hhERPA} = \frac{1}{2} \int_0^1 \sum_{pqrs} (g_{pqrs}^{\lambda=1} - g_{pqrs}^{\lambda=0}) (\Gamma_{pqrs}^{hhERPA,\lambda} - \Gamma_{pqrs}^{\lambda=0}) \quad (4.5.2)$$

$$E_c^{ppERPA} = \frac{1}{2} \int_0^1 \sum_{pqrs} (g_{pqrs}^{\lambda=1} - g_{pqrs}^{\lambda=0}) (\Gamma_{pqrs}^{ppERPA,\lambda} - \Gamma_{pqrs}^{\lambda=0}) \quad (4.5.3)$$

These equations provide different ways to estimate the energy of a fully-correlated many-electron system based on the adiabatic connection combined with ERPA. The energy formulas are distinguished by the labels *phERPA*, *hhERPA* and *ppERPA* to indicate the ERPA variant used to approximate the 2-RDMs, either the particle-hole, hole-hole, or particle-particle approximation. The AC-ERPA energy expressions,

E_c^{hhERPA} and E_c^{ppERPA} , are then alternatives to particle-hole AC-ERPA for adding dynamic correlation to multideterminant wavefunction approximations. Mathematically, there is no reason to prefer any of these formulations: which method works best will depend on how accurately one can approximate the 2-RDM for each λ value.

In particular, Eqs. (4.5.2) and (4.5.3) for the *hhERPA* and *ppERPA*, respectively, are equivalent even under the approximations considered (see the end of subsection 4.4.1). This arises because double-electron removal and double-electron attachment are complementary solutions of the hh-ERPA equation. The equivalence in the correlation energy obtained from the $N - 2$ -electron and $N + 2$ -electron processes was been proven by Scuseria for pp-RPA [37]. We confirmed these results by implementing both correlation energy formulas, Eqs. (4.5.2) and (4.5.3).

4.6 Examples

To show how AC-ERPA method can be used in practice, we derive explicit expressions for a noninteracting reference wavefunction (Hartree-Fock) and for an interacting Hamiltonian that captures static electron correlation (double occupied configuration interaction, DOCI).

Hartree-Fock: If a noninteracting Hamiltonian is used as the reference Hamiltonian, the ground-state wavefunction is a Slater determinant and AC-ERPA provides an approximation to the correlation energy. While RPA is often used in the context of Kohn-Sham density functional theory, we consider it in the context of the Hartree-Fock method, $\Psi_0^{\lambda=0} = \Phi^{HF}$. The noninteracting Hamiltonian, the Fock operator, is

defined by an effective one-electron Hamiltonian:

$$\hat{H}^{\lambda=0} = \sum_{pq} h_{pq}^{\lambda=0} a_p^\dagger a_q \quad (4.6.1)$$

$$h_{pq}^{\lambda=0} = h_{pq} + \sum_{rs} \langle pr || qs \rangle \gamma_{rs}$$

The energy expectation value is the sum over the energies of the occupied molecular orbitals:

$$E_0^{\lambda=0} = \langle \Phi^{HF} | \hat{H}^{\lambda=0} | \Phi^{HF} \rangle = \sum_{pq} h_{pq}^{\lambda=0} \gamma_{pq} = \sum_i^{occ} \epsilon_i \quad (4.6.2)$$

This expression follows from using the above Hamiltonian definition, Eq. (4.6.1), together with the HF 1-RDM elements given by:

$$\gamma_{pq} = n_p \delta_{pq} \quad (4.6.3)$$

The occupation number n_p is 1 for occupied spin-orbitals and 0 for unoccupied ones. Conventionally, these orbitals are labeled with indexes, i, j, k, l and a, b, c, d , respectively. In the case of HF, the 2-RDM has a simple structure and can be expressed in terms of the 1-RDMs as:

$$\Gamma_{pqrs} = \gamma_{pr} \gamma_{qs} - \gamma_{ps} \gamma_{qr} \quad (4.6.4)$$

As an independent particle model, Hartree-Fock does not account for electron

correlation. The energy functional of this wavefunction model reads:

$$\begin{aligned}
E_0^{HF} &= \langle \Phi^{HF} | \hat{H}^{\lambda=1} | \Phi^{HF} \rangle \\
&= \sum_{pq} h_{pq}^{\lambda=1} \gamma_{pq} + \frac{1}{2} \sum_{pqrs} g_{pqrs}^{\lambda=1} \Gamma_{pqrs} \\
&= \sum_i^{occ} \epsilon_i - \frac{1}{2} \sum_{ij}^{occ} \langle ij || ij \rangle
\end{aligned} \tag{4.6.5}$$

where the second term in the last line corrects for double-counting of electron-electron repulsion.

The correlation energy correction to this energy with the particle-hole-AC-ERPA method can be evaluated as:

$$\begin{aligned}
E_c^{phERPA} &= \frac{1}{2} \int_0^1 d\lambda \sum_{pqrs} g_{pqrs}^{\lambda=1} (\Gamma_{pqrs}^{phERPA;\lambda} - \gamma_{pr}\gamma_{qs} + \gamma_{ps}\gamma_{qr}) \\
&= \frac{1}{2} \int_0^1 d\lambda \sum_{pqrs} g_{pqrs}^{\lambda=1} \left(\sum_{n \neq 0} (n_p - n_r)(n_q - n_s) c_{pr;n}^\lambda c_{qs;n}^\lambda - n_q \delta_{ps} \delta_{qr} + n_p n_q \delta_{ps} \delta_{qr} \right) \\
&= \frac{1}{2} \int_0^1 d\lambda \sum_{pqrs} g_{pqrs}^{\lambda=1} \left(\sum_{n \neq 0} (n_p - n_r)(n_q - n_s) c_{pr;n}^\lambda c_{qs;n}^\lambda + (n_p - 1) n_q \delta_{ps} \delta_{qr} \right) \\
&= \frac{1}{2} \int_0^1 d\lambda \sum_{pqrs} g_{pqrs}^{\lambda=1} \left(\sum_{n \neq 0} (n_p - n_r)(n_q - n_s) c_{pr;n}^\lambda c_{qs;n}^\lambda \right) \\
&\quad + \frac{1}{2} \int_0^1 d\lambda \sum_{pq} g_{pqqp}^{\lambda=1} (n_p - 1) n_q
\end{aligned} \tag{4.6.6}$$

This results from (1) inserting into the AC formula Eq. (4.5.1) the 2-RDMs definitions at λ and $\lambda = 0$ given by Eq. (4.4.7) and Eq. (4.6.4), respectively and then (2) noticing that the fock operator, Eq. (4.6.1), does not have two electron interaction terms ($g_{pqrs}^{\lambda=0} = 0$). The last two lines in the correlation energy formula, E_c^{phERPA} , have one term involving a sum over the (positive) solutions to the ph-RPA equation and pure

exchange term.

As it has been proven elsewhere [26, 38], the particle-hole eigenvalue problem, Eq. (4.4.2), by which the coefficients are evaluated along the perturbation path, becomes the ph-RPA one, where the non-zero elements in \mathbf{A}^λ and \mathbf{M} matrices correspond to excitations between occupied (i,j) and virtual orbitals (a,b) determined by the HF reference:

$$A_{ai,bj}^\lambda = \delta_{ab}\delta_{ij}(\epsilon_a - \epsilon_i) + \lambda \langle ab||ij \rangle \quad (4.6.7)$$

$$A_{ai,jb}^\lambda = \lambda \langle aj||ib \rangle \quad (4.6.8)$$

$$M_{ai,bj} = -\delta_{ab}\delta_{ij} \quad (4.6.9)$$

Therefore, the particle-hole ERPA correlation formula, Eq. (4.6.6), is equivalent to the one formulated by Toulouse, labeled the particle-hole RPax-I [14, 39]. In this method the antisymmetrized two-electron integrals appear in the RPA matrix equation but not in the correlation energy expression.

On the other hand, taking the hh-ERPA correlation energy expression, Eq. (4.5.2), and inserting Eq. (4.4.15) and (4.6.4) for the 2-RDMs at λ and $\lambda = 0$, leads to:

$$\begin{aligned} E_0^{hhERPA} &= \frac{1}{2} \int_0^1 d\lambda \sum_{pqrs} g_{pqrs}^{\lambda=1} (\Gamma_{pqrs}^{hhERPA;\lambda} - \gamma_{pr}\gamma_{qs} + \gamma_{ps}\gamma_{qr}) \\ &= \frac{1}{2} \int_0^1 d\lambda \sum_{pqrs} g_{pqrs}^{\lambda=1} \left(\sum_n (n_p + n_q - 1)(n_r + n_s - 1) (c_{pq;n}^\lambda - c_{qp;n}^\lambda)(c_{rs;n}^\lambda - c_{sr;n}^\lambda) \right) \\ &\quad - \frac{1}{2} \int_0^1 d\lambda \sum_{pq} n_p n_q (g_{pqqp}^{\lambda=1} - g_{pqqp}^{\lambda=1}) \end{aligned} \quad (4.6.10)$$

Note that in the pp-ERPA approach the last term includes both coulomb and exchange contributions, while in ph-ERPA (compare Eq. (4.6.6)) there is only an exchange

contribution.

This hh-ERPA AC equation, Eq. (4.6.10), corresponds to the pp-RPA equation derived by Yang and colleagues [28]. To see this, notice that, for HF, the hh-ERPA matrix equation, Eq. (4.4.10), reduces to:

$$\begin{aligned}
 A_{ij,kl}^\lambda &= -2\delta_{ik}\delta_{jl}(\epsilon_i + \epsilon_j) + \lambda \langle kl||ij \rangle \\
 A_{ab,cd}^\lambda &= 2\delta_{ac}\delta_{bd}(\epsilon_a + \epsilon_b) + \lambda \langle cd||ab \rangle \\
 A_{ij,ab}^\lambda &= -\lambda \langle ab||ij \rangle \\
 M_{ij,kl} &= \delta_{ik}\delta_{jl} - \delta_{il}\delta_{jk} \\
 M_{ab,cd} &= -(\delta_{ac}\delta_{bd} - \delta_{ad}\delta_{bc})
 \end{aligned}$$

where the non-zero elements in the LHS matrix \mathbf{A}^λ includes terms involving only occupied spin-orbitals ($A_{ij,kl}$; associated with double ionizations), terms involving only virtual orbital indexes ($A_{ab,cd}$; corresponding to double electron attachments) and off-diagonal coupling terms between them ($A_{ij,ab}$). These equations actually correspond to the pp-RPA ones, although in our case, we derived them for the two-electron removal process, instead of two-electron addition. Additionally, we did not make the restriction that $j > i$ and $b > a$, thus leading to the factor of two in the matrix elements $A_{ij,kl}$ and $A_{ab,cd}$.

The origin of the correlation energy added from ph- and pp-RPA methods lies on the connection between the HF determinant and double excited configurations, specifically through the off diagonal terms in the RPA matrix equations. Furthermore, it has been proven numerically and analytically, the relation between ph-RPA and pp-RPA and the ring and ladder coupled cluster double (CCD) approximations,

respectively [37, 40].

DOCI: Finally, let's consider the case in which the ground state is described by the double occupied configuration interaction model (DOCI):

$$|\Psi_0^{DOCI}\rangle = \sum_{m_p \in \{0,1\} \sum m_p = N/2} c_m \prod_p^K (a_{p\alpha}^\dagger a_{p\beta}^\dagger)^{m_p} |0\rangle = |\Psi_0^{\lambda=0}\rangle \quad (4.6.11)$$

where the product runs over all pairs of spin-orbitals K and m_p denotes their pair occupation number. DOCI is the only size-consistent configuration interaction method and provides a good description of many static correlation effects, though it misses most dynamic correlation. DOCI is an especially interesting model for static correlation because while exact DOCI calculations are very difficult, there are several computationally affordable approaches that give near-exact DOCI energies for many systems. Most, but not all, of those approaches are based on (various parameterizations of) the antisymmetric product of interacting geminals.

AC-ERPA can be used to estimate the residual correlation energy in DOCI wavefunctions because the DOCI wavefunction is the exact eigenfunction of the pairing Hamiltonian:

$$\begin{aligned} \hat{H}^{\lambda=0} &= \sum_{\sigma} \sum_p h_{pp} a_{p\sigma}^\dagger a_{p\sigma} + \frac{1}{2} \sum_{\sigma\tau} \sum_{p \neq q} g_{pqpq} a_{p\sigma}^\dagger a_{q\tau}^\dagger a_{q\tau} a_{p\sigma} \\ &+ \frac{1}{2} \sum_{\sigma} \sum_{pq} g_{pqqp} a_{p\sigma}^\dagger a_{q\sigma}^\dagger a_{p\sigma} a_{q\sigma} \\ &+ \frac{1}{2} \sum_{\sigma \neq \tau} \sum_{pq} g_{ppqq} a_{p\sigma}^\dagger a_{p\tau}^\dagger a_{q\tau} a_{q\sigma} \end{aligned} \quad (4.6.12)$$

where σ and τ indicate the spin component of the orbital, α or β . The expectation

value of this Hamiltonian is a linear function of the DOCI 1- and 2-RDMs:

$$\begin{aligned}
E_0^{\lambda=0} &= \langle \Psi_0^{DOCI} | \hat{H}^{\lambda=0} | \Psi_0^{DOCI} \rangle \\
&= \sum_{\sigma} \sum_p h_{pp} \gamma_{p\sigma p\sigma} + \frac{1}{2} \sum_{\sigma\tau} \sum_{p \neq q} g_{ppqq} \Gamma_{p\sigma q\tau p\sigma q\tau} \\
&+ \frac{1}{2} \sum_{\sigma} \sum_{pq} g_{ppqp} \Gamma_{p\sigma q\sigma q\sigma p\sigma} + \frac{1}{2} \sum_{\sigma \neq \tau} \sum_{pq} g_{ppqq} \Gamma_{p\sigma p\tau q\sigma q\tau} \quad (4.6.13)
\end{aligned}$$

As a seniority zero wavefunction model (encompassing only electronic configurations with all electrons paired), DOCI 1- and 2-RDMs have a sparse structure; γ is a diagonal matrix:

$$\gamma_{p\sigma q\sigma} = \gamma_{p\alpha q\alpha} = \gamma_{p\beta q\beta} = n_{p\sigma} \delta_{pq} \quad (4.6.14)$$

with n_p between 0 and 1, while Γ includes only the seniority two sector in the off-diagonal (configurations with all but two electrons paired):

$$\Gamma_{p\sigma p\tau q\sigma q\tau} = \Gamma_{p\alpha p\beta q\alpha q\beta} = \Gamma_{p\beta p\alpha q\beta q\alpha} \quad (4.6.15)$$

and the seniority zero sector in the diagonal:

$$\begin{aligned}
\Gamma_{p\sigma q\tau p\sigma q\tau} &= \Gamma_{p\alpha q\alpha p\alpha q\alpha} = \Gamma_{p\beta q\beta p\beta q\beta} \\
&= \Gamma_{p\alpha q\beta p\alpha q\beta} = \Gamma_{p\beta q\alpha p\beta q\alpha} \quad (4.6.16)
\end{aligned}$$

For DOCI, the correlation energy is numerically equivalent to the difference between the energies at the fully and partially interacting limits: $E_c = E_0^{\lambda=1} - E_0^{\lambda=0}$, since for this wavefunction model the first-order correction to the energy, corresponding to the expectation value of the exact Hamiltonian, $H^{\lambda=1}$, for the DOCI wavefunction,

is equal to $E_0^{DOCI} = \langle \Psi_0^{\lambda=0} | H^{\lambda=1} | \Psi_0^{\lambda=0} \rangle = E_0^{\lambda=0}$. This happens because $H^{\lambda=1}$ only couples the seniority zero and seniority two sectors of the wavefunction.

Inserting the definitions of the Hamiltonian Eq. (4.6.12) and the RDMs into Eq. (4.5.1), the fully correlated energy can be evaluated from the particle-hole channel of ERPA through:

$$\begin{aligned}
E_c^{phERPA} &= \frac{1}{2} \int_0^1 d\lambda \sum_{pqrs} (g_{pqrs}^{\lambda=1} - g_{pqrs}^{\lambda=0}) \Gamma_{pqrs}^{phERPA;\lambda} - \frac{1}{2} \int_0^1 d\lambda \sum_{pqrs} (g_{pqrs}^{\lambda=1} - g_{pqrs}^{\lambda=0}) \Gamma_{pqrs}^{\lambda=0} \\
&= \frac{1}{2} \int_0^1 d\lambda \sum_{pqrs} (g_{pqrs}^{\lambda=1} - g_{pqrs}^{\lambda=0}) \left(\sum_{n \neq 0} (n_p - n_r)(n_q - n_s) c_{pr;n}^\lambda c_{qs;n}^\lambda \right) \\
&\quad + \frac{1}{2} \int_0^1 d\lambda \sum_{pqrs} (g_{pqrs}^{\lambda=1} - g_{pqrs}^{\lambda=0}) (n_p n_q \delta_{pr} \delta_{qs} - n_q \delta_{ps} \delta_{qr}) \\
&= \frac{1}{2} \int_0^1 d\lambda \sum_{pqrs} (g_{pqrs}^{\lambda=1} - g_{pqrs}^{\lambda=0}) \left(\sum_{n \neq 0} (n_p - n_r)(n_q - n_s) c_{pr;n}^\lambda c_{qs;n}^\lambda \right) \quad (4.6.17)
\end{aligned}$$

where the second term in the first line and the elements in the third line vanish for DOCI. The recovered correlation energy can thus be evaluated using terms associated with the excited states' transition density matrices integrated over the adiabatic connection path.

The analogous result for the the hole-hole channel also has a simple form, given by:

$$\begin{aligned}
E_0^{hhERPA} &= \frac{1}{2} \int_0^1 d\lambda \sum_{pqrs} (g_{pqrs}^{\lambda=1} - g_{pqrs}^{\lambda=0}) \sum_n (n_p + n_q - 1)(n_r + n_s - 1) (c_{pq;n}^\lambda - c_{qp;n}^\lambda)(c_{rs;n}^\lambda - c_{sr;n}^\lambda) \\
&\quad (4.6.18)
\end{aligned}$$

Using either of the energy equations derived above, we expect to recover the

missing dynamic electron correlation in the DOCI approximation. Vu et al. have analyzed the performance of AC based on ph-ERPA for a variational 2-RDM DOCI formulation [18]. However, to our knowledge, neither ph-ERPA for exact DOCI nor pp-ERPA in the hole-hole channel has been studied.

4.7 Computational details

Restricted HF and DOCI results were obtained from PySCF quantum chemistry package [41, 42]. Unless otherwise specified the cc-pVDZ atomic orbital basis set was used [43]. Orbital optimization was considered with the DOCI model based on a multi-configuration self-consistent field procedure (MCSCF) taking all electrons and orbitals as active. A convergence tolerance of $1e^{-4}$ was used for the gradient and $1e^{-7}$ for the energy. When the scale of the problem permitted it, Full Configuration Interaction (FCI) results were obtained from PySCF to be used as reference. For larger problems, the heat-bath configuration interaction (HCI) wavefunction model [8] was used, generated and optimized with PyCI [44]. The threshold ϵ , used by the HCI variational optimization algorithm, was set to 10^{-4} .

All of the following AC-ERPA results were obtained using our general implementation of Eq. (4.5.1)-(4.5.3). The procedure we followed is outlined below and illustrated in Fig. 4.1 :

1. Build the Hamiltonian for the non-interacting system $\hat{H}^{\lambda=0}$ represented by its one- and two-electron integral matrix terms.
2. Set the number of steps in the AC path between 0 and 1. At every λ value:
 - (a) Build the AC Hamiltonian, Eq. (4.2.3), in terms of the linearly interpolated

one- and two-electron integrals, Eq. (4.2.4).

- (b) Construct the ERPA eigenvalue problem (Eq. (4.4.3) for the particle-hole ERPA, or Eq. (4.4.11) for the hole-hole/particle-particle variant).
- (c) Solve the generalized eigenvalue problem. This step can involve inversion of the metric matrix requiring a threshold to avoid numerical ill-conditioning.
- (d) Select the solutions with $\omega > 0$ and ortho-normalize the eigenvectors. A more general approach is to select the solutions with positive eigenvector norm:

$$\mathbf{C}_n^\lambda \mathbf{M} \mathbf{C}_n^\lambda > 0 \quad (4.7.1)$$

- (e) Compute the transition matrices between the ground and excited states (Eq. 4.4.5 or 4.4.13) and reconstruct the corresponding 2-RDM, $\mathbf{\Gamma}^\lambda$ (Eq. 4.4.7 or 4.4.15, respectively).
- (f) Evaluate the integrand (Eq. 4.5.1 or 4.5.2) from the two-electron integrals for the real and model Hamiltonian systems ($\mathbf{g}^{\lambda=1}$ and $\mathbf{g}^{\lambda=0}$, respectively), the approximated 2-RDM, $\mathbf{\Gamma}^\lambda$, and the non-interacting system 2-RDM, $\mathbf{\Gamma}^{\lambda=0}$.

3. Integrate over the AC path

All one- and two-electron integrals needed for steps 1 and 2a were generated by the PySCF package and expressed in the molecular orbital basis. For the computations based on the DOCI wavefunction model, the electron integrals representing the seniority-zero Hamiltonians were expressed in the optimized orbital basis. For step 2b a spin-adapted version of the ERPA equations was used. To handle potential singularities

in the metric matrix \mathbf{M} , a 10^{-7} tolerance value was used with a Moore-Penrose pseudo-inverse procedure in step (2c). For instance in ph-ERPA the singularities can arise from orbital rotations (elements $a_p^\dagger a_q$) between orbitals with occupation numbers close to 0.5. The matrix inversion algorithm effectively removes these terms from the eigenvector solutions. It is worth noticing that as a result, the number of eigenvectors included in the approximation of the 2-RDM at different coupling values (step 2d) can differ and affect the quality of the results. Finally, for step 3, a Gauss-Legendre quadrature of order five was used to evaluate the adiabatic connection integrand. Not that only singlet excited states contribute to the Hartree-Fock correlation energy through ph-RPA. However, for ph-ERPA with DOCI as the reference, and the procedures based on hh/pp-(E)RPA, both singlet and triplet excited states contribute.

4.8 Results and discussion

To assess the accuracy of the hole-hole (and particle-particle) AC-ERPA approaches for recovering electron correlation, we studied the symmetric dissociation reactions of small model systems. For comparison purposes, the results from the particle-hole AC-ERPA method are also included. Two wavefunction models are considered for the zeroth-order description of the system: RHF and orbital-optimized doubly-occupied CI (OO-DOCI). The AC-ERPA based methods are denoted as phDOCI for the ph-ERPA with DOCI as the reference and hh/ppDOCI for the hh/pp-ERPA variant. When RHF is the reference, these methods become the ph-RPA and hh/pp-RPA approaches. These RPA methods are also known in the literature as ph-RPax-I and full pp-RPA, respectively. We will examine H_2 , H_6 chain, HF and N_2 to explore

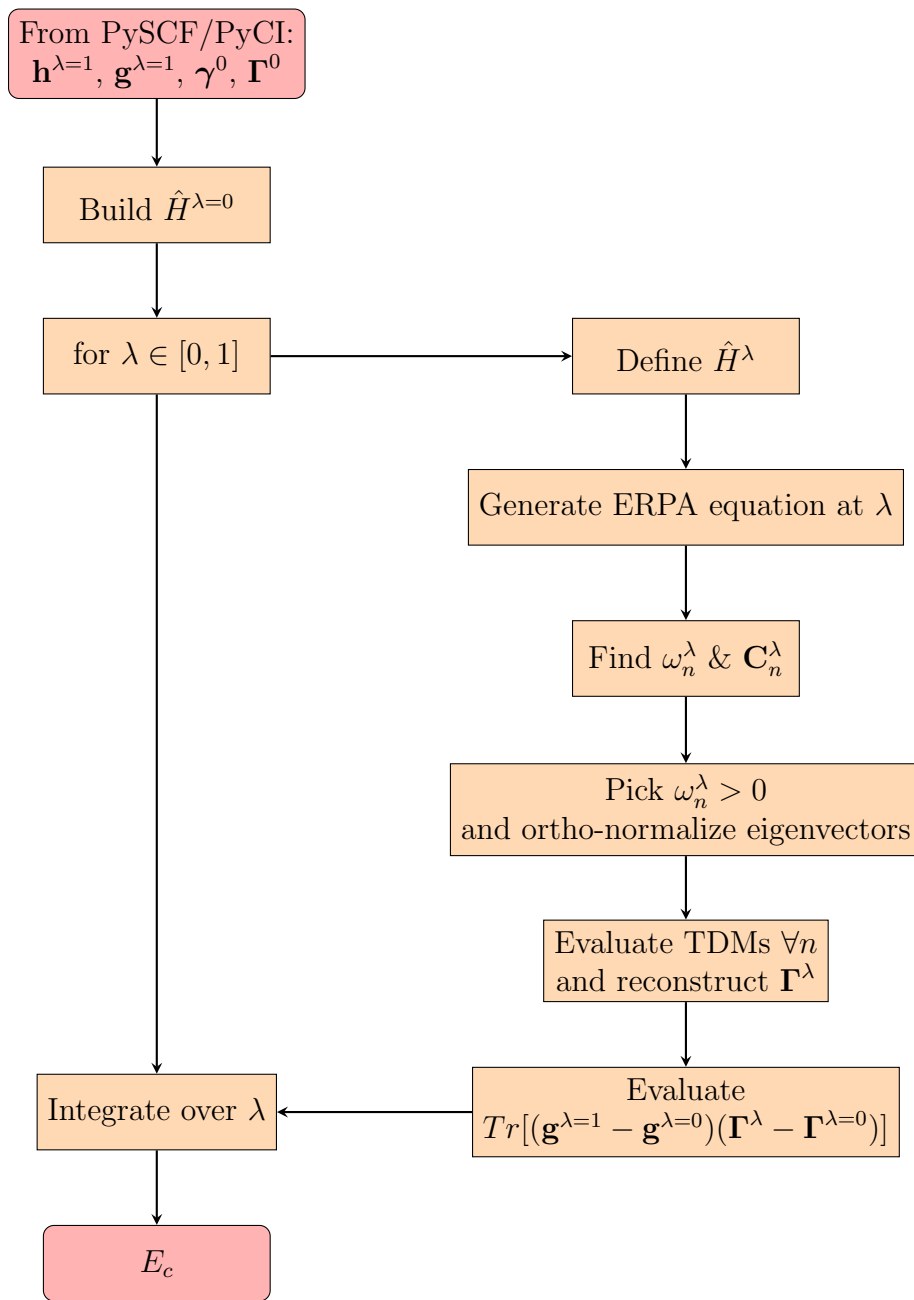


Figure 4.1: General procedure for computing the correlation energy via AC-ERPA.

different bonding types. Results from FCI (or HCI) are referenced as (essentially) exact solutions in the given basis set.

H₂

We begin by revisiting the dissociation of the hydrogen molecule, H₂ with ph-, pp- and hh-RPA (Fig. 4.2). Panel 4.2a presents the total energies, while panel 4.2b shows the errors relative to FCI, defined as the absolute value of the energy difference, $|E(\text{method}) - E(\text{FCI})|$. This reaction is a paradigmatic model used to test the performance of wavefunction methods in different electron correlation regimes. The goal here is to examine the behavior of the three RPA methods.

From Fig. 4.2a it is evident that the RHF wavefunction model (a single Slater determinant) becomes extremely inaccurate as the H–H bond stretches. The difference between the RHF and FCI curves increases with the bond length, exceeding 0.25 Hartree at the dissociation limit, taken here at 10 \AA . At intermediate bond distances the energy gap between the H₂ occupied and virtual molecular orbitals decreases and the multireference character of the wavefunction increases. Moreover, at the dissociation limit, RHF fails to give the correct product (two isolated hydrogen atoms), because it forces both electrons to occupy the same spatial orbital.

Adding the RPA corrections to the HF energy recovers some, but not all, of the missing electron correlation for all bond lengths. Around equilibrium (0.8 \AA) where RHF is qualitatively correct and the energy error is due to the absence of dynamic correlation, the RPA methods describe the H₂ molecule satisfactorily. The particle-hole variant reduces the error to just 0.004 Hartree, whereas the hole-hole variant reduces it to 0.016 Hartree. However, at intermediate bond lengths, RPA approaches are still too repulsive. For these geometries, RHF does not account for the static correlation effects (orbitals with fractional occupations) and assuming the constant 1-RDM from RHF in the AC formula becomes a rough approximation. As expected, the

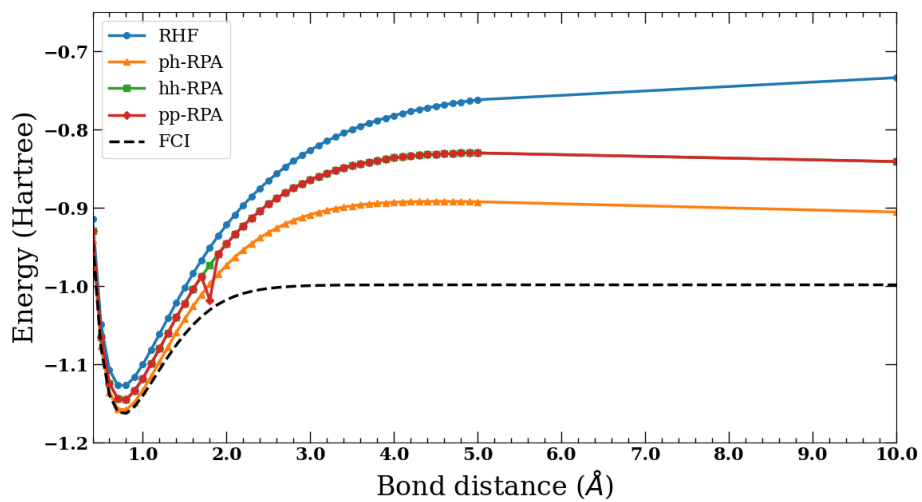
hole-hole and particle-particle RPA curves are essentially indistinguishable, differing only due to issues associated with numerical stability in the spin-recoupling region.

Compared to particle-hole, hh-RPA consistently recovers less of the correlation energy. ph-RPA produces the closest energies to FCI, with differences below 0.1 Hartree across all bond lengths. Nonetheless, towards the dissociation limit, at 10\AA , all RPA variants significantly reduce the RHF error by roughly 0.1 Hartree (even more for ph-RPA). Moreover, although, our results do not show this, it has been reported that at longer bond distances, the RPA methods converge to the correct dissociation limit [28]. DOCI is exact for all 2-electron systems, so using ph- and pp-ERPA to correct the DOCI reference gives no correction for H_2 .

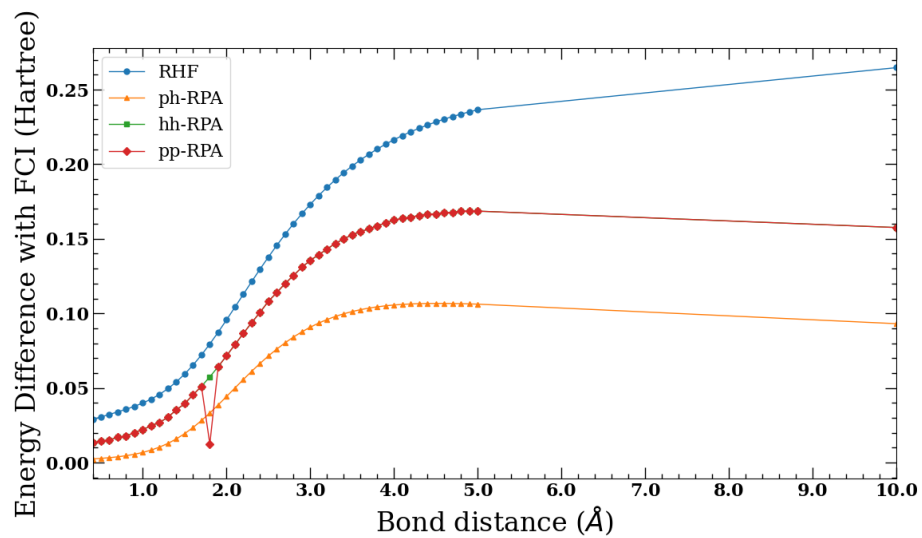
HF

Next, we analyze another bond-breaking reaction: the dissociation of hydrogen fluoride HF, a molecule that serves as a model for systems with ionic character. At the dissociation limit, taken here as 7.0 a.u., HF dissociate into neutral hydrogen and fluorine atoms, so there is a change from ionic- to covalent-like bonding with bond stretching. In this case, we use DOCI to provide a better initial model. The HF potential energy surfaces computed with DOCI, hhDOCI and phDOCI using the 6-31G basis set are depicted in Fig. 4.3. Panel 4.3a presents the total energies while the energy differences relative to FCI, $|E(\text{method}) - E(\text{FCI})|$, are presented in panel 4.3b. Here, the HCI results are used as the reference.

Since DOCI accounts for the static correlation necessary to describe the bond breaking, it produces a dissociation profile with the right shape, unlike RHF in the previous example (see Fig. 4.3a). However, DOCI is systematically above HCI due to the lack of dynamic correlation contributions. This is corroborated by the substantial



(a)



(b)

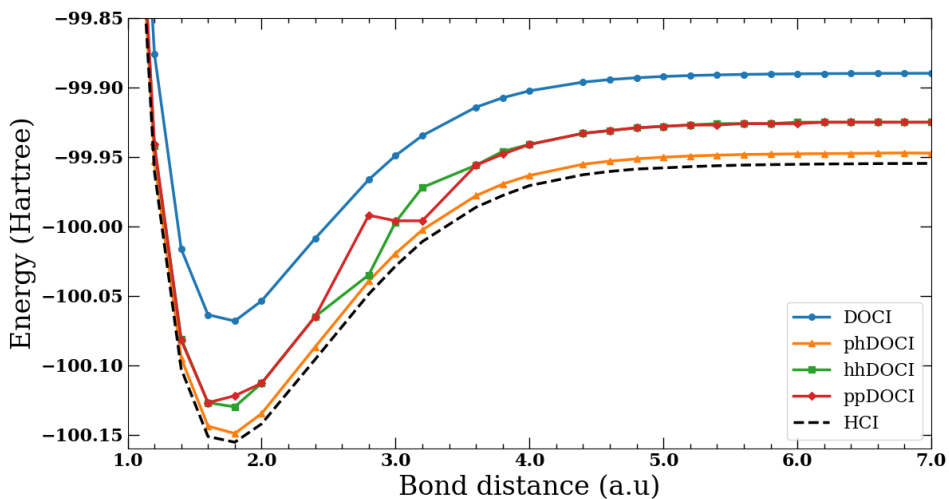
Figure 4.2: Dissociation curve of H₂ in the cc-pVDZ basis set. (a) Total energies and (b) energy differences (relative to FCI).

improvement across all bond distances that both AC-ERPA based approaches yield. The DOCI error decreases by approximately 0.03 Hartree with hhDOCI and 0.05 Hartree with phDOCI. Similar to the observation with H_2 case, phDOCI variant recovers more dynamic correlation than hhDOCI.

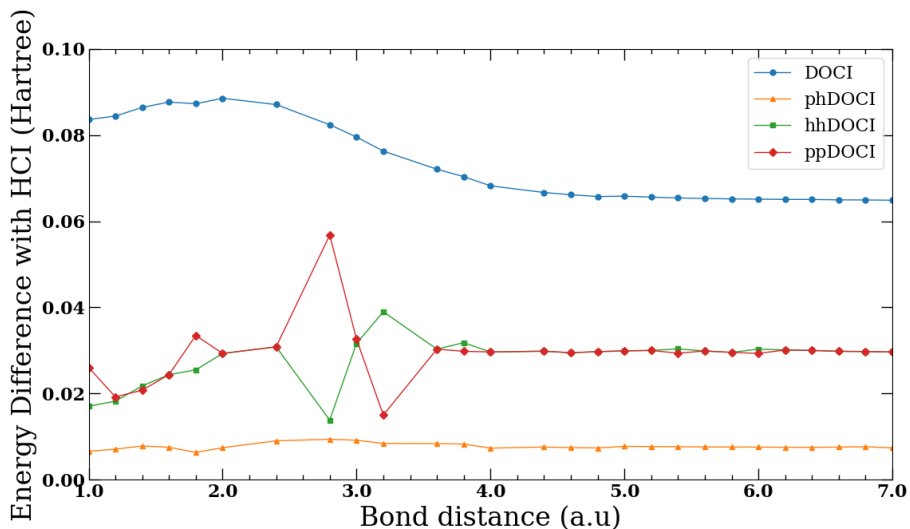
While the hole-hole and particle-particle channels of ERPA are mathematically equivalent, from Fig. 4.3a it is evident that they are not always numerically equivalent. Removing this instability requires careful hand-tuning of the tolerance value used to invert the metric matrix when solving the ERPA generalized eigenvalue problem. Specially ppERPA appears to be sensible to these instabilities even near the equilibrium bond length (around 2.8 a.u.). Removing instabilities from the metric matrix of the ppERPA eigenvalue problem corresponds to removing problematic two-electron addition operators (of the type $a_p^\dagger a_q^\dagger$) from the linear expansion of the $N + 2$ -electron states. This in turn eliminates associated matrix elements from the lambda-dependent transition pairing matrix entering the ppERPA approximation of the 2-RDM (see Eq. 4.4.17). As a result, an unbalance between contributions to the correlation energy from the perturbation dependent and independent terms in Eq. (4.4.17) can be generated. The differences between hhDOCI and ppDOCI in the 2.2 to 4.0 a.u. region, where the nature of the HF bond is changing, are likely due to incorrect inclusion of $(N + 2)$ -electron states in the sum over states for the hhERPA 2-RDMs Eq. (4.4.15), while these states are omitted from the complementary equation Eq. (4.4.17).

Although the hhDOCI method still undercorrelates the electrons, the curve it produces is qualitatively correct and in Fig. 4.3a appears parallel to the phDOCI and FCI curves. It's unsurprising, then, that the hhDOCI dissociation energy, estimated here as the difference between the energy at 7.0 a.u. 1.8 a.u., is 205 mHartrees,

which is almost as good as phDOCI (202 mHartree). By comparison, HCl gives 201 mHartree but the DOCI dissociation energy is relatively poor, 178 mHartree, due mostly to the lack of dynamic correlation near equilibrium.



(a)



(b)

Figure 4.3: Dissociation curve of FH in the 6-31G basis set. (a) Total energies and (b) energy differences calculated as the absolute value relative to HCl.

H₆ chain

The H₆ chain is a classic strongly correlated model system where, conveniently, DOCI is exact in the dissociation limit. Recall that the correlation energy is the integral along the adiabatic connection path,

$$E_c = \int_0^1 W(\lambda) d\lambda \quad (4.8.1)$$

where the integrand as a function of the interaction strength, $W(\lambda)$, is given by those in the AC-ERPA equations, Eqs. (4.6.18) and (4.6.17). For a H–H separation of 1.0Å, DOCI provides a comparatively decent approximation with a energy 0.0308 Hartree above the FCI result (–3.3266 Hartree).

The contribution to the correlation energy by the hhDOCI and phDOCI methods along the adiabatic connection path is presented in Fig 4.4. The correlation energy is given by the area under the curves. In agreement with observations in the previous examples, the dynamic correlation energy contribution from hhDOCI is substantially less than that from phDOCI. The hhDOCI reduces DOCI error relative to FCI to 0.0216 Hartree, whereas phDOCI reduces the error to 0.0180 Hartree. Noticeably, the hhDOCI integrand is almost a linear function of the coupling parameter λ . This implies that fewer points along the AC path are needed to approximate the integral, which reduces the computational cost of hhDOCI relative to phDOCI.

N₂

Finally, we look at the dissociation of the nitrogen molecule N₂, which is a classic example of multiple bond-breaking, which is known to be a very difficult problem for single-reference quantum chemistry methods. Figure 4.5a presents the dissociation

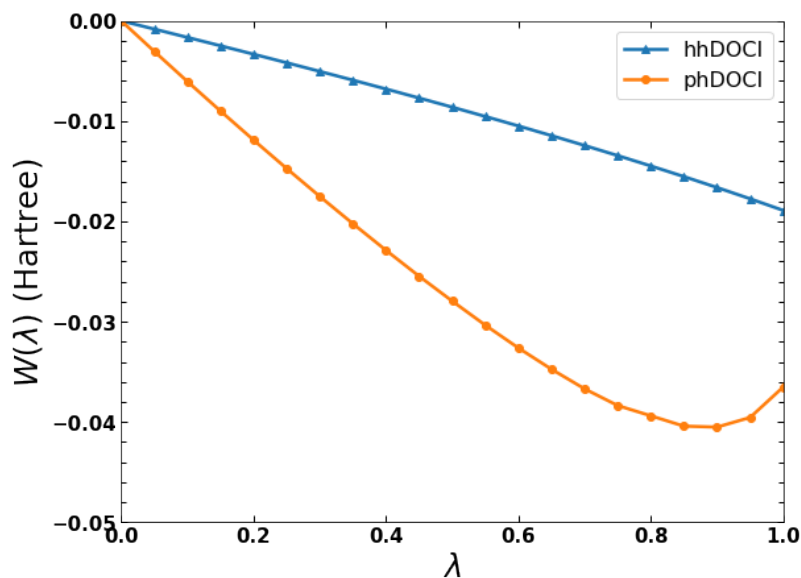


Figure 4.4: AC integrand for the DOCI reference for H_6 with H–H distance of 1.0\AA using 6-31G basis set. The correlation energy is given by the area under the $W(\lambda)$ curves. The hhDOCI underestimates the correlation energy relative to phDOCI.

curves for the DOCI, phDOCI and hhDOCI methods using the cc-pVDZ basis set. Here, the HCI results are taken as the best approximation to the exact solution.

Both AC-ERPA methods accurately describe the N_2 molecule around the equilibrium geometry at 1.2\AA bond distance. For example, phDOCI has an error of only 0.028 Hartree above HCI, whereas hhDOCI has an error three times larger (0.084 Hartree) at 1.1\AA (see Fig. 4.5b). However, the quality of the AC-ERPA deteriorates at intermediate and stretched bond lengths (roughly above 1.5\AA), especially for hhDOCI.

The disappointing results can be attributed to the fact that DOCI, as a closed shell wavefunction model, cannot properly describe the spin-coupling between open-shell nitrogen atoms in the bond-breaking region of the potential energy curve. Consequently, it is reasonable that using a constant 1-RDM and the zeroth-order 2-RDM in the AC-ERPA equations is a poor approximation. Moreover, the differences in potential

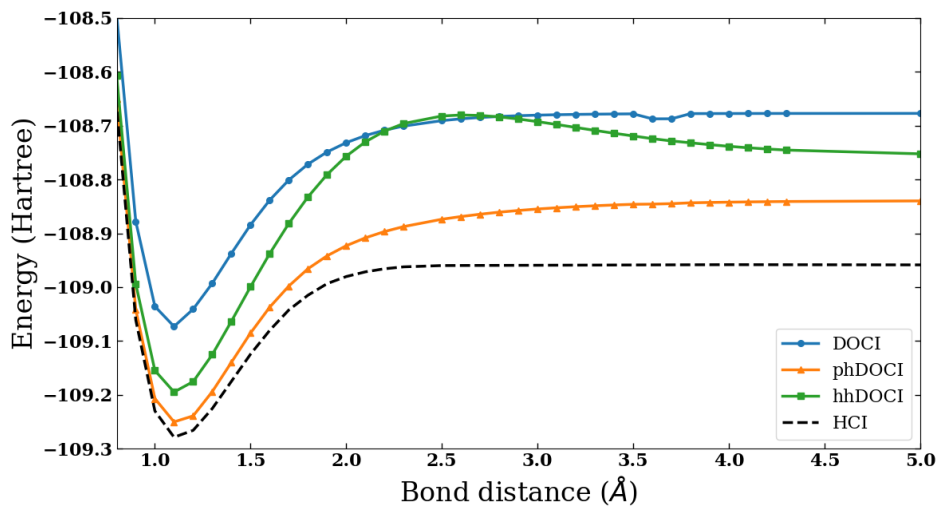
energy surfaces obtained from phDOCI and hhDOCI are more pronounced in this system, with hhDOCI presenting a bump at intermediate bond lengths (roughly between 2.0 and 3.5 Å). Since, for the DOCI reference, the AC correlation energy from ph-ERPA and hh-ERPA depends only on the respective transition density matrices (Eqs. 4.6.17 and 4.6.18, respectively), the notable difference in hhDOCI's performance suggests that the ERPA approximation to the resolution of the identity is poorer for hhDOCI than for phDOCI.

In summary, hhERPA methods provides comparable, but somewhat worse, results than phERPA where dynamic correlation effects are prevalent (e.g. near equilibrium geometries). Where static correlation is not completely captured by the DOCI reference, phDOCI and hhDOCI are both disappointing, but hhDOCI is substantially worse.

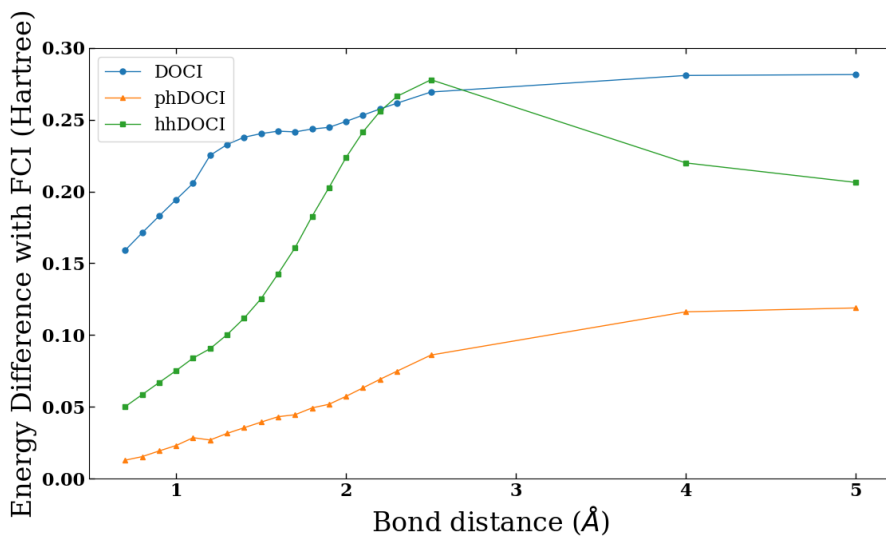
4.9 Conclusions

We propose alternative formulations to add dynamic correlation to multideterminant wavefunction approximations based on the adiabatic connection approximation (Eqs. (4.5.2) and (4.5.3)). The methods use the hole-hole and particle-particle channels of extended random phase approximation to approximate the 2-RDM along the adiabatic connection path. Specifically, resolutions of identity in terms of double electron attached (or removed) states are used to rewrite the λ -dependent 2-RDMs in the AC formula can be rewritten in terms of pairing transition density matrix elements. These matrices in turn are approximated to first order using hh/pp-ERPA (Eq. 4.4.10).

The correlation energy corrections via these alternative ERPA channels follow the same approximations as the particle-hole counterpart [13]. Specifically, the 1-RDM is



(a)



(b)

Figure 4.5: Dissociation curve of N_2 in the cc-pVDZ basis set. (a) Total energies and (b) energy differences calculated as the absolute value relative to HCl.

assumed constant along the adiabatic connection path and is taken from the zeroth-order approximation. The pairing transition density matrices are approximated using first-order excitation operators (e.g. Eq. 4.4.8), and the ERPA equations are evaluated with the 1-RDM and 2-RDM at $\lambda = 0$.

We assessed the accuracy of the AC-ERPA methods based on the hole-hole and particle-particle channels using model systems with strong multiconfigurational character, comparing our results against accurate results from FCI or HCI. Numerical analysis confirmed the equivalence between the hh- and pp-AC-ERPA procedures. For the Hartree-Fock reference, these two methods correspond to pp-RPA.

Unfortunately, the main problem with these new AC-ERPA approaches is that they do not improve over the particle-hole variant in terms of accuracy or computational efficiency. The computational cost of the AC-ERPA corrections based on the hole-hole (or equivalently particle-particle) channel is similar to that of the particle-hole variant, scaling as m^6 for m molecular orbitals. Furthermore, they share the same limitation as the particle-hole AC-ERPA in that the best performance is achieved when the zeroth-order wavefunction is a good approximation.

Nonetheless, these new formulations may still be valuable as alternative *ab initio* methods for modeling electron correlation in molecular systems. They may be promising in the correlation energy corrections for excited states, where particle-hole ERPA is prone to breaking due to orbital rotation instabilities. Additionally, as extensions of pp-RPA to correlated wavefunction models, their may be promising in the simulation of dispersion interactions.

Philosophically, these approaches are appealing because, unlike most previous approaches to correcting seniority-zero models, they do not freeze the seniority-zero

sector of the wavefunction/reduced density matrix. The performance of these models might be improved if we did not let them correct seniority-zero elements of the 2-RDM, which are believed to be accurate in DOCI. However, we know that seniority-zero sector should relax in response to dynamic correlation effects, and should not be frozen. These ERPA-based approaches do relax the seniority-zero sector, but are obviously not especially effective at doing so.

References

- [1] Patrick A Lee. From high temperature superconductivity to quantum spin liquid: progress in strong correlation physics. *Reports on Progress in Physics*, 71(1): 012501, dec 2007.
- [2] Myron B. Salamon and Marcelo Jaime. The physics of manganites: Structure and transport. *Rev. Mod. Phys.*, 73:583–628, Aug 2001.
- [3] J. R. Heflin, K. Y. Wong, O. Zamani-Khamiri, and A. F. Garito. Nonlinear optical properties of linear chains and electron-correlation effects. *Phys. Rev. B*, 38:1573–1576, Jul 1988.
- [4] Hao Hong, Chunchun Wu, Zixun Zhao, Yonggang Zuo, Jinhuan Wang, Can Liu, Jin Zhang, Fangfang Wang, Jiangang Feng, Huaibin Shen, Jianbo Yin, Yuchen Wu, Yun Zhao, Kehai Liu, Peng Gao, Sheng Meng, Shiwei Wu, Zhipei Sun, Kaihui Liu, and Jie Xiong. Giant enhancement of optical nonlinearity in two-dimensional materials by multiphoton-excitation resonance energy transfer from quantum dots. *Nature Photonics*, 15(7):510–515, 2021. ISSN 1749-4893. doi: 10.1038/s41566-021-00801-2. URL <https://doi.org/10.1038/s41566-021-00801-2>.

- [5] James Shee, Matthias Loipersberger, Diptarka Hait, Joonho Lee, and Martin Head-Gordon. Revealing the nature of electron correlation in transition metal complexes with symmetry breaking and chemical intuition. *The Journal of Chemical Physics*, 154(19):194109, 05 2021. ISSN 0021-9606.
- [6] B. Huron, J. P. Malrieu, and P. Rancurel. Iterative perturbation calculations of ground and excited state energies from multiconfigurational zeroth-order wavefunctions. *The Journal of Chemical Physics*, 58(12):5745–5759, 06 1973. ISSN 0021-9606.
- [7] Robert J. Buenker and Sigrid D. Peyerimhoff. Individualized configuration selection in ci calculations with subsequent energy extrapolation. *Theoretica chimica acta*, 35(1):33–58, 1974. ISSN 1432-2234.
- [8] Adam A. Holmes, Norm M. Tubman, and C. J. Umrigar. Heat-bath configuration interaction: An efficient selected configuration interaction algorithm inspired by heat-bath sampling. *Journal of Chemical Theory and Computation*, 12:3674–3680, 8 2016. ISSN 1549-9618.
- [9] A. C. Hurley, John Edward Lennard-Jones, and John Anthony Pople. The molecular orbital theory of chemical valency xvi. a theory of paired-electrons in polyatomic molecules. *Proceedings of the Royal Society of London. Series A. Mathematical and Physical Sciences*, 220(1143):446–455, 1953.
- [10] Tecmer, Paweł and Boguslawski, Katharina and Johnson, Paul and Limacher, Peter A and Chan, Matthew and Verstraelen, Toon and Ayers, Paul W. Assessing the accuracy of new geminal-based approaches. *JOURNAL OF PHYSICAL CHEMISTRY A*, 118(39):9058–9068, 2014. ISSN 1089-5639.

- [11] Steven R. White. Density matrix formulation for quantum renormalization groups. *Physical Review Letters*, 69:2863–2866, 11 1992. ISSN 0031-9007.
- [12] Garnet Kin-Lic Chan and Sandeep Sharma. The density matrix renormalization group in quantum chemistry. *Annual Review of Physical Chemistry*, 62:465–481, 5 2011. ISSN 0066-426X.
- [13] Katarzyna Pernal. Electron correlation from the adiabatic connection for multireference wave functions. *Physical Review Letters*, 120:013001, 1 2018. ISSN 0031-9007.
- [14] Julien Toulouse, Wuming Zhu, János G. Ángyán, and Andreas Savin. Range-separated density-functional theory with the random-phase approximation: Detailed formalism and illustrative applications. *Phys. Rev. A*, 82:032502, Sep 2010.
- [15] János G. Ángyán, Ru Fen Liu, Julien Toulouse, and Georg Jansen. Correlation energy expressions from the adiabatic-connection fluctuation-dissipation theorem approach. *Journal of Chemical Theory and Computation*, 7:3116–3130, 10 2011. ISSN 15499618.
- [16] Katarzyna Pernal. Intergeminal correction to the antisymmetrized product of strongly orthogonal geminals derived from the extended random phase approximation. *Journal of Chemical Theory and Computation*, 10:4332–4341, 10 2014. ISSN 1549-9618.
- [17] Ewa Pastorczak and Katarzyna Pernal. Correlation energy from the adiabatic

- connection formalism for complete active space wave functions. *Journal of Chemical Theory and Computation*, 14:3493–3503, 7 2018. ISSN 15499626.
- [18] Nam Vu, Ion Mitxelena, and A Eugene DePrince. An adiabatic connection for doubly-occupied configuration interaction wave functions. *The Journal of chemical physics*, 151:244121, 12 2019. ISSN 1089-7690.
- [19] Elvis Maradzike, Michał Hapka, Katarzyna Pernal, and A. Eugene DePrince. Reduced density matrix-driven complete active space self-consistent field corrected for dynamic correlation from the adiabatic connection. *Journal of Chemical Theory and Computation*, 16:4351–4360, 7 2020. ISSN 1549-9618.
- [20] Pavel Beran, Mikuláš Matoušek, Michał Hapka, Katarzyna Pernal, and Libor Veis. Density matrix renormalization group with dynamical correlation via adiabatic connection. *Journal of Chemical Theory and Computation*, 17, 2021. ISSN 15499626.
- [21] Kerstin Andersson, Per-Åke Malmqvist, and Björn O. Roos. Second-order perturbation theory with a complete active space self-consistent field reference function. *The Journal of Chemical Physics*, 96(2):1218–1226, 01 1992. ISSN 0021-9606.
- [22] Yang Guo, Kantharuban Sivalingam, and Frank Neese. Approximations of density matrices in N-electron valence state second-order perturbation theory (NEVPT2). I. Revisiting the NEVPT2 construction. *The Journal of Chemical Physics*, 154(21):214111, 06 2021. ISSN 0021-9606.

- [23] David Bohm and David Pines. A collective description of electron interactions. i. magnetic interactions. *Phys. Rev.*, 82:625–634, Jun 1951.
- [24] David Pines and David Bohm. A collective description of electron interactions: Ii. collective vs individual particle aspects of the interactions. *Phys. Rev.*, 85: 338–353, Jan 1952.
- [25] David Bohm and David Pines. A collective description of electron interactions: Iii. coulomb interactions in a degenerate electron gas. *Phys. Rev.*, 92:609–625, Nov 1953.
- [26] Koushik Chatterjee and Katarzyna Pernal. Excitation energies from extended random phase approximation employed with approximate one- and two-electron reduced density matrices. *The Journal of Chemical Physics*, 137:204109, 2012.
- [27] Helen van Aggelen, Brecht Verstichel, Guillaume Acke, Matthias Degroote, Patrick Bultinck, Paul W. Ayers, and Dimitri Van Neck. Extended random phase approximation method for atomic excitation energies from correlated and variationally optimized second-order density matrices. *Computational and Theoretical Chemistry*, 1003:50–54, 1 2013. ISSN 2210271X.
- [28] Exchange-correlation energy from pairing matrix fluctuation and the particle-particle random-phase approximation. *Physical Review A*, 88:030501, 9 2013. ISSN 1050-2947.
- [29] Helen van Aggelen, Yang Yang, and Weitao Yang. Exchange-correlation energy from pairing matrix fluctuation and the particle-particle random phase approximation. *The Journal of Chemical Physics*, 140, 5 2014. ISSN 0021-9606.

- [30] Katarzyna Pernal. Exact and approximate adiabatic connection formulae for the correlation energy in multireference ground and excited states. *The Journal of chemical physics*, 149:204101, 11 2018. ISSN 1089-7690.
- [31] Ewa Pastorzak and Katarzyna Pernal. Electronic excited states from the adiabatic-connection formalism with complete active space wave functions. *Journal of Physical Chemistry Letters*, 9:5534–5538, 2018. ISSN 19487185.
- [32] Daria Drwal, Ewa Pastorzak, and Katarzyna Pernal. Excited states in the adiabatic connection fluctuation-dissipation theory: Recovering missing correlation energy from the negative part of the density response spectrum. *The Journal of Chemical Physics*, 154:164102, 4 2021. ISSN 0021-9606.
- [33] A. D. McLACHLAN and M. A. BALL. Time-dependent hartree—fock theory for molecules. *Reviews of Modern Physics*, 36:844–855, 7 1964. ISSN 0034-6861.
- [34] Filipp Furche and Troy Van Voorhis. Fluctuation-dissipation theorem density-functional theory. *The Journal of Chemical Physics*, 122, 4 2005. ISSN 0021-9606.
- [35] D. J. Rowe. Equations-of-motion method and the extended shell model. *Reviews of Modern Physics*, 40:153–166, 1968. ISSN 00346861.
- [36] János G. Ángyán, Ru Fen Liu, Julien Toulouse, and Georg Jansen. Correlation energy expressions from the adiabatic-connection fluctuation-dissipation theorem approach. *Journal of Chemical Theory and Computation*, 7:3116–3130, 10 2011. ISSN 15499618.
- [37] Gustavo E. Scuseria, Thomas M. Henderson, and Ireneusz W. Bulik. Particle-particle and quasiparticle random phase approximations: Connections to coupled

- cluster theory. *The Journal of Chemical Physics*, 139:104113, 9 2013. ISSN 0021-9606.
- [38] Katarzyna Pernal. Correlation energy from random phase approximations: A reduced density matrices perspective. *International Journal of Quantum Chemistry*, 118:e25462, 1 2018. ISSN 00207608.
- [39] Bastien Mussard, Peter Reinhardt, János G. Ángyán, and Julien Toulouse. Spin-unrestricted random-phase approximation with range separation: Benchmark on atomization energies and reaction barrier heights. *The Journal of Chemical Physics*, 142:154123, 4 2015. ISSN 0021-9606.
- [40] Xinguo Ren, Patrick Rinke, Christian Joas, and Matthias Scheffler. Random-phase approximation and its applications in computational chemistry and materials science. *Journal of Materials Science*, 47:7447–7471, 11 2012. ISSN 0022-2461.
- [41] Qiming Sun, Timothy C Berkelbach, Nick S Blunt, George H Booth, Sheng Guo, Zhendong Li, Junzi Liu, James D McClain, Elvira R Sayfutyarova, Sandeep Sharma, et al. Pyscf: the python-based simulations of chemistry framework. *Wiley Interdisciplinary Reviews: Computational Molecular Science*, 8(1):e1340, 2018.
- [42] Qiming Sun, Xing Zhang, Samraghi Banerjee, Peng Bao, Marc Barbry, Nick S Blunt, Nikolay A Bogdanov, George H Booth, Jia Chen, Zhi-Hao Cui, et al. Recent developments in the pyscf program package. *The Journal of Chemical Physics*, 153(2):024109, 2020.

- [43] Jr. Dunning, Thom H. Gaussian basis sets for use in correlated molecular calculations. I. The atoms boron through neon and hydrogen. *The Journal of Chemical Physics*, 90(2):1007–1023, 01 1989. ISSN 0021-9606.
- [44] Michelle Richer, Gabriela Sánchez-Díaz, Farnaz Heidar-Zadeh, Marco Martínez-González, Valerii Chuiko, and Paul W. Ayers. Pyci: A python-scriptable library for arbitrary determinant ci. Unpublished manuscript.

Chapter 5

PyEOM: A software package for equations-of-motion methods.

5.1 What is PyEOM?

PyEOM is an open source research-level library developed in Python for computing electronic structure properties of excited states. As its name indicates, its structure is based on the equations-of-motion (EOM) framework (see Chapter 2). It allows its users to model electronic transitions, including one- and two-electron removal, one- and two-electron attachment, and electronic excitations. By relying on reduced density matrices (RDMs), PyEOM supports a broad variety of multireference wavefunction approaches, including *Configuration Interaction* (CI) [1], *Antisymmetrized Geminal Products* (AGP) [2, 3], and the *Density Matrix Renormalization Group* (DMRG) [4, 5]. The residual dynamic correlation energy can be approximated through the adiabatic connection approach combined with ERPA (AC-ERPA) [6].

As a tool developed for research, PyEOM favors a clear and simple implementation

over optimized performance. We strive to ensure that the PyEOM source code itself is comprehensively documented, including useful tests, scripts, and examples. The computational cost of these methods scale as either the third or sixth power of the size of the spin-orbital basis set; the memory demands are controlled by the need to store several four-dimensional arrays. Both of these bottlenecks could be circumvented by well-known strategies (e.g., iterative diagonalization and auxiliary basis sets) but we judged that these innovations were undesirable for prototyping new methods, where robustness, flexibility, and controlled errors are more important than performance.

5.2 Why PyEOM?

We started developing PyEOM because we needed to prototype and test new excited state approaches based on the equations-of-motion method. Many *ab initio* packages (Gaussian [7], Q-Chem [8], GAMESS [9]) support computation of excited states for traditional wavefunction methods like *Hartree-Fock* (HF), CI, *Coupled Cluster* (CC), and or *Multi-Configuration Self-Consistent Field* (MCSCF). However, closed-source code, combined with abstract, highly optimized low-level implementations of *ab initio* methods, often makes it cumbersome to understand, modify, or extend these packages. We considered using other free and open-source libraries like PySCF [10, 11], GQPC [12], and Psi4 [13] that have routines for several post-HF methods, provide necessary inputs like the one- and two-electron integrals and the density matrices, and share our philosophical preferences for the development of open-source software tools for the scientific community. However, these packages tended to be monolithic and had a steep learning curve, so we opted to build a compact, stand-alone, library to support our research needs. As we felt our library could be useful to others, we decided to

release it independently. By leveraging our EOM-based methods, researchers can efficiently compute excited states from correlated wavefunctions, facilitating more comprehensive electronic structure analyses.

PyEOM was designed to be integrated into Python scripting workflows with open source post-HF packages such as PyCI [14], our robust library for configuration interaction (CI) wavefunctions, PySCF, or GQCP. This integration ensures that users can take full advantage of the existing functionalities in PyCI while extending its capabilities for excited state computations. The following sections will present the structure of PyEOM followed by examples showcasing its distinguishing features (Section 5.5).

5.3 Intended user

Using PyEOM requires familiarity with the fundamental concepts of electronic structure theory. Additionally, users need some experience in computational electronic structure theory, since an *ab initio* calculation (e.g, Gaussian or PySCF) is necessary to generate input data. Extending the capabilities of PyEOM requires basic knowledge of object-oriented computer programming in Python.

5.4 Structure of PyEOM

PyEOM is written entirely in Python, using NumPy and SciPy’s linear algebra routines. Its source code can be accessed through GitHub at <https://github.com/gabrielasd/eomee>, including tutorials, example scripts and scientific documentation.

PyEOM uses a class hierarchy to implement different types of excited states based

on the equations-of-motion framework described in Chapter 2 [15]. Each method can be implemented as a class definition, templated from an abstract base class. Currently, there are **five** main excited-state classes that allow one to construct and solve the EOM eigenvalue problem for a given molecular system (specified through its Hamiltonian \hat{H} and reference state RDMs) as shown in Fig. 5.1. These main methods appear listed in Table 5.1, and are named, respectively, the Ionization Potential (IP), Electron Affinity (EA), Double Ionization Potential (DIP), Double Electron Attachment (DEA), and Excitation Energy (EE) EOM classes. Additionally, for closed shell systems, pure singlet and triplet transitions can be computed using subclasses of EE, DIP and DEA. These spin-adapted implementations of EE-EOM, DIP-EOM, and DEA-EOM are the last six classes listed in Table 5.1.

Table 5.1: Supported EOM Methods.

Excited state	GEVP	Class
$\Psi^{(N)}$	(5.4.5)	EE [16]
$\Psi^{(N-1)}$	(5.4.3)	IP [17, 18]
$\Psi^{(N+1)}$	(5.4.3)	EA [17]
$\Psi^{(N-2)}$	(5.4.5)	DIP
$\Psi^{(N+2)}$	(5.4.5)	DEA
$\Psi^{(N)}$ singlet	(5.4.5)	EES
$\Psi^{(N)}$ triplet	(5.4.5)	EET
$\Psi^{(N-2)}$ singlet	(5.4.5)	DIPS
$\Psi^{(N-2)}$ triplet	(5.4.5)	DIPT
$\Psi^{(N+2)}$ singlet	(5.4.5)	DEAS
$\Psi^{(N+2)}$ triplet	(5.4.5)	DEAT

At present, the methods in PyEOM are limited to those which can be fully expressed in terms of the one- and two-electron reduced density matrices (1- and 2-RDMs) of the (ground state) reference wavefunction.

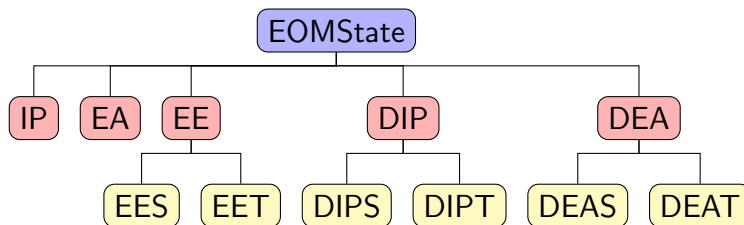


Figure 5.1: PyEOM class inheritance diagram.

5.4.1 EOM state (EOMState) base class

All supported electronic transitions are based on the `EOMState` class. Within this class, the λ th excited state wavefunction is defined as a linear combination of transition operators, $\hat{q}_n^{\dagger(\pm\kappa)}$, applied to a reference N -electron state, $|\Psi^{(N)}\rangle$:

$$|\Psi_\lambda^{(N\pm\kappa)}\rangle = \sum_n c_{n;\lambda} \hat{q}_n^{\dagger(\pm\kappa)} |\Psi^{(N)}\rangle \quad (5.4.1)$$

The operators $\hat{q}_n^{\dagger(\pm\kappa)}$, where n is a generic multi-index, form an (incomplete) basis for the transition operator. In PyEOM, the $\hat{q}_n^{\dagger(\pm\kappa)}$ operators are approximated with strings of the second-quantized operators for creating (a_p^\dagger) and annihilating (a_p) electrons from spin-orbitals. This general notation in Eq. (5.4.1) is used to provide a common framework for electronic transitions, including those which change the number of electrons. Usually, the reference state is chosen as the ground state, $|\Psi^{(N)}\rangle = |\Psi_0^{(N)}\rangle$.

Analogous to CI methods, the parameters of the wavefunction, $c_{n;\lambda}$, are optimized solving an eigenvalue problem,

$$\mathbf{AC}_\lambda = \Delta E_\lambda \mathbf{MC}_\lambda \quad (5.4.2)$$

where the obtained eigenvalues, ΔE_λ , correspond to the transition energies between

the reference state and the λ th excited state $\Delta E_\lambda = E_\lambda - E_0$. More explicit expressions for \mathbf{A} and \mathbf{M} will be given in the next section, but, roughly, they correspond respectively to matrix elements of a transition-energy operator and an overlap matrix, projected onto the basis used to describe the final (post-transition) state of the system.

The base `EOMState` class allows us to construct and store the left- and right-hand-side matrices of the eigenvalue problem, \mathbf{A} and \mathbf{M} , for different “flavors” of electron transition. These matrices are stored as dense NumPy arrays and can be accessed as attributes of the `EOMState` class. The total number of expected solutions λ , determined by the basis set of transition operators $\hat{q}_n^{\dagger(\pm\kappa)}$ is an attribute of the class; this is important because the matrices are not always full rank. Additionally, the `solve_dense` and `solve_sparse` methods of `EOMState` class implement solutions to the generalized eigenvalue problem Eq. (5.4.2), using NumPy and SciPy, respectively.

5.4.2 Built-in EOM methods

PyEOM supports excited states based on the most common approximations to $\hat{q}_n^{\dagger(\pm\kappa)}$, as summarized in table 5.2:

Table 5.2: Excited states in PyEOM.

Process	Operator basis	State
Electron removal (IP)	a_p	$ \Psi_\lambda^{(N-1)}\rangle = \sum_p c_{p;\lambda} a_p \Psi_0^{(N)}\rangle$
Electron attachment (EA)	a_p^\dagger	$ \Psi_\lambda^{(N+1)}\rangle = \sum_p c_{p;\lambda} a_p^\dagger \Psi_0^{(N)}\rangle$
Double electron removal (DIP)	$a_p a_q$	$ \Psi_\lambda^{(N-2)}\rangle = \sum_{pq} c_{pq;\lambda} a_p a_q \Psi_0^{(N)}\rangle$
Double electron addition (DEA)	$a_p^\dagger a_q^\dagger$	$ \Psi_\lambda^{(N+2)}\rangle = \sum_{pq} c_{pq;\lambda} a_p^\dagger a_q^\dagger \Psi_0^{(N)}\rangle$
Electronic excitation (EE)	$a_p^\dagger a_q$	$ \Psi_\lambda^{(N)}\rangle = \sum_{pq} c_{pq;\lambda} a_p^\dagger a_q \Psi_0^{(N)}\rangle$

IP class: One-electron-removed states are described by the Ionization Potential (IP) subclass of `EOMState`. The associated left- and right-hand side matrix elements have the form:

$$\begin{aligned}\langle \Psi_0^{(N)} | a_m^\dagger, [\hat{H}, a_n] | \Psi_0^{(N)} \rangle &= A_{mn}(\gamma, \Gamma) \\ \langle \Psi_0^{(N)} | a_m^\dagger a_n | \Psi_0^{(N)} \rangle &= M_{mn}(\gamma, \Gamma)\end{aligned}\tag{5.4.3}$$

These terms can be evaluated using the reference wavefunction's 1- and 2-RDMs and the Hamiltonian operator's one- and two-electron integrals.

EA class: The Electron Affinity (EA) subclass of `EOMState` stores the left- and right-hand side matrix terms for the EOM of the form:

$$\begin{aligned}\langle \Psi_0^{(N)} | a_m, [\hat{H}, a_n^\dagger] | \Psi_0^{(N)} \rangle &= A_{mn}(\gamma, \Gamma) \\ \langle \Psi_0^{(N)} | a_m a_n^\dagger | \Psi_0^{(N)} \rangle &= M_{mn}(\gamma, \Gamma)\end{aligned}\tag{5.4.4}$$

This class represents electron attachment, and, like the IP class, the eigenvalue equation can be expressed in terms of the reference wavefunction's 1- and 2-RDMs and the 1- and 2-electron integrals. These IP and EA approaches are also known in the literature as the extended Koopman's theorem (EKT) [17, 18]. IP-EOM is exact for (a) all one-electron systems and (b) certain ionized states if the reference wavefunction is exact (within a given basis); EA-EOM is only exact for the vacuum (zero-electron) reference state.

EE class: The Excitation Energy (**EE**) subclass of **EOMState** models electronic excitations using left- and right-hand side matrices with the form:

$$\begin{aligned}\langle \Psi_0^{(N)} | [a_p^\dagger a_q, [\hat{H}, a_s^\dagger a_r]] | \Psi_0^{(N)} \rangle &= A_{pq,rs}(\gamma, \Gamma) \\ \langle \Psi_0^{(N)} | [a_p^\dagger a_q, a_s^\dagger a_r] | \Psi_0^{(N)} \rangle &= M_{pq,rs}(\gamma, \Gamma)\end{aligned}\quad (5.4.5)$$

Instances of this class represent the particle-hole extended random phase approximation (ph-ERPA) [16]. The **EEm** class inherits the **EE** method, and corresponds to changing the metric matrix to $M_{pq,rs} = \langle \Psi_0^{(N)} | a_p^\dagger a_q a_s^\dagger a_r | \Psi_0^{(N)} \rangle$. EE-EOM is exact only for 1-electron systems.

DIP class: One can describe two-electron-removed states using the Double Ionization Potential (DIP) subclass of **textttEOMState**. DIP class implements the left- and right-hand side matrix elements for the EOM of the form:

$$\begin{aligned}\langle \Psi_0^{(N)} | [a_p^\dagger a_q^\dagger, [\hat{H}, a_s a_r]] | \Psi_0^{(N)} \rangle &= A_{pq,rs}(\gamma, \Gamma) \\ \langle \Psi_0^{(N)} | [a_p^\dagger a_q^\dagger, a_s a_r] | \Psi_0^{(N)} \rangle &= M_{pq,rs}(\gamma, \Gamma)\end{aligned}\quad (5.4.6)$$

The **DIPm** class inherits the DIP method, and corresponds to changing the metric matrix to $M_{pq,rs} = \langle \Psi_0^{(N)} | a_p^\dagger a_q^\dagger a_s a_r | \Psi_0^{(N)} \rangle$. In general, DIP-EOM is exact only for 2-electron systems.

DEA class: Two-electron addition is modeled with the Double Electron Attachment (DEA) subclass of `EOMState`, where the left- and right-hand side matrix elements are

$$\begin{aligned} \langle \Psi_0^{(N)} | [a_p a_q, [\hat{H}, a_s^\dagger a_r^\dagger]] | \Psi_0^{(N)} \rangle &= A_{pq,rs}(\gamma, \Gamma) \\ \langle \Psi_0^{(N)} | [a_p a_q, a_s^\dagger a_r^\dagger] | \Psi_0^{(N)} \rangle &= M_{pq,rs}(\gamma, \Gamma) \end{aligned} \quad (5.4.7)$$

The `DEAm` class inherits the `DEA` class, and corresponds to changing the metric matrix to $M_{pq,rs} = \langle \Psi_0^{(N)} | a_p a_q a_s^\dagger a_r^\dagger | \Psi_0^{(N)} \rangle$. DEA-EOM is exact only for the vacuum (zero-electron) reference state.

5.5 Using PyEOM

The following examples demonstrate how `PyEOM` can be incorporated into *ab initio* computational workflows. The examples are based on the current version of the package and will evolve with the package. Users are referred to the GitHub repository and the `PyEOM` website for the most up-to-date documentation and examples. Here we focus on `PyEOM`'s main features:

- specifying a molecular system
- setting up and running EOM/ERPA calculations
- processing results
- estimating the residual correlation energy
- adding new EOM methods

Through these examples we use the Beryllium atom and H_4 chain molecule as simple demonstration systems; the resulting calculations are easily performed on a laptop computer.

5.5.1 Molecular system specification

PyEOM is intended to be broadly applicable to any many-fermion system; it does not make any assumptions about the number of fermions, their interactions, or their electronic state but instead relies on the user to provide the elements of the 1- and 2-body integrals and the 1- and 2-body reduced density matrices, denoted h_{pq} , g_{pqrs} , γ_{pq} and Γ_{pqrs} , respectively. These parameters must be generated by external *ab initio* packages, either from within the QC-Devs ecosystem (GBasis [19], ModelHamiltonian [20], HORTON [21], PyCI [14]) or from external packages (PySCF [10, 11], Gaussian [7], etc.). These inputs are specified as 2- or 4-dimensional NumPy arrays. The specific definition for these input variables is defined in the following subsections, together with some associated utility functions.

Hamiltonian: PyEOM’s built-in methods are based on the Hamiltonian operator expressed in second quantization as:

$$\hat{H} = \sum_{pq} h_{pq} a_p^\dagger a_q + \frac{1}{2} \sum_{pqrs} g_{pqrs} a_p^\dagger a_q^\dagger a_s a_r \quad (5.5.1)$$

where

$$h_{pq} = \int \chi_p^*(\mathbf{x}) \left(-\frac{\nabla^2}{2} - \sum_A \frac{Z_A}{r_{1A}} \right) \chi_q(\mathbf{x}) d\mathbf{x} \quad (5.5.2)$$

$$g_{pqrs} = \int \int \chi_p^*(\mathbf{x}_1) \chi_q^*(\mathbf{x}_2) \frac{1}{r_{12}} \chi_r(\mathbf{x}_1) \chi_s(\mathbf{x}_2) d\mathbf{x}_1 d\mathbf{x}_2 \quad (5.5.3)$$

define the one- and two-electron integral matrix elements in terms of the spin-orbital basis $\chi(\mathbf{x})$. The variable \mathbf{x} denotes the combined spin and spatial coordinates of the electron. Note that we use **physicist's** notation to represent the two-electron integrals, g_{pqrs} .

The orbitals defining the Hamiltonian can be classified as: restricted, if an alpha and beta pair of orbitals share the same spatial component; unrestricted, if the alpha and beta pair have different spatial component; or generalized (spin-free), in which the one-electron function can have a mixture of alpha and beta spin functions.

PyEOM methods are represented in the generalized spin-orbital basis but in quantum chemistry computations typically a restricted or unrestricted orbital basis is used. Restricted and unrestricted Hamiltonians can be expressed as generalized ones by preserving the symmetry of the spin-orbital basis and setting mixed spin electron integral components to zero. The following snippet of code shows how to use the utility function `spinize` from the `eomee.tools` module to build spin-resolved electron integrals h_{pq} and g_{pqrs} starting from the molecular orbital integrals from a restricted HF calculation stored as NumPy arrays.

```

1  import numpy as np
2  from eomee.tools import spinize
3
4  one_mo = np.load("be_sto3g_oneint.npy")

```

```

5 two_mo = np.load("be_sto3g_twoint.npy")
6 one_sp = spinize(one_mo) # h_pq
7 two_sp = spinize(two_mo) # g_pqrs

```

The loaded arrays `one_mo` and `two_mo` have dimensions of the number of spatial molecular orbitals, (k, k) and (k, k, k, k) , respectively, while the spin-resolved electron integrals `one_sp` and `two_sp` have dimensions (m, m) and (m, m, m, m) , with $m = 2 \times k$ being the number of spin-orbitals.

Wavefunction: In PyEOM the N -electron ground state is defined through its one- and two-electron reduced density matrices (RDMs), γ and Γ , respectively, with matrix elements given by:

$$\begin{aligned}\gamma_{pq} &= \langle \Psi_0^{(N)} | a_p^\dagger a_q | \Psi_0^{(N)} \rangle \\ \Gamma_{pqrs} &= \langle \Psi_0^{(N)} | a_p^\dagger a_q^\dagger a_s a_r | \Psi_0^{(N)} \rangle\end{aligned}\tag{5.5.4}$$

For a single Slater determinant wavefunction (e.g., Hartree-Fock), the 1- and 2-RDMs have a very simple structure and one can use the utility function `hartreefock_rdm`s from the `eomee.tools` module to generate them from the definition of the number of basis set orbitals and the number of alpha and beta electrons:

```

1 from eomee.tools import hartreefock_rdm
2
3 # HF 1- and 2-RDMs for Be in a minimal basis.
4 # I.e., 2 alpha and 2 beta electrons with 5 spatial MOs
5 rdm1, rdm2 = hartreefock_rdm(5, (2, 2))

```

For other (variational) wavefunction methods, free and open-source electronic structure packages such as PySCF, GQCP or PyCI can be used to obtain spin-resolved

RDMs. Usually, for restricted and unrestricted post-HF wavefunction methods, only the non-zero matrix elements are computed. The utility function `spinize_rdm`s can be used to reconstruct the generalized density matrices from the sub-matrices corresponding to the non-zero spin-blocks of the 1- and 2-RDMs. These are: the alpha-alpha and beta-beta spin-blocks in the case of the 1-RDM, and the alpha-alpha-alpha, beta-beta-beta-beta and alpha-beta-alpha-beta four-dimensional tensor blocks in the case of the 2-RDM:

```
1  import numpy as np
2  from eomee.tools import spinize_rdm
3
4  # Load 1- and 2-RDMs nonzero spin-blocks
5  dm1aa, dm2bb = np.load("be_sto3g_onedm.npy")
6  dm2aa, dm2ab, dm2bb = np.load("be_sto3g_twodm.npy")
7  # Convert from the unrestricted to the generalized format
8  rdm1 = spinize_rdm(dm1aa, dm2bb)
9  rdm2 = spinize_rdm(dm2aa, dm2ab, dm2bb)
```

When interfacing with external packages one must ensure that their definitions for the 1-RDM and (especially) the 2-RDM matches the one in Eq. (5.5.4).

5.5.2 Running a calculation

Creating an EOM wavefunction: Once a Hamiltonian and its RDMs are defined, an instance of an EOM method can be created using:

```
1  myeom = eom_method(one_mo, two_mo, rdm1, rdm2)
2
3  print("Number of solutions: ", myeom.neigs)
4  print("Left-hand-side matrix: \n", myeom.lhs)
```

```
5 print("Metric matrix: ", myeom.rhs)
```

Here `eom_method` denotes any of the built-in EOM classes listed in Table 5.1 since they share a common interface.

Finding eigenvalues and eigenvectors: One then solves for the transition energies (eigenvalues) and the associated transition operators (eigenvectors) using:

```
1 # Solve the EOM eigenvalue problem
2 ev, cv = myeom.solve_dense()
3 print("Excitation energies: ", ev)
```

The eigenvalues (and eigenvectors) are listed from smallest to largest. For some EOM methods like the excitation energies `EE`, the spectrum has negative elements (associated with de-excitations in `EE-EOM`) that appear first.

Example ionization energy calculation: The following example finds the ionization potentials of the Beryllium atom using the Extended Koopmans' Theorem:

```
1 from eomee import IP
2
3 # Generate the EKT eigenvalue problem
4 ekt = IP(one_sp, two_sp, rdm1, rdm2)
5
6 # Solve the EKT eigenvalue problem
7 ev, cv = ekt.solve_dense()
8 print("Ionization potentials: ", ev)
```

Example excited state calculation: Similarly, the excitation energies of Beryllium can be computed using:

```

1  from eomee import EE
2
3  # Generate the particle-hole EOM/ERPA eigenproblem
4  erpa = EE(one_sp, two_sp, rdm1, rdm2)
5
6  # Solve the ERPA eigenvalue problem
7  ev, cv = erpa.solve_dense()
8  print("Excitation energies: ", ev)

```

If the HF density matrices were used, this calculation is equivalent to the time-dependent HF (TDHF) method [22] also known as the particle-hole random phase approximation (ph-RPA).

If only the singlet transitions were of interest, one can instead create an instance of the class `EES` from the module `eomee.spinadapted.particlehole`:

```

1  from eomee.spinadapted.particlehole import EES
2
3  # Generate the singlet spin-adapted particle-hole EOM
4  pheom = EES(one_sp, two_sp, rdm1, rdm2)
5
6  # Solve the spin-adapted ERPA eigenvalue problem
7  ev, cv = pheom.solve_dense()
8  print("Singlet excitation energies: ", ev)

```

This last method is only suitable for closed-shell systems like Beryllium.

5.5.3 Post-processing EOM results

Once the eigenvalues ΔE_λ and eigenvectors \mathbf{C}_λ for a excitation process of interest are computed, one can obtain the corresponding transition RDMs; these are the

key quantities for evaluating oscillator strengths for the modelled transitions. The transition RDM between the ground state, $\Psi_0^{(N)}$, and the λ th ($N-1$)-electron excited state, $\Psi_\lambda^{(N-1)}$, is computed from the eigenvectors of the IP-EOM equation, $c_{q;\lambda}$, as follows:

$$\langle \Psi_0^{(N)} | a_p^\dagger | \Psi_\lambda^{(N-1)} \rangle = \sum_q c_{q;\lambda} \langle \Psi_0^{(N)} | a_p^\dagger a_q | \Psi_0^{(N)} \rangle \quad (5.5.5)$$

These quantities are computed using the `compute_tdm` method of the IP class:

```
1 tdm = ekt.compute_tdm(cv[0])
```

In this example the transition matrix between the ground state and the first ionized state is evaluated. This method is useful for post-processing. E.g., Fig. 5.2 depicts the Feynman-Dyson orbitals for the two lowest ionization energies of CO. The orbital amplitudes were obtained through an EKT calculation using the 1- and 2-RDMs from a Heat-Bath Configuration Interaction (HCI) calculation with $\epsilon_1 = 5 \times 10^{-4}$ in the 6-31G basis set. The Dyson orbitals were then evaluated on a two-dimensional grid of point using `GBasis`.

5.5.4 Correlation energy corrections

PyEOM also provides routines to compute the residual correlation energy for general multideterminant wavefunction approximations using the AC-ERPA approach (see Chapter 4):

$$\begin{aligned} E_c &= \langle \Psi_0^{\lambda=1} | \hat{H} | \Psi_0^{\lambda=1} \rangle - \langle \Psi_0^{\lambda=0} | \hat{H} | \Psi_0^{\lambda=0} \rangle \\ &= \frac{1}{2} \int_0^1 \sum_{pqrs} (g_{pqrs}^{\lambda=1} - g_{pqrs}^{\lambda=0}) (\Gamma_{pqrs}^\lambda - \Gamma_{pqrs}^{\lambda=0}) d\lambda \end{aligned} \quad (5.5.6)$$

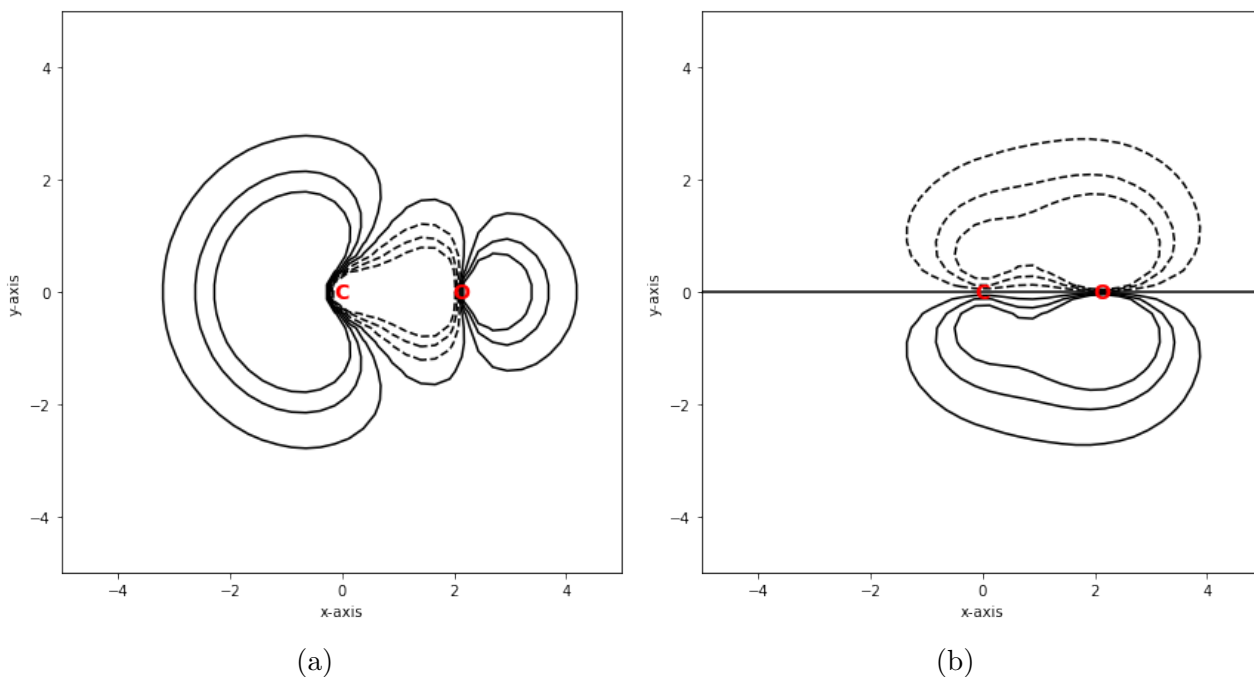


Figure 5.2: Dyson orbitals contour plots from Extended Koopmans' Theorem at the HCl/6-31G level of theory for CO molecule. (a) σ transition (b) π transition.

where $g_{pqrs}^{\lambda=1}$ and $g_{pqrs}^{\lambda=0}$ are the two-electron integrals from the real and model Hamiltonians, respectively, and Γ_{pqrs}^{λ} and $\Gamma_{pqrs}^{\lambda=0}$ are the 2-RDMs at every perturbation strength value λ and for the reference state, respectively.

The method `eval_ecorr` in the modules for the spin-adapted implementations of EE, DIP, and DEA-EOM implements this equation. At present, PyEOM only supports this functionality for closed-shell systems. To run this type of calculation the user needs to specify:

- (a) the Hamiltonian for the real/fully-interacting system (`h1` and `v1` array elements),
- (b) the Hamiltonian corresponding to a given wavefunction approximation (`h0` and `v0` arrays)

(c) the 1- and 2-RDMs for the approximate wavefunction (`rdm1` and `rdm2` arrays).

In the cases where the model system is described by the HF or the doubly-occupied configuration interaction (DOCI) wavefunction approximations, PyEOM provides utility functions `make_spinized_fock_hamiltonian` and `make_doci_ham_spinized` to help build the necessary one- and two-electron integrals (part (b)). For example,

```

1  from eomee.tools import make_spinized_fock_hamiltonian
2
3  # Build the Hamiltonian for the HF wfn (Fock operator)
4  h0, v0 = make_spinized_fock_hamiltonian(one_mo, two_mo)

```

Other model Hamiltonians such as the Pariser-Parr-Pople [23, 24], Hubbard [25], Hückel [26], Heisenberg [27], and Richardson-Gaudin [28, 29] model Hamiltonians are available through the ModelHamiltonian package [20].

The following example showcases this method for the correction based on the particle-hole ERPA approach:

```

1  from eomee.tools import spinize, hartreefock_rdms
2  from eomee.tools import make_spinized_fock_hamiltonian
3  from eomee.spinadapted.particlehole import eval_ecorr
4
5  # 1) Load the electron integral matrices
6  one_mo = np.load("h4_chain_1.40_631g_oneint.npy")
7  two_mo = np.load("h4_chain_1.40_631g_twoint.npy")
8  h1 = spinize(one_int)
9  v1 = spinize(two_int)
10
11 # 2) Build Hamiltonian at lambda=0 (Fock operator)
12 h0, v0 = make_spinized_fock_hamiltonian(one_mo, two_mo)
13

```

```

14 # 3) HF 1- and 2-RDMs in molecular orbital basis
15 nelects = (2,2) # number of alpha and beta electrons
16 nbasis = one_mo.shape[0] # number of molecular orbitals
17 rdm1, rdm2 = hartreefock_rdms(nbasis, *nelects)
18
19 # 4) Compute the correction to the HF energy
20 ecorr_hf = eval_ecorr(h0, v0, h1, v1, rdm1, rdm2)
21 print("Correlation energy = ", ecorr_hf)

```

The AC-ERPA correction (via the particle-particle channel) can also be computed if the same function from the `eomee.spinadapted.holehole` module is used instead.

5.6 Extensions to PyEOM

To add new methods to PyEOM, the base class `EOMState` must be subclassed. This procedure requires the methods `neigs`, `_compute_lhs` and `_compute_rhs` specifying the number of excited state solutions and the expressions of the matrices **A** and **M**, respectively, to be defined. For instance, the code snippet below implements a new flavor of EOM to compute $(N - 1)$ -electron states following the matrix expressions:

$$\begin{aligned}
 A_{mn}(\gamma, \Gamma) &= \left\langle \Psi_0^{(N)} \left| \left\{ a_m^\dagger, \left[\hat{H}, a_n \right] \right\} \right| \Psi_0^{(N)} \right\rangle \\
 &= - \sum_q h_{nq} \gamma_{mq} - \frac{1}{2} \sum_{qrs} (g_{nqrs} - g_{nqsr}) \Gamma_{mqrs} \\
 M_{mn}(\gamma, \Gamma) &= \left\langle \Psi_0^{(N)} \left| a_m^\dagger a_n \right| \Psi_0^{(N)} \right\rangle = \gamma_{pq}
 \end{aligned} \tag{5.6.1}$$

```

1 from eomee.base import EOMState
2

```

```
3 class IPa(EOMState):
4     def neigs(self):
5         # Number of eigenvalues and eigenvectors expected
6         # from full matrix diagonalization
7         return self._n
8
9     def _compute_lhs(self):
10        # Define the matrix A as a function of one- and
11        # two-electron integrals and DMs
12        #  $A_{mn} = -h_{nq} \gamma_{mq} - 0.5 \langle nq || rs \rangle \Gamma_{mqr}$ 
13        one_body = np.dot(self._dm1, self._h)
14        two_body = np.tensordot(
15        self._dm2, self._v, ((1, 2, 3), (1, 2, 3))
16        )
17        two_body *= 0.5
18        two_body += one_body
19        return -two_body
20
21    def _compute_rhs(self):
22        # Expression for matrix M as a function of one- and
23        # two-electron integrals and DMs
24        return self._dm1
```

5.7 Summary

This chapter introduces PyEOM, a library for developing new EOM-based excited state methods. The creation of PyEOM was motivated by our desire to model electronic transitions using multireference wavefunctions and the equations-of-motion ansatz.

The distinctive feature of PyEOM is that multiple excited state properties (e.g. ionization potentials, electron affinities and excitation energies) are treated using a unified framework, simply by providing the information about the system (specifically, its 1- and 2-electron integrals) and reference state (specifically, its 1- and 2-RDMs) of interest. With this framework, it is easy to implement new EOM approaches and ERPA approaches, as demonstrated in section 5.6. Our hope is that PyEOM will help researchers quickly test ideas for new correlated electronic structure theory methods and, to achieve this goal, PyEOM contains several methods that can be combined with one another. Future work will focus on performance improvements and methodological extensions, especially to EOM methods relying upon higher-order reduced density matrices.

References

- [1] Attila Szabo and Neil S Ostlund. *Modern Quantum Chemistry: Introduction to Advanced Electronic Structure Theory*. Courier Corporation, 2012.
- [2] Paul A. Johnson, Paul W. Ayers, Peter A. Limacher, Stijn De Baerdemacker, Dimitri Van Neck, and Patrick Bultinck. A size-consistent approach to strongly correlated systems using a generalized antisymmetrized product of nonorthogonal geminals. *Computational and Theoretical Chemistry*, 1003:101–113, 2013. ISSN 2210271X.
- [3] Paweł Tecmer, Katharina Boguslawski, Paul A. Johnson, Peter A. Limacher, Matthew Chan, Toon Verstraelen, and Paul W. Ayers. Assessing the accuracy of new geminal-based approaches. *The Journal of Physical Chemistry A*, 118:9058–9068, 10 2014. ISSN 1089-5639.
- [4] Steven R. White. Density matrix formulation for quantum renormalization groups. *Physical Review Letters*, 69:2863–2866, 11 1992. ISSN 0031-9007.
- [5] Garnet Kin-Lic Chan and Sandeep Sharma. The density matrix renormalization group in quantum chemistry. *Annual Review of Physical Chemistry*, 62:465–481, 5 2011. ISSN 0066-426X.

- [6] Katarzyna Pernal. Electron correlation from the adiabatic connection for multireference wave functions. *Physical Review Letters*, 120:013001, 1 2018. ISSN 0031-9007.
- [7] M. J. Frisch, G. W. Trucks, H. B. Schlegel, G. E. Scuseria, M. A. Robb, J. R. Cheeseman, G. Scalmani, V. Barone, G. A. Petersson, H. Nakatsuji, X. Li, M. Caricato, A. V. Marenich, J. Bloino, B. G. Janesko, R. Gomperts, B. Mennucci, H. P. Hratchian, J. V. Ortiz, A. F. Izmaylov, J. L. Sonnenberg, D. Williams-Young, F. Ding, F. Lipparini, F. Egidi, J. Goings, B. Peng, A. Petrone, T. Henderson, D. Ranasinghe, V. G. Zakrzewski, J. Gao, N. Rega, G. Zheng, W. Liang, M. Hada, M. Ehara, K. Toyota, R. Fukuda, J. Hasegawa, M. Ishida, T. Nakajima, Y. Honda, O. Kitao, H. Nakai, T. Vreven, K. Throssell, J. A. Montgomery, Jr., J. E. Peralta, F. Ogliaro, M. J. Bearpark, J. J. Heyd, E. N. Brothers, K. N. Kudin, V. N. Staroverov, T. A. Keith, R. Kobayashi, J. Normand, K. Raghavachari, A. P. Rendell, J. C. Burant, S. S. Iyengar, J. Tomasi, M. Cossi, J. M. Millam, M. Klene, C. Adamo, R. Cammi, J. W. Ochterski, R. L. Martin, K. Morokuma, O. Farkas, J. B. Foresman, and D. J. Fox. Gaussian~16 Revision C.01, 2016. Gaussian Inc. Wallingford CT.
- [8] Yihan Shao, Zhengting Gan, Evgeny Epifanovsky, Andrew T.B. Gilbert, Michael Wormit, Joerg Kussmann, Adrian W. Lange, Andrew Behn, Jia Deng, Xintian Feng, Debashree Ghosh, Matthew Goldey, Paul R. Horn, Leif D. Jacobson, Ilya Kaliman, Rustam Z. Khaliullin, Tomasz Kuś, Arie Landau, Jie Liu, Emil I. Proynov, Young Min Rhee, Ryan M. Richard, Mary A. Rohrdanz, Ryan P. Steele, Eric J. Sundstrom, H. Lee Woodcock III, Paul M. Zimmerman, Dmitry Zuev, Ben Albrecht, Ethan Alguire, Brian Austin, Gregory J. O. Beran,

Yves A. Bernard, Eric Berquist, Kai Brandhorst, Ksenia B. Bravaya, Shawn T. Brown, David Casanova, Chun-Min Chang, Yunqing Chen, Siu Hung Chien, Kristina D. Closser, Deborah L. Crittenden, Michael Diedenhofen, Robert A. DiStasio Jr., Hainam Do, Anthony D. Dutoi, Richard G. Edgar, Shervin Fatehi, Laszlo Fusti-Molnar, An Ghysels, Anna Golubeva-Zadorozhnaya, Joseph Gomes, Magnus W.D. Hanson-Heine, Philipp H.P. Harbach, Andreas W. Hauser, Edward G. Hohenstein, Zachary C. Holden, Thomas-C. Jagau, Hyunjun Ji, Benjamin Kaduk, Kirill Khistyayev, Jaehoon Kim, Jihan Kim, Rollin A. King, Phil Klunzinger, Dmytro Kosenkov, Tim Kowalczyk, Caroline M. Krauter, Ka Un Lao, Adèle D. Laurent, Keith V. Lawler, Sergey V. Levchenko, Ching Yeh Lin, Fenglai Liu, Ester Livshits, Rohini C. Lochan, Arne Luenser, Prashant Manohar, Samuel F. Manzer, Shan-Ping Mao, Narbe Mardirossian, Aleksandr V. Marenich, Simon A. Maurer, Nicholas J. Mayhall, Eric Neuscamman, C. Melania Oana, Roberto Olivares-Amaya, Darragh P. O'Neill, John A. Parkhill, Trilisa M. Perrine, Roberto Peverati, Alexander Prociuk, Dirk R. Rehn, Edina Rosta, Nicholas J. Russ, Shaama M. Sharada, Sandeep Sharma, David W. Small, Alexander Sodt, Tamar Stein, David Stück, Yu-Chuan Su, Alex J.W. Thom, Takashi Tsuchimochi, Vitalii Vanovschi, Leslie Vogt, Oleg Vydrov, Tao Wang, Mark A. Watson, Jan Wenzel, Alec White, Christopher F. Williams, Jun Yang, Sina Yeganeh, Shane R. Yost, Zhi-Qiang You, Igor Ying Zhang, Xing Zhang, Yan Zhao, Bernard R. Brooks, Garnet K.L. Chan, Daniel M. Chipman, Christopher J. Cramer, William A. Goddard III, Mark S. Gordon, Warren J. Hehre, Andreas Klamt, Henry F. Schaefer III, Michael W. Schmidt, C. David Sherrill, Donald G. Truhlar, Arieh Warshel, Xin Xu, Alán Aspuru-Guzik, Roi Baer, Alexis T.

- Bell, Nicholas A. Besley, Jeng-Da Chai, Andreas Dreuw, Barry D. Dunietz, Thomas R. Furlani, Steven R. Gwaltney, Chao-Ping Hsu, Yousung Jung, Jing Kong, Daniel S. Lambrecht, WanZhen Liang, Christian Ochsenfeld, Vitaly A. Rassolov, Lyudmila V. Slipchenko, Joseph E. Subotnik, Troy Van Voorhis, John M. Herbert, Anna I. Krylov, Peter M.W. Gill, and Martin Head-Gordon. Advances in molecular quantum chemistry contained in the q-chem 4 program package. *Molecular Physics*, 113(2):184–215, 2015. ISSN 0026-8976.
- [9] Giuseppe M. J. Barca, Colleen Bertoni, Laura Carrington, Dipayan Datta, Nuwan De Silva, J. Emiliano Deustua, Dmitri G. Fedorov, Jeffrey R. Gour, Anastasia O. Gunina, Emilie Guidez, Taylor Harville, Stephan Irle, Joe Ivanic, Karol Kowalski, Sarom S. Leang, Hui Li, Wei Li, Jesse J. Lutz, Ilias Magoulas, Joani Mato, Vladimir Mironov, Hiroya Nakata, Buu Q. Pham, Piotr Piecuch, David Poole, Spencer R. Pruitt, Alistair P. Rendell, Luke B. Roskop, Klaus Ruedenberg, Tosaporn Sattasathuchana, Michael W. Schmidt, Jun Shen, Lyudmila Slipchenko, Masha Sosonkina, Vaibhav Sundriyal, Ananta Tiwari, Jorge L. Galvez Vallejo, Bryce Westheimer, Marta Wloch, Peng Xu, Federico Zahariev, and Mark S. Gordon. Recent developments in the general atomic and molecular electronic structure system. *The Journal of Chemical Physics*, 152(15):154102, April 2020. ISSN 0021-9606, 1089-7690.
- [10] Qiming Sun, Timothy C Berkelbach, Nick S Blunt, George H Booth, Sheng Guo, Zhendong Li, Junzi Liu, James D McClain, Elvira R Sayfutyarova, Sandeep Sharma, et al. Pyscf: the python-based simulations of chemistry framework. *Wiley Interdisciplinary Reviews: Computational Molecular Science*, 8(1):e1340, 2018.

- [11] Qiming Sun, Xing Zhang, Samraghi Banerjee, Peng Bao, Marc Barbry, Nick S Blunt, Nikolay A Bogdanov, George H Booth, Jia Chen, Zhi-Hao Cui, et al. Recent developments in the pyscf program package. *The Journal of Chemical Physics*, 153(2):024109, 2020.
- [12] To learn about gqcp, please refer to its website. URL <https://gqcg.github.io/GQCP/landing-page.html>.
- [13] Daniel G. A. Smith, Lori A. Burns, Andrew C. Simmonett, Robert M. Parrish, Matthew C. Schieber, Raimondas Galvelis, Peter Kraus, Holger Kruse, Roberto Di Remigio, Asem Alenaizan, Andrew M. James, Susi Lehtola, Jonathon P. Misiewicz, Maximilian Scheurer, Robert A. Shaw, Jeffrey B. Schriber, Yi Xie, Zachary L. Glick, Dominic A. Sirianni, Joseph Senan O’Brien, Jonathan M. Waldrop, Ashutosh Kumar, Edward G. Hohenstein, Benjamin P. Pritchard, Bernard R. Brooks, III Schaefer, Henry F., Alexander Yu. Sokolov, Konrad Patkowski, III DePrince, A. Eugene, Uğur Bozkaya, Rollin A. King, Francesco A. Evangelista, Justin M. Turney, T. Daniel Crawford, and C. David Sherrill. PSI4 1.4: Open-source software for high-throughput quantum chemistry. *The Journal of Chemical Physics*, 152(18):184108, 05 2020. ISSN 0021-9606.
- [14] Michelle Richer, Gabriela Sánchez-Díaz, Farnaz Heidar-Zadeh, Marco Martínez-González, Valerii Chuiko, and Paul W. Ayers. Pyci: A python-scriptable library for arbitrary determinant ci. Unpublished manuscript.
- [15] D. J. Rowe. Equations-of-motion method and the extended shell model. *Reviews of Modern Physics*, 40:153–166, 1968. ISSN 00346861.
- [16] Koushik Chatterjee and Katarzyna Pernal. Excitation energies from extended

- random phase approximation employed with approximate one- and two-electron reduced density matrices. *The Journal of Chemical Physics*, 137:204109, 2012.
- [17] Orville W Day, Darwin W Smith, and Claude Garrod. A generalization of the hartree-fock one-particle potential. *International Journal of Quantum Chemistry*, 8:501–509, 1974.
- [18] Ernest R. Davidson, Joseph Vincent Ortiz, and Viktor N. Staroverov. Complete-active-space extended koopmans theorem method. *The Journal of Chemical Physics*, 155:051102, 8 2021. ISSN 0021-9606.
- [19] Taewon David Kim, Leila Pujal, Michelle Richer, Marco Martínez-González, Maximilian van Zyl, Alireza Tehrani, Valerii Chuiko, Gabriela Sánchez-Díaz, William Adams, Xiaomin Huang, Braden D. Kelly, Esteban Vöhringer-Martinez, Toon Verstraelen, Farnaz Heidar-Zadeh, and Paul W. Ayers. GBasis: A Python library for evaluating functions, functionals, and integrals expressed with gaussian basis functions. Unpublished manuscript.
- [20] Valerii Chuiko, Addison Richards, Gabriela Sánchez-Díaz, Marco Martínez-González, Michelle Richer, Farnaz Heidar-Zadeh, and Paul W. Ayers. Modelhamiltonian: A python-scriptable library for generating 0-, 1-, and 2-electron integrals. Unpublished manuscript.
- [21] Toon Verstraelen, Paweł Tecmer, Farnaz Heidar-Zadeh, Cristina E González-Espinoza, Matthew Chan, Taewon D Kim, Katharina Boguslawski, Stijn Fias, Steven Vandenbrande, Diego Berrocal, and Paul W Ayers. HORTON 2.1.1, 2017. <http://theochem.github.io/horton/2.1.1/>.

- [22] A. D. McLACHLAN and M. A. BALL. Time-dependent hartree—fock theory for molecules. *Reviews of Modern Physics*, 36:844–855, 7 1964. ISSN 0034-6861.
- [23] J. A. Pople. Electron interaction in unsaturated hydrocarbons. *Trans. Faraday Soc.*, 49:1375–1385, 1953. doi: 10.1039/TF9534901375. URL <http://dx.doi.org/10.1039/TF9534901375>.
- [24] Rudolph Pariser and Robert G. Parr. A Semi-Empirical Theory of the Electronic Spectra and Electronic Structure of Complex Unsaturated Molecules. II. *The Journal of Chemical Physics*, 21(5):767–776, 05 1953. ISSN 0021-9606.
- [25] J. Hubbard and Brian Hilton Flowers. Electron correlations in narrow energy bands. *Proceedings of the Royal Society of London. Series A. Mathematical and Physical Sciences*, 276(1365):238–257, 1963.
- [26] Erich Hückel. Quantentheoretische beiträge zum benzolproblem: I. die elektronenkonfiguration des benzols und verwandter verbindungen. *Zeitschrift für Physik*, 70(3–4):204–286, March 1931. ISSN 1434-601X.
- [27] W. Heisenberg. Zur theorie des ferromagnetismus. *Zeitschrift für Physik*, 49 (9–10):619–636, September 1928. ISSN 1434-601X.
- [28] R. W. Richardson. Exact eigenstates of the pairing-force hamiltonian. ii. *Journal of Mathematical Physics*, 6(7):1034–1051, July 1965. ISSN 1089-7658.
- [29] Michel Gaudin. *La fonction d'onde de Bethe*. Elsevier Masson, Barcelona, Spain, 1983.

Chapter 6

Conclusion

6.1 Summary

Developing *ab initio* methods for excited states is challenging, especially for strongly-correlated systems. This thesis explores approaches to molecular excited state properties that are computationally efficient, yet applicable to strongly-correlated systems. Specifically, we explore strategies that combine the fundamental Equation-of-Motion (EOM) approach with the types of correlated wavefunction ansätze that are suitable for strongly-correlated systems, and assessed these strategies for neutral and ionic excited states. To control the computational cost, excited-state wavefunctions are generated from a reference (typically the ground-state) wavefunction through the action of a transition operator expanded in some suitable, but small, basis set for the excitation process of interest. By suitably truncating the basis set for the transition operator, we can model excitation processes from the ground state's 1- and 2-RDMs; the resulting EOM methods can be applied to any wavefunction method that provides these quantities, including the wavefunctions of highly-accurate *ab initio* approaches.

Chapter 2 examines the theoretical background and accuracy of various excited-state methods within the EOM framework. Taking the simplest basis set approximation to the transition operator together with various (in principle equivalent) EOM eigenvalue problem formulations, the working equations to optimize the parameters of the excited-state wavefunction are derived. This leads to traditional approaches such as the extended Koopman’s Theorem (EKT) for ionization energies as well as new/alternative expressions. For example, in analogy to the particle-hole extended random phase approximation to obtain electronic excitations from correlated ground state wavefunctions, an expression for the process of double ionization, labeled hole-hole ERPA, is derived. In addition, the accuracy of different EOM formulations for the processes of ionization, electron excitation, and double ionization is compared. In all cases, the excited states are determined by diagonalizing the transition-Hamiltonian in the basis of excited configurations generated from the ground-state wavefunction. We observed that in general established approaches produced better results for the transition energies considered (i.e., lowest ionization potentials, excitation energies and double ionization energies).

The approaches presented in Chapter 2 are best suited for *ab initio* methods relying on variational optimization of the wavefunction. In these cases, obtaining the ground state 2-RDMs is usually straightforward. However, for non-variational wavefunction methods, such as coupled cluster or geminal product approximations that rely on a projected formulation of the Schrödinger equation, the *transition* reduced density matrices are more accessible. Chapter 3 extends the Flexible Ansatz for N-electron Configuration Interaction (FanCI) framework for multideterminant wavefunctions to electronic transitions based on EOM; we call the resulting approach

FanEOM. The proposed method leads to an overdetermined system of equations that can be cast into a rectangular generalized eigenvalue problem. However, in general, solving rectangular eigenvalue problems is rather difficult. Among the methods we explored for solving the FanEOM eigenproblem, left-multiplying by the conjugate-transpose of the right-hand-side of the equation and solving the eigenproblem in the least-squares sense gave the best results. Since the FanEOM eigenvalue problem is not symmetric, complex solutions are possible, though we did not find the imaginary part of the eigenvalues to be significant for the systems we tested.

In Chapter 4 we explored using the EOM framework to estimate the residual dynamic correlation energy in correlated wavefunction methods. For example, we can use the hole-hole/particle-particle channel of extended random phase approximation (ERPA) from chapter 2 to approximate the 2-RDMs along the adiabatic connection path. By employing a resolution of identity in terms of double electron removed (or attached) states, the λ -dependent 2-RDMs in the AC formula can be rewritten in terms of pairing transition density matrix elements. These matrices are in turn approximated using hh/pp-ERPA. The correlation energy corrections via this alternative ERPA channel follow the same approximations as the particle-hole counterpart [1]. Our numerical performance assessment indicated that, in general, less of the residual (dynamic) correlation was recovered by the hole-hole ERPA, and particle-hole ERPA should be preferred.

In order to perform the computational tests discussed in chapters 2-4, I was actively involved in the development of software, including PyCI [2], a Python library for (parameterized) configuration interaction calculations and AtomDB, a database of atomic reference data. In addition to these collaborative efforts, I developed

the PyEOM library discussed in chapter 5. PyEOM is based on the unified EOM framework presented in Chapter 2. Its goal is to facilitate studies like those in this thesis, where different formulations of the EOM problem are explored, rather than provide production-level EOM calculations. PyEOM is well-suited to its intended user base because of its modular design, clear and simple implementation, and thorough documentation. PyEOM is designed as a flexible post-processing tool for almost any electronic structure package, allowing users to model a wide variety of electronic transitions and a variety of other dynamic properties (e.g. oscillator strengths) for post-Hartree-Fock methods where the 1- and 2-RDMs are available.

6.2 Future work

The work presented in this thesis lays a robust foundation for several avenues of future research and development. Here, we outline some potential directions for extending and enhancing the methodologies developed in this thesis:

Using the EOM formulations presented in Chapter 2, various properties of neutral and ionized excited states can be evaluated from the correlated ground state’s 1- and 2-RDMs. Consequently, these EOM methodologies can also be applied to assess other properties relevant to molecular reactivity in strongly correlated systems, such as the chemical potential, chemical hardness, and polarizability [3–5]. We performed some preliminary computations of spin-polarized chemical reactivity indicators used to describe radical reactivity, with promising results. Further studies along these lines are certainly warranted.

Among the unconventional EOM methods we explored, the most interesting results corresponded to the IPa approach for ionized states. This method, based on the

examples studied in Chapter 2, provides qualitatively good results using only the 1-RDM of the reference ground state. IPa seems promising as an efficient alternative to the extended Koopmans’ theorem (EKT), especially for post-processing methods where the 2-RDM is not readily available. We would also like to use the left-hand side of the extended Koopmans’ theorem and extended Random Phase Approximation, related to the orbital Lagrangian and Hessian, for orbital optimization [6, 7].

In Chapter 2, we looked at several EOM formulations for neutral and charged excited states, but we limited ourselves to transition operators that involved a product of at most two creation/annihilation operators. This restriction controlled the cost of the calculations and ensured that only the 1- and 2-electron reduced density matrices were needed. To improve the accuracy of the EOM methods, particularly the double ionization EOM approach (labeled as the hole-hole ERPA), a straightforward solution would be to introduce terms that depend on three or four creation/annihilation operators [8, 9]. Alternatively, using the 3-RDM and the same transition operators, the basic form of the EOM could be used, so that the killer condition does not need to be invoked [10]. Techniques such as cumulant reconstructions of the higher-order RDMs could be used to reduce the additional cost that would be incurred were the 3- and 4-RDMs evaluated directly. Note, however, that the 3- and 4-RDMs have simple, easy to compute and store, forms for seniority-zero wavefunctions, making it feasible to include more complex transition operators and/or avoid the killer condition for seniority-zero theories [11–13].

In Chapter 4, the AC-ERPA methods assume a linear dependence with the interaction strength parameter of the adiabatic connection Hamiltonian and a constant 1-RDM along the adiabatic connection path. Future work could explore adiabatic connections

like the Harris-Jones path [14]; that would allow us to relax, or perhaps even eliminate, the assumption that the 1-RDM remains constant. Other nonlinear parameterizations of the Hamiltonian, associated with generalized adiabatic connections, can also be used [15]. Additionally, inspired by the recent work of Knowles, better zeroth-order Hamiltonian approximations with a desired functional form could be determined [16]. Such explorations may lead to new insights and improvements in the accuracy of the correlation energy correction through the adiabatic connection methods.

At the moment, the EOM package uses a generalized implementation of the working equations for the excited state approximations in Chapter 2. However, the consequent need to store multiple high dimensional tensors (e.g. the two-electron integrals and 2-RDMs) causes poor memory scaling. We can reduce the time and memory requirements of EOM methods using a restricted form of the EOM working equations. Alternatively, we can use tensor/array compression techniques such as density fitting and Cholesky decomposition [17, 18].

References

- [1] Katarzyna Pernal. Electron correlation from the adiabatic connection for multireference wave functions. *Physical Review Letters*, 120:013001, 1 2018. ISSN 0031-9007.
- [2] Michelle Richer, Gabriela Sánchez-Díaz, Farnaz Heidar-Zadeh, Marco Martínez-González, Valerii Chuiko, and Paul W. Ayers. Pyci: A python-scriptable library for arbitrary determinant ci. Unpublished manuscript.
- [3] Paul W. Ayers and Junia Melin. Computing the fukui function from ab initio quantum chemistry: approaches based on the extended koopmans’ theorem. *Theoretical Chemistry Accounts*, 117(3):371–381, 2007. ISSN 1432-2234.
- [4] Peter Politzer, Jane S. Murray, and Felipe A. Bulat. Average local ionization energy: A review. *Journal of Molecular Modeling*, 16(11):1731–1742, 2010.
- [5] Dilan Yildiz and Uğur Bozkaya. Assessment of the extended koopmans’ theorem for the chemical reactivity: Accurate computations of chemical potentials, chemical hardnesses, and electrophilicity indices. *Journal of Computational Chemistry*, 37:345–353, 1 2016. ISSN 01928651.
- [6] George B. Bacskay. A quadratically convergent hartree—fock (qc-scf) method.

- application to closed shell systems. *Chemical Physics*, 61:385–404, 10 1981. ISSN 03010104.
- [7] George B. Bacskay. A quadratically convergent hartree-fock (qc-scf) method. application to open shell orbital optimization and coupled perturbed hartree-fock calculations. *Chemical Physics*, 65:383–396, 3 1982. ISSN 03010104.
- [8] Koushik Chatterjee and Katarzyna Pernal. Excitation energies from extended random phase approximation employed with approximate one- and two-electron reduced density matrices. *The Journal of Chemical Physics*, 137:204109, 2012.
- [9] Hervé Molique and Jerzy Dudek. Particle-particle hole-hole tda - and beyond - for the nuclear pairing hamiltonian. *International Journal of Modern Physics E*, 16:298–309, 2007. ISSN 02183013.
- [10] Loren Greenman and David A. Mazziotti. Electronic excited-state energies from a linear response theory based on the ground-state two-electron reduced density matrix. *The Journal of Chemical Physics*, 128, 3 2008. ISSN 0021-9606.
- [11] Frank Weinhold and Jr. Wilson, E. Bright. Reduced Density Matrices of Atoms and Molecules. II. On the N-Representability Problem. *The Journal of Chemical Physics*, 47(7):2298–2311, 10 1967. ISSN 0021-9606.
- [12] III DePrince, A. Eugene and David A. Mazziotti. Cumulant reconstruction of the three-electron reduced density matrix in the anti-Hermitian contracted Schrödinger equation. *The Journal of Chemical Physics*, 127(10):104104, 09 2007. ISSN 0021-9606.

- [13] Ward Poelmans, Mario Van Raemdonck, Brecht Verstichel, Stijn De Baerdemacker, Alicia Torre, Luis Lain, Gustavo E. Massaccesi, Diego R. Alcoba, Patrick Bultinck, and Dimitri Van Neck. Variational optimization of the second-order density matrix corresponding to a seniority-zero configuration interaction wave function. *Journal of Chemical Theory and Computation*, 11(9): 4064–4076, 2015. PMID: 26575902.
- [14] Helen van Aggelen, Yang Yang, and Weitao Yang. Exchange-correlation energy from pairing matrix fluctuation and the particle-particle random phase approximation. *The Journal of Chemical Physics*, 140, 5 2014. ISSN 0021-9606.
- [15] Mikuláš Matoušek, Michał Hapka, Libor Veis, and Katarzyna Pernal. Toward more accurate adiabatic connection approach for multireference wavefunctions. *The Journal of Chemical Physics*, 158(5):054105, 02 2023. ISSN 0021-9606.
- [16] Peter J. Knowles. Perturbation-adapted perturbation theory. *Journal of Chemical Physics*, 156, 1 2022. ISSN 10897690.
- [17] Edward G. Hohenstein and C. David Sherrill. Density fitting and Cholesky decomposition approximations in symmetry-adapted perturbation theory: Implementation and application to probe the nature of π - π interactions in linear acenes. *The Journal of Chemical Physics*, 132(18):184111, 05 2010. ISSN 0021-9606.
- [18] Neil Shenvi, Helen van Aggelen, Yang Yang, and Weitao Yang. Tensor hypercontracted pprpa: Reducing the cost of the particle-particle random phase approximation from $\mathcal{O}(r^6)$ to $\mathcal{O}(r^4)$. *The Journal of Chemical Physics*, 141: 024119, 7 2014. ISSN 0021-9606.

Appendix A

A.0.1 Electron affinity from extended Koopmans' theorem

Inserting the definition of the one-electron addition operator \hat{Q}_λ^{+1} , Eq. 2.3.9, into the EOM equation 5.4.3 results in an analogous EKT equation for the process of electron attachment:

$$\sum_n \langle \Psi_0^N | a_m [\hat{H}, a_n^\dagger] | \Psi_0^N \rangle c_{n;\lambda} = \Delta E_\lambda^{N-1} \sum_n \langle \Psi_0^N | a_m a_n^\dagger | \Psi_0^N \rangle c_{n;\lambda}; \forall m \quad (\text{A.0.1})$$

where ΔE_λ^{N-1} represents the electron affinity. The terms are defined as follows:

$$\begin{aligned} A_{mn} &= \langle \Psi_0^N | a_m [\hat{H}, a_n^\dagger] | \Psi_0^N \rangle \\ &= h_{mn} + \sum_{qs} \langle mq || ns \rangle \gamma_{qs} - \sum_p h_{pn} \gamma_{pm} - \frac{1}{2} \sum_{pqs} \langle pq || sn \rangle \Gamma_{pqsm} \end{aligned} \quad (\text{A.0.2})$$

$$\begin{aligned} M_{mn} &= \langle \Psi_0^N | a_m a_n^\dagger | \Psi_0^N \rangle \\ &= \delta_{mn} - \gamma_{nm} \end{aligned} \quad (\text{A.0.3})$$

Here, the left-hand-side matrix, A_{mn} , includes the one-electron integrals h_{pq} , two-electron integrals $\langle pq||rs\rangle$, and the one- and two-electron reduced density matrices γ_{pq} and Γ_{pqrs} , respectively. The metric matrix M_{mn} is the overlap matrix between the $N + 1$ electron configurations generated from the ground state by the basis set of creation operators that define the one-electron addition operator \hat{Q}_λ^{+1} .

A.0.2 Other Equation-of-motion formulations for ionization potential

Different variants of the Equation-of-motion (EOM) approach can be employed to compute ionization potentials (IPs, see Chapter 2). Based on the anticommutator form of EOM that excludes the killer condition on the right-hand side, Eq. 2.2.18, one obtains:

$$\sum_n \left\langle \Psi_0^N \left| \left[a_m^\dagger, \left[\hat{H}, a_n \right] \right]_+ \right| \Psi_0^N \right\rangle c_{n;\lambda} = \Delta E_\lambda^{N-1} \sum_n \left\langle \Psi_0^N \left| a_m^\dagger a_n \right| \Psi_0^N \right\rangle c_{n;\lambda}; \forall m \quad (\text{A.0.4})$$

and similarly, for the nested commutator form 5.4.5:

$$\sum_n \left\langle \Psi_0^N \left| \left[a_m^\dagger, \left[\hat{H}, a_n \right] \right] \right| \Psi_0^N \right\rangle c_{n;\lambda} = \Delta E_\lambda^{N-1} \sum_n \left\langle \Psi_0^N \left| a_m^\dagger a_n \right| \Psi_0^N \right\rangle c_{n;\lambda}; \forall m \quad (\text{A.0.5})$$

These approaches will be labeled as IPam and IPcm respectively. They differ from the IPa and IPc methods described in Chapter 2 in the metric matrix on the RHS, which now corresponds to the one-electron reduced density matrix (1-RDM).

A.0.3 Particle-particle extended random phase approximation (pp-ERPA)

Taking the double-electron attachment operator Eq. 2.3.37 with the commutator form of the EOM, Eq. (2.2.17), leads to the pp-ERPA equation:

$$\sum_{ij} \langle \Psi_0^N | [a_k a_l, [\hat{H}, a_i^\dagger a_j^\dagger]] | \Psi_0^N \rangle c_{ij;\lambda} = \Delta E_\lambda \sum_{ij} \langle \Psi_0^N | [a_k a_l, a_i^\dagger a_j^\dagger] | \Psi_0^N \rangle c_{ij;\lambda}; \forall k, l \quad (\text{A.0.6})$$

where:

$$\begin{aligned} A_{kl,ji} &= \langle \Psi_0^N | [a_k a_l, [\hat{H}, a_i^\dagger a_j^\dagger]] | \Psi_0^N \rangle \\ &= 2h_{li}\delta_{kj} - 2h_{ki}\delta_{lj} + 2h_{ki}\gamma_{jl} - 2h_{li}\gamma_{jk} + 2\delta_{lj} \sum_p h_{pi}\gamma_{pk} + 2\delta_{ki} \sum_p h_{pj}\gamma_{pl} \\ &\quad + \langle lk||ij \rangle + \sum_q \langle ql||ij \rangle \gamma_{qk} - \sum_q \langle qk||ij \rangle \gamma_{ql} + 2 \sum_r \langle lk||jr \rangle \gamma_{ir} \\ &\quad + 2\delta_{ki} \sum_{qr} \gamma_{qr} \langle ql||jr \rangle - 2\delta_{li} \sum_{qr} \langle qk||jr \rangle \\ &\quad + 2 \sum_{qr} \langle ql||ir \rangle \Gamma_{qjrk} - 2 \sum_{qr} \langle qk||ir \rangle \Gamma_{qjrl} \\ &\quad + \delta_{li} \sum_{pqr} \langle pq||jr \rangle \Gamma_{pqrk} - \delta_{ki} \sum_{pqr} \langle pq||jr \rangle \Gamma_{pqrl} \end{aligned} \quad (\text{A.0.7})$$

$$\begin{aligned}
U_{kl,ji} &= \left\langle \Psi_0^N \left| \left[a_k a_l, a_i^\dagger a_j^\dagger \right] \right| \Psi_0^N \right\rangle \\
&= \delta_{il} \delta_{jk} - \delta_{ik} \delta_{jl} + \delta_{ik} \gamma_{jl} - \delta_{il} \gamma_{jk} + \delta_{jl} \gamma_{ik} - \delta_{jk} \gamma_{il}
\end{aligned} \tag{A.0.8}$$

A.0.4 Commutator identities

Given the transition operator $(\hat{Q}_\lambda^{\pm\kappa})^\dagger$ and its complex conjugate $\hat{Q}_\lambda^{\pm\kappa}$, the following commutator identity holds:

$$\begin{aligned}
0 &= \left\langle \Psi_0^N \left| \left[\hat{Q}_\lambda^{\pm\kappa}, \left[\hat{H}, (\hat{Q}_\lambda^{\pm\kappa})^\dagger \right] \right] \right| \Psi_0^N \right\rangle + \left\langle \Psi_0^N \left| \left[\hat{H}, \left[(\hat{Q}_\lambda^{\pm\kappa})^\dagger, \hat{Q}_\lambda^{\pm\kappa} \right] \right] \right| \Psi_0^N \right\rangle \\
&+ \left\langle \Psi_0^N \left| \left[(\hat{Q}_\lambda^{\pm\kappa})^\dagger, \left[\hat{Q}_\lambda^{\pm\kappa}, \hat{H} \right] \right] \right| \Psi_0^N \right\rangle
\end{aligned} \tag{A.0.9}$$

Similarly, for the anticommutator, the identity is given by:

$$\begin{aligned}
0 &= \left\langle \Psi_0^N \left| \left[\hat{H}, \left[\hat{Q}_\lambda^{\pm\kappa}, (\hat{Q}_\lambda^{\pm\kappa})^\dagger \right]_+ \right] \right| \Psi_0^N \right\rangle - \left\langle \Psi_0^N \left| \left[(\hat{Q}_\lambda^{\pm\kappa})^\dagger, \left[\hat{H}, \hat{Q}_\lambda^{\pm\kappa} \right]_+ \right] \right| \Psi_0^N \right\rangle \\
&+ \left\langle \Psi_0^N \left| \left[\hat{Q}_\lambda^{\pm\kappa}, \left[(\hat{Q}_\lambda^{\pm\kappa})^\dagger, \hat{H} \right]_+ \right] \right| \Psi_0^N \right\rangle
\end{aligned} \tag{A.0.10}$$

These relations justify the presence of complementary pairs of eigenvalues in the solutions of the commutator and anticommutator forms of the equation-of-motion described in Chapter 2.

A.0.5 Additional data

In this section, we provide additional ionization potential data for the test set of second-row atoms (He, Be, C, Ne) and the 1,3-dipolar molecules, computed using the different forms of EOM (EKT, IPa, IPc, IPam, IPcm) with Heat-bath Configuration Interaction (HCI) reduced density matrices. The HCI ground state is not an eigenfunction

of the Hamiltonian operator; as a result, the EKT and IPc left-hand-side matrices are not Hermitian. The effect this has on the computed ionization potentials can be assessed based on the results in table A.2. This table presents the lowest ionization energies for the test set of atoms and molecules evaluated using symmetrized forms of the eigenvalue problems (e.g., Eq. 2.2.24) for the electron removal operator Eq. 2.3.3, labeled as EKT1/2 and IPc1/2.

Table A.1: Lowest ionization potentials (in eV) computed from 1- and 2-RDMs at the aug-cc-pVDZ HF (KT) and HCI levels (EKT, IPa, IPc, IPam, IPcm)

	Label	KT	IP	IPa	IPc	IPam	IPcm	HCI
He	1s	24.96	24.36	24.88	26.96	25.09	26.69	24.36
Be	2s	8.42	9.29	7.62	11.89	8.42	10.62	9.29
C	2p	11.78	11.09	11.68	13.63	11.89	13.33	11.07
Ne	2p	23.21	21.49	23.68	27.04	23.93	26.64	21.49
NNO	2 π	13.40	11.61	13.10	17.16	13.44	16.65	12.06
NNNH	4 π	11.01	11.22	10.73	14.48	11.00	14.05	10.10
HCNO	2 π	11.09	10.91	10.87	14.82	11.19	14.28	10.29
HCNNH	4 π	9.54	8.64	9.27	12.83	9.52	12.39	8.93
H ₂ CNCH	4 π	8.57	9.88	8.27	11.55	8.50	11.18	8.02

Table A.2: Lowest ionization potentials (in eV) computed from 1- and 2-RDMs at the aug-cc-pVDZ HCI level (EKT, EKT1/2, IPc, IPc1/2)

	Label	EKT	EKT1/2	IPc	IPc1/2
He	1s	24.36	24.36	26.96	26.96
Be	2s	9.29	9.29	11.89	11.89
C	2p	11.09	11.09	13.63	13.63
Ne	2p	21.49	21.5	27.04	27.04
NNO	2 π	11.61	7.45	17.16	17.16
NNNH	4 π	11.22	9.56	14.48	14.47
HCNO	2 π	10.91	10.52	14.82	14.82
HCNNH	4 π	8.64	9.51	12.83	12.82
H ₂ CNCH	4 π	9.88	5.15	11.55	11.55